TRANSIENT HEATING IN BÉNARD CONVECTION

Thesis by

Richard Carl Nielsen

In Partial Fulfillment of the Requirements
for the Degree of
Doctor of Philosophy

California Institute of Technology

Pasadena, California

1971

(Submitted May 21, 1971)

ACKNOWLEDGMENTS

The author wishes to express his deep appreciation to Professor Rolf Sabersky for his guidance, advice and patience during the course of this research. Thanks are extended to Professors Allan Acosta and Duncan Rannie for their encouragement and their stimulating discussions. The help of Professor Dave Welch, Mr. Don Laird and Mr. Fred McDonald in the design and construction of the experimental apparatus is deeply valued.

Special thanks are due to Mrs. Julie Powell and Mrs. Georgeia Hutchinson for the typing of the manuscript and to others on the California Institute of Technology staff for their cooperation.

Part of this research was sponsored by the National Science Foundation through Grant GK-572. Financial assistance was provided by the John and Fannie Hertz Foundation. The author is very grateful for this aid.

Finally, the author wishes to thank his wife for her cooperation and encouragement and especially for help in the reduction of the data from these experiments.

ABSTRACT

Experimental results are presented for a study of the effects of time-dependent heating on Bénard convection, where the fluids were 5 centistoke (cs), 100 cs and 500 cs viscosity grades of silicone oil. Fluid layer depths were 0.00635 m, 0.01270 m and 0.01905 m. For each run the heat flux at the lower surface was approximately constant, which in dimensionless units was between 9.2×10^2 and 1.9×10^7. The study examined the effects of different heating rates on the onset of convection, the change of the Rayleigh number with time and the development of motion. Visual observations were made from shadowgraph images, which were recorded photographically.

A supplementary analytical analysis of the onset of motion was performed. The results of the work support the trends of the critical time data found in the experiments.

On the basis of the experimental results the conculsions are that as the heat flux at the lower surface is increased, the temperature difference required for the initiation of convection increases while the time to the onset of motion decreases. For the higher heating rates a "new" small closed cell pattern is observed shortly after the onset of motion. This pattern does not appear in the steady-state system. Because of the "large" (approximately greater than 100) Prandtl number, specifying the time and the heat flux at the lower surface is sufficient to characterize the state of the fluid layer.

TABLE OF CONTENTS

CONTENTS (continued)

LIST OF FIGURES

LIST OF TABLES

LIST OF SYMBOLS

General

a	Wave number
c_p	Specific heat at constant pressure
d	Fluid layer depth
g	Acceleration due to gravity
H	Dimensionless heat flux at the lower surface = $(g\beta d^4/\varkappa\nu k)(-\partial T/\partial z)_{z=0}$
H_T	Dimensionless total heat generation rate = $g\beta d^4 Q_T/\varkappa\nu k$
k	Thermal conductivity
Nu	Nusselt number = $(d/k\Delta T)(-\partial T/\partial z)_{z=0}$
p	Pressure
Pr	Prandtl number = $\nu/\varkappa$
Q_T	Total heat generation rate
Ra	Rayleigh number = $g\beta d^3\Delta T/\varkappa\nu$
t	Time
T	Temperature
u_i	Velocity components
u, v, w	Velocity components
x_i	Cartesian coordinates
x, y, z	Cartesian coordinates

1. General (continued)

β	Thermal coefficient of expansion
δ_{rn}	Kronecker delta
ΔT	Temperature difference between lower and upper surface
ϵ	Thermal thickness = $\frac{2}{d\Delta T}\int_0^d [T(z, t) - T(d, t)]dz$
$\varkappa$	Thermal diffusivity
μ	Dynamic viscosity
ν	Kinematic viscosity
ρ	Density
τ	Dimensionless time = $t(\varkappa/d^2)$

Subscript:

cr	Value of quantity at critical time

2. Chapter III and Appendix B

e_n	Function, defined in equation (B15)
E_{rn}	Function, defined in equation (36)
f	Horizontal spatial dependence, defined in equation (23)
K_{rn}	Coefficient, defined in equation (36)
R	Characteristic Rayleigh number = $g^* \beta^* d^{*3} \Delta\Theta^* / \varkappa^* \nu^*$
T_r^*	Reference temperature
T_0^*	Upper surface temperature

2. Chapter III and Appendix B (continued)

W_n	Fourier velocity function, defined in equation(33)
α	Heating parameter, defined in equation (44)
δ	Heating parameter, defined in equation (43)
$\Delta\Theta^*$	Characteristic temperature difference
ζ^*	Bulk viscosity
λ_i	Direction vector = (0, 0, 1)
Π	Pressure, defined in equation (8)
ρ_r^*	Reference density
$\bar{\Phi}^*$	Dissipation function
θ	Temperature
θ_n	Fourier time-dependent coefficients
Θ_n	Fourier temperature function, defined in equation (33)
ω	Vertical velocity
ω_n	Fourier time-dependent coefficients

Superscript:

$\bar{(\ )}$	Conduction quantity
$(\ )'$	Perturbation quantity
$(\ )^*$	Dimensional quantity

3. Chapters VI, VII and VIII

A	Dimensionless wave number = ad

3. Chapters VI, VII and VIII (continued)

EP	Thermal thickness
HT	Dimensionless total heat generation rate
NU	Nusselt number
Ra_d	Rayleigh number
RAD	Rayleigh number
TAU	Dimensionless time
-CR	Value of quantity at onset of motion

4. Appendix C

ℓ	Thickness of layers 1 and 3
p	Laplace transform parameter
q	Coefficient = $\sqrt{p/\varkappa}$
β_{ij}	Property coefficient, given in equation (C12)
$\zeta_1, \zeta_2, \zeta_3, \zeta_4$	Property coefficients, defined in equation (C9)
μ_{ij}	Property coefficient, given in equation (C15)
ξ	Property coefficient, defined in equation (C9)
σ_2, σ_4	Property coefficients, defined in equation (C9)
φ	Function, defined in equation (C9)

Subscript:

$(\ )_i$	Layer of material i

4. Appendix C (continued)

Superscript:

$\bar{(\ )}$	Laplace transform

5. Appendix D

A	Surface heating area
C_Q	Constant, defined in equation (D10)
i_1, i_2, I	Current
r	Resistance
R_0	Resistance = R_2R_4/R_3
R_1, R_2, R_3, R_4	Leg resistances
T_0	Initial temperature
V	Bridge total voltage drop
α_R	Temperature coefficient of resistance = $\Delta R/\Delta T$
δ	Effective imbalance = $\Delta V/V$
δ_0	Initial effective imbalance
ΔR	Imbalance resistance
ΔR_0	Initial imbalance resistance
ΔV	Bridge voltage imbalance
ΣR	Resistance = $R_1+R_2+R_3+R_4$
ΣR_0	Resistance = $R_0+R_2+R_3+R_4$

6. Appendix E

a, b, A, B	Constants in Walther viscosity equation
t	Temperature, Celsius
T	Temperature, Kelvin
VTC	Viscosity temperature coefficient = 1 - ν(50 C)/ν(25 C)
Δk, $\Delta \rho$, Δc_p	Change of quantity per unit temperature

Subscript:

0	Value of property at 0 C

I. INTRODUCTION

When a layer of fluid contained between two flat, horizontal plates has the lower surface maintained at a higher temperature than the upper surface, a number of interesting natural convection phenomena can be observed. The fundamental observation is that if the temperature difference is "small enough" no convection occurs; the heat is transferred solely by conduction. This is because the viscous forces and thermal diffusivity act to dissipate any motion generated by the buoyancy of the system. As the temperature difference is raised, a point is reached where the dissipative forces can no longer completely dampen out the motion generated by the buoyancy force. This point is the first time that a balance can be maintained between these two opposing forces. This boundary between no convection and convection can be given, for the simple system of constant properties, solely in terms of a single, dimensionless parameter, the Rayleigh number, Ra.

Once motion occurs, it takes place in an ordered array, with the normally seen pattern being "vermiculated" (randomly curved) rolls, that is, a repetitive pattern of hot rising bands of fluid adjacent to cold descending ribbons of fluid. When attempting to describe this motion, a basic characteristic measure of the flow is the horizontal scale of the planform, which is normally given in terms of the total wave number, a. Other parameters that are used to characterize the

tate of the fluid layer are the previously mentioned Rayleigh number, ıe Prandtl number and the Nusselt number.

As the Rayleigh number is increased, the roll pattern becomes nstable. The planform is replaced by a steady, three-dimensional ..iotion. This, too, eventually becomes unstable and turns into a pattern involving periodic disturbances of a single frequency. As the Rayleigh number is further increased, another periodic disturbance appears at twice the frequency. Higher order disturbances continue to appear until the motion is so complicated as to be called "turbulent".

For transient heating of the fluid layer, starting from an initially isothermal condition, the sequence of events has not been as extensively explored and a number of pertinent questions may be asked. The first is how long does it take for motion to occur and is this length of time completely describable by only two parameters: the Rayleigh number and a second number characteristic of the conduction problem? This additional parameter could be based on the heat transfer rate at, say, the lower surface, or on some average rate given in terms of a "thermal thickness". Another question one could ask refers to the planform of motion. Is the motion uniquely determined by the Rayleigh number and (possibly) the Prandtl number, or are there other important parameters? Once motion does occur, does the system successively assume all the states described above for the steady-state system as the corresponding Rayleigh numbers are reached in a transient manner; or are some of the states bypassed as the system

approaches a steady-state condition? As time progresses, what is the heat transfer in the fluid layer?

The present investigation is directed towards answering these questions through a series of experiments in which emphasis is laid on the visual observation of the motion as well as on the quantitative determination of the temperatures and heat transfer rates of the system as a function of time. A complementary, analytical study is also carried out on the stability boundary of infinitesimal disturbances and the influence of the temperature profile shape on the initiation of convection.

II. REVIEW OF PREVIOUS WORK ON BÉNARD CONVECTION

Previous work, both experimental and theoretical, published in the literature on the steady-state phenomena associated with the fluid layer heated from below affords a rather thorough understanding of the physical processes involved in describing the system. This is particularly true for the region between the onset of motion and the point at which the pattern of motion becomes three-dimensional.

The first mention of this type of natural convection problem was made by Thomson (1882), who studied the patterns associated with the evaporative cooling of water. The first quantitative experiments were carried out by Bénard (1900, 1901). Because of his pioneering work, this natural convection phenomena is often called Bénard convection and the flow pattern, Bénard cells. He used very thin layers of highly viscous fluids and from visual observations found that the motion normally occurred in a honeycomb pattern, that is, a repetition of hexagonal cells. In his experiments the upper surface was exposed to the atmosphere, allowing the appearance of surface tension gradients. Papers by Block (1956) and Pearson (1958) indicated that Bénard's experiments were probably governed by surface tension gradients instead of buoyancy forces. Subsequent investigations have indicated that the honeycomb pattern was due to free surface effects and was not the preferred pattern when the upper surface was a solid boundary.

An excellent review of work involving evaporative convection and surface tension effects is given by Berg, Acrivos and Boudart (1966).

In an attempt to determine the governing criteria for the onset of convection, Lord Rayleigh (1916) presented an analytical investigation of the problem for the case of two stress free, but rigid boundaries (hereafter called "free" boundaries). He found that the onset of motion could be completely described by a single parameter, now called the Rayleigh number, Ra. The other physical parameter that appears in the analysis, the Prandtl number, Pr, did not enter into the stability boundary calculations. Lord Rayleigh also showed that there was a unique wave number associated with the critical Rayleigh number, but the linearized analysis was unable to determine the planform of motion.

The work was extended to the case of two rigid, no slip boundaries (hereafter called "rigid" boundaries) by Jeffreys (1926, 1928) and Low (1929). The two authors also considered the case of the upper surface free and the lower surface rigid. Their work was generalized and extended by Pellew and Southwell (1940), who showed that it was not necessary to specify the cell shape to carry out the analysis, but only the total wave number. The analysis also predicted that at the critical Rayleigh number the motion would start as an aperiodic growth of the initial disturbance. This result is now known as the "principle of exchange of stabilities".

These papers, along with others pertaining to meteorological conditions, can be found in an anthology edited by Saltzman (1962a).

The definitive analytical determination of the critical values of the Rayleigh number and the wave number was made for the various boundary conditions, free-free, rigid-free and rigid-rigid, by Reid and Harris (1958). These analytical results along with some of the experimentally determined Rayleigh numbers are shown in Table 1.

To check out the early theoretical work, experiments were carried out by Schmidt and Milverton (1935) to determine the onset of convection. A subsequent study was done by Schmidt and Saunders (1938) on the relation between heat transfer and the Rayleigh number for values greater than the critical. This work included a determination of the wave number of the motion, using an optical system that viewed the fluid layer from the side. Earlier, Mull and Reiher (1930) had carried out detailed experiments with air on Nusselt number versus Rayleigh number over a wide range of Rayleigh numbers. Similar experiments were conducted by de Graaf and van der Held (1953).

Malkus (1954 a) reported a series of experiments which indicated that as the Rayleigh number was increased, there were discrete changes in the slope of the heat flux versus Rayleigh number curve. The transition points were checked by Willis and Deardorff (1967 b). Both series of experiments made use of a "quasi-steady" approach in which a large temperature difference was initially imposed on the system. The apparatus was then insulated, and the temperature was slowly allowed to decay towards an isothermal fluid layer. For "slow enough" decay rates the results should closely approximate a steady-state system. Truly steady-state results were recently presented by

Krishnamurti (1968 c, 1969, 1970 a, 1970 b, 1970 c), who also showed that the breaks in the curve were accompanied by changes in flow pattern.

Very detailed experiments, utilizing optical studies over a wide range of Rayleigh numbers and Prandtl numbers, were reported by Silveston (1958) and Schmidt and Silveston (1959). These experiments were the first systematically cataloguing the patterns of motion that are observed at the various Rayleigh numbers.

Numerous experiments have been carried out that report critical Rayleigh number, heat transfer as a function of Rayleigh number, detailed temperature profiles and, in a few instances, flow patterns. Among these are Catton and Edwards (1967), Chen and Whitehead (1968), Deardorff and Willis (1965, 1967 a, 1967 b), di Frederico and Foraboschi (1966), Dropkin and Somerscales (1965), Gille (1967), Globe and Dropkin (1959), Goldstein and Chu (1966, 1968, 1969), Goldstein and Graham (1969), Ingersoll (1966), Koschmieder (1966, 1967), Leontiev and Kirdyashkin (1968, 1969), Rossby (1966, 1969), Somerscales and Dropkin (1966), Somerscales and Gazda (1968, 1969), Thompson and Sogin (1966) and Willis and Deardorff (1967 a, 1967 b, 1970). A collection of some of the recommended heat transfer correlations from the above sources is contained in Table 2. Also listed are some of the theoretical predictions of Nusselt number versus Rayleigh number.

The linear analysis that is able to predict the onset of motion cannot determine the type of flow pattern that will evolve. Because

the non-linear terms are neglected, the linear approximation cannot predict temperature profiles and velocity fields. The inclusion of the non-linear terms introduces some very formidable problems for the theoretician.

The first one to attack the non-linear problem was Pillow (1952), who assumed that the flow field consisted of a series of two-dimensional rolls in which the motion was rapid enough to utilize boundary layer approximations for the flow in the roll cell. Similar analyses, using different boundary conditions, different Prandtl number ranges, and improved mathematical techniques, have been carried out by Robinson (1965, 1967b, 1969), Turcotte (1967), Turcotte and Oxburgh (1967) and Wesseling (1969).

In an attempt to explain the observed changes in slope in the heat flux versus Rayleigh number curve, Malkus (1954b, 1956, 1961, 1963) developed a theory of thermal turbulence. To make the problem tractable, he introduced several assumptions. One of the important assumptions introduced into the analysis was that the flow pattern that was observed was the one that transported the maximum amount of heat across the fluid layer. Using this basic assumption, Howard (1963) and subsequently Busse (1969) examined the upper bounds that can be placed on heat transfer from integrated forms of the equations of motion.

Malkus' theory of thermal turbulence did not make use of the detailed flow patterns, but only of the average quantities. The first attempts to examine the region above the critical Rayleigh number in a

detailed fashion were done by Gor'kov (1958) and Malkus and Veronis (1958).

Even with non-linear analyses the number of possible planforms is infinite, and a method had to be devised to select which of the motions would be observed in an experimental situation. Malkus and Veronis chose the criterion of maximum heat transport as the possible selection mechanism, with the result that two-dimensional rolls turned out to be the "preferred" pattern. Subsequent work by Schlüter, Lortz and Busse (1965) used the criterion that the observed motion was the one that was most stable to disturbances. The result was that three-dimensional patterns were unstable and that two-dimensional rolls were again the preferred pattern.

Busse (1967 b) showed that for the case of infinite Prandtl number and rigid boundaries, the two-dimensional solution became unstable to three-dimensional disturbances at a Rayleigh number of 22,600. Busse (1970) recently discussed two of the instability mechanisms which make the two-dimensional flow unstable.

Heat transfer predictions based on single wave number flows were made by Howard (1965), Roberts (1966) and Stewartson (1966), using asymptotic expansions of the governing equations for large Rayleigh number.

Theoretical work designed to predict the salient features of turbulent flow include, in addition to those already mentioned, the works of Elder (1966, 1967), Herring (1966, 1969), Howard (1966),

Kraichnan (1962, 1964 a, 1964 b), Ledoux, Schwarzchild and Spiegel (1961), Spiegel (1962, 1966, 1967) and Townsend (1962).

The prediction of heat transfer, cell size, stability, flow in two dimensions and preferred cell shape has been the goal of many of the papers on Bénard convection. These works include those of Busse (1962, 1967 a), Catton (1966), Chorin (1967), Deardorff (1964, 1965, 1968), Elder (1969), Foster (1969 a), Fromm (1965), Gough (1969), Herring (1963, 1964), Kuo (1961), Kuo and Platzman (1961), Leontiev and Kirdyashkin (1965, 1966), Nakagawa (1960), Newell, Lange and Aucoin (1970), Newell and Whitehead (1969), Platzman (1965), Plows (1968), Saltzman (1962 b), Schneck and Veronis (1967), Segel (1962, 1963, 1964, 1965 a, 1965 b), Somerville (1970 a, 1970 b), Speigel (1970), Stuart (1964), Toomre (1969), Veronis (1966) and Wantland (1970).

Periodically, the field of thermal convection has been surveyed and summarized. The most detailed summary, but one where the analytical work was essentially restricted to linear analysis was the monograph by Chandrasekhar (1961). One of the earliest surveys of the field was performed by Stommel (1947). More recent surveys include those of Brindley (1967), Ostrach (1957, 1964), Segel (1966) and Stuart (1960).

In all the analytical works discussed so far, the assumptions have been made that the materials bounding the fluid layer were perfect conductors of heat; that there were no lateral boundaries; and that the Boussinesq (1903) approximation was permissible. In the approximation all physical properties are assumed constant, except

for the density in the buoyancy force term where the change with temperature is taken into account. In most of the experiments that have been mentioned, attempts have been made to meet these conditions by using small temperature differences across the fluid depth, leading to small property changes; using bounding materials, such as copper and aluminum, that have high thermal conductivities and thermal diffusivities compared to those of the fluids used (the notable exception being mercury); and using small fluid layer depths compared to the lateral dimensions of the fluid chamber.

Concerning the lateral boundary problem, there have been several theoretical papers and some experimental works directed towards predicting and establishing the effect of vertical sidewalls on the initiation of convection, the size of the cellular structure, and the change in the heat transfer once convection is established.

The first attempt at measuring lateral boundary effects was made by Soberman (1958). The most systematic experimental study on the effect of vertical sidewalls on heat transfer was carried out by Catton and Edwards (1967). Other experimental papers that used chambers where the lateral boundaries would have an effect on the motion in the fluid layer are those by Koschmieder (1966), Ostrach and Pneuli (1963) and Sun and Edwards (1970).

Among the important analytical papers concerned with predicting the effect of lateral boundaries are those by Catton (1970), Charlson and Sani (1970), Davis (1967, 1968), Edwards (1969), Edwards and Catton (1969), Liang, Vidal and Acrivos (1969), Pneuli (1964), Pneuli

ıd Iscovici (1968) and Segel (1969). One result indicated by these apers was that as the lateral boundaries were moved together, the :ritical Rayleigh number increased.

If the motion in the fluid layer is in the form of hexagons, a free parameter in the linear analysis is the direction of motion in the center of the cell. It was observed in some of the early experiments that the direction of flow was different for gases and liquids. Graham (1933) was the first to speculate that this fact was due to the opposite variations of viscosity with temperature for the two groups of fluids. This hypothesis was confirmed by von Tippelskirch (1956), who found that the direction of flow in a layer of sulfur changed at about 153 C, the point at which the temperature dependence of viscosity changed.

Analytical works which included studies on the effect of property variation on the initiation of convection, the effect on the preferred planform of cellular motion and the effect on the motion in a hexagonal cell are those by Busse (1962, 1967 a), Davis and Segel (1965, 1968), Jenssen (1963), Liang, Vidal and Acrivos (1969), Palm (1960), Palm and Øiann (1964), Plam, Ellingsen and Gjevik (1967) and Segel and Stuart (1962).

Several experimental studies have appeared recently. One by Liang, et al, was concerned with flow direction. Hoard, Robertson and Acrivos (1970) examined the effect of property variation on the critical Rayleigh number, while the work of Somerscales and Dougherty (1969, 1970) determined the critical Rayleigh number and examined the flow direction problem.

The last area to be considered is the effect of the properties of the bounding materials on the response of a fluid layer to thermal instability. The theoretical papers to date have considered two types of thermal boundary conditions and tested their effect on the initiation of convection. The first boundary condition assumed that the heat transfer from the boundary could be characterized by a film coefficient, while the second assumed that the bounding materials were of finite conductivity with the necessary match of temperature and heat flux at the boundary.

The first paper to consider the boundary effect was that of Sparrow, Goldstein and Jonsson (1964), who utilized the film coefficient approach. More recent papers by Hurle, Jakeman and Pike (1967), Jakeman (1968) and Nield (1968) have assumed finite conductivity materials of various configurations. The main finding of these papers is that the critical Rayleigh number and the critical wave number are decreased when the bounding materials are not perfect conductors.

The writer is aware of only one experimental paper in which the problem of finite conductivity is considered. This is the work of Koschmieder (1969), who confirmed the predicted change in the critical wave number.

In the works cited above, the conditions have been steady or at least quasi-steady. There have, however, been some experiments and analytical studies concerned with the influence of time dependency on the convection phenomena.

In some early experiments reported by Graham (1933), Chandra (1938) and Dassanayake (1950), the latter reported by Sutton (1950), it was found that it was possible to sustain convection at Rayleigh numbers well below the critical value, particularly for thin fluid layers. Graham, although presenting no numerical data, described the motion as being columnar in nature. Sutton, in discussing the results of Chandra and Dassanayake, speculated that the reduced critical Rayleigh number was due to a non-linear temperature profile caused by transient heating, in contrast to the linear profile when the conduction state was steady. He advanced some qualitative arguments to substantiate his hypothesis. [Berg, Acrivos and Boudart (1966) have more recently speculated that the anomalous stability results reported by Chandra and Dassanayake were due to the smoke-gas suspension used for visualization. Berg, et al, theorized that the suspension had sufficiently different properties to cause the irregular results.] In experiments reported by de Graaf and van der Held (1953), critical Rayleigh numbers as low as 1400 were obtained. The authors agreed with Sutton that this lowering could be caused by transient effects.

The first experimental work specifically studying the effect of time dependency on the initiation of convection was that of Soberman (1959). His experiments approximated the case of constant heat flux at the lower surface for an initially isothermal system. He found that rapid heating did indeed affect the critical Rayleigh number. As the heating rate, H, was increased beyond that required to initiate steady-

state convection, the critical Rayleigh number was increased with the data falling on the curve $Ra_{cr} = 90.7 H^{.394}$.

Spangenberg and Rowland (1961) used a layer of water in which the top surface was free to evaporate. They found that the upper surface temperature decreased approximately linearly until convection was initiated. The critical Rayleigh number was 1193 (compared to 1108). Similar experiments were carried out by Foster (1965b) over a wider range of parameters. In some recent work Foster (1969b) used deep layers (greater than 0.05 m) of water and silicone oil to study the length of time required for the initiation of convection for the analogous problem of linearly increasing lower surface temperature.

Several experimental works have been published using time-dependent density gradients which were created by solute concentrations instead of temperature differences. The works are generally analogous to the case of a step increase of the lower surface temperature. These papers include those of Blair and Quinn (1969), Mahler and Schechter (1970) and Plevan and Quinn (1966).

Onat and Grigull (1970) reported results for deep layers of several different working fluids when the lower surface was subjected to constant heat flux.

In a quite different form of heating, that of increasing or decreasing the two surface temperatures at the same constant rates, Krishnamurti (1967, 1968b) reported data on changes in the critical Rayleigh number, critical wave number, planform shape and heat transfer.

The first theoretical paper to include the effect of time-dependency in an explicit way was that of Morton (1957). He assumed that the temperature profile was not far from the linear one and found that for this case the critical Rayleigh number was affected very little.

Goldstein (1959) described an approach in which the point of instability was chosen as that point for which the growths of the velocity and temperature perturbations were stationary. He then chose a particular conduction problem and found that for this case the critical Rayleigh number and critical wave number could be increased over their steady-state values by rapid heating.

Lick (1965) considered the case of rapid heating and examined the growth rates of disturbances when the growth rates were much larger than the time characteristic of changes in the temperature profile. This approximation allowed him to introduce an approximate temperature profile to study the general effects of rapid heating on growths of disturbances as opposed to selecting a few conduction profiles and obtaining more exact results.

Starting from an approach similar to that used by Goldstein (1959), Foster (1965 a) treated the time dependency as an initial-value problem. In the methods developed by Morton, Goldstein and Lick, time had been reduced to a parameter with the result that profile history was not important, while Foster's analysis was dependent on the profile used. He chose two conduction problems, both with the free boundary conditions. The first was the profile generated by a step increase in the temperature at the lower surface, while the second

case was for a linear increase of temperature with time at the lower surface.

Because of Foster's initial-value approach, no true critical point can be defined. However, it is possible to determine the time it takes for a disturbance to grow a certain amount from an initial state. This leads to a correlation between the Rayleigh number, the wave number, and the time for a certain growth to occur. In the "quasi-static" approach where time is only a parameter, the results are independent of Prandtl number. In Foster's method, however, with the time dependency explicitly used, the Prandtl number does appear as a parameter in the results.

Foster (1968) studied the effect of boundary conditions, thermal and kinematic, on critical times in a semi-infinite layer of fluid, subject to either a step change or linear increase with time of the lower surface temperature.

Using methods similar to Foster's, Mahler, Schechter and Wissler (1968) and Mahler and Schechter (1970) looked at the problem of time-dependent density gradients caused by solute concentrations.

Following techniques developed by Lick (1965), Currie (1966, 1967) used the "quasi-static" assumption and a similar approximate profile to examine the growth rates of disturbances in a semi-infinite layer of fluid. He also calculated the stability boundary for the approximate profile. Comparing his work with the experimental results of Soberman (1959) and Spangenberg and Rowland (1961), he found reasonable agreement. One important feature of the stability boundary

was its minimal character, with the lowest critical Rayleigh number of about 1340. The critical wave number, however, only increased with rising heating rates.

Robinson (1967 a) discussed the validity of the "quasi-static" approximation near the point of instability using estimates of the time scales involved. A detailed comparison of the "quasi-static" approximation and the initial-value approach has recently been made by Gresho and Sani (1971), who examined the problem of a step increase in temperature at the lower surface.

Krishnamurti (1967, 1968 a), utilizing perturbation expansion techniques fashioned after Schlüter, Lortz and Busse (1965), calculated the response of a fluid layer when both surface temperatures were increased or decreased at equal and constant rates.

Several analytical papers have examined the effect of modulation on the stability of the fluid layer. Gershuni and Zhukhovitshii (1963) and Venezian (1968, 1969) investigated the stability problem when the surface temperatures were subject to periodic variation. The alternate case of gravity modulation has been examined in the more recent papers of Davis (1970) and Gresho and Sani (1970).

The main thrust of the present work is to provide experimental data that will be useful in predicting the behavior of a fluid layer in response to time-dependent heating. The experimental results will provide insight into the flow mechanisms involved to give the theoretician more information on which to develop his model.

A second aspect of the present work will be developed in the next chapter. It is concerned with the effect of an assumed approximate temperature profile in the fluid on the stability boundary as determined by the method of Goldstein (1959).

III. THEORETICAL WORK

In determining the stability of a fluid layer subject to time-dependent heating, the method first developed by Goldstein (1959) will be followed. For completeness, the basic steps of the analysis will be retraced here.

In making an analytical investigation of the response of a fluid layer to heating from below, shown schematically in Figure 1, the starting point is the equations of motion. In Cartesian notation the equations are

$$\frac{\partial \rho^*}{\partial t^*} + \frac{\partial}{\partial x_j^*}(\rho^* u_j^*) = 0 \tag{1}$$

$$\rho^*\left(\frac{\partial u_i^*}{\partial t^*} + u_j^* \frac{\partial u_i^*}{\partial x_j^*}\right) = -\frac{\partial p^*}{\partial x_i^*} - \rho^* g^* \lambda_i + \frac{\partial}{\partial x_j^*}\left[\mu^*\left(\frac{\partial u_i^*}{\partial x_j^*} + \frac{\partial u_j^*}{\partial x_i^*}\right)\right] + \frac{\partial}{\partial x_i^*}\left[\left(\zeta^* - \frac{2}{3}\mu^*\right)\frac{\partial u_j^*}{\partial x_j^*}\right] \tag{2}$$

$$\rho^* c_p^*\left(\frac{\partial T^*}{\partial t^*} + u_j^* \frac{\partial T^*}{\partial x_j^*}\right) = \frac{\partial}{\partial x_j^*}\left(k^* \frac{\partial T^*}{\partial x_j^*}\right) + T^*\beta^*\left(\frac{\partial p^*}{\partial t^*} + u_j^* \frac{\partial p^*}{\partial x_j^*}\right) + \Phi^* \tag{3}$$

where the starred quantities are dimensional, Φ^* is the dissipation function and $\underline{\lambda} = (0, 0, 1)$. Along with the equations of motion, an equation of state is required in the form of, say, $\rho^* = \rho^*(p^*, T^*)$.

In tackling this problem, the use of the above equations would lead to extremely difficult, if not intractable, analyses. In almost all the work that is done in natural convection a simplified set of equations is used, which is the lowest order approximation to the general equations. The simplified equations make use of the Boussinesq (1903) approximation, which can be stated as follows: (a) all properties are assumed constant, except in the body force term where the variation of density with temperature is taken into account; and (b) the right hand side of the energy equation (3) is neglected, except for the heat flux diffusion term. A detailed derivation of the Boussinesq approximation is given by Mihaljan (1962). Other derivations have been given by Chandrasekhar (1961) [but see the note in the appendix of Thompson and Sogin (1966)], Malkus (1969) and Spiegel and Veronis (1960). The resulting equations of motion and equation of state are given below:

$$\frac{\partial u_i^*}{\partial x_j^*} = 0 \tag{4}$$

$$\frac{\partial u_i^*}{\partial t^*} + u_j^* \frac{\partial u_i^*}{\partial x_j^*} = -\frac{1}{\rho_r^*} \frac{\partial p^*}{\partial x_i^*} - \frac{\rho^*}{\rho_r^*} g^* \lambda_i + \nu^* \frac{\partial^2 u_i^*}{\partial x_j^* \partial x_j^*} \tag{5}$$

$$\frac{\partial T^*}{\partial t^*} + u_j^* \frac{\partial T^*}{\partial x_j^*} = \varkappa^* \frac{\partial^2 T^*}{\partial x_j^* \partial x_j^*} \tag{6}$$

$$\rho^* = \rho_r^* \left[1 - \beta^* \left(T^* - T_r^* \right) \right] \tag{7}$$

Before proceeding with the analysis, the pressure term is redefined as follows:

$$\frac{1}{\rho_r^*} p^* = \Pi^* - g^* x_i^* \lambda_i \tag{8}$$

Substituting (8) into (5), the momentum equation can be written as

$$\frac{\partial u_i^*}{\partial t^*} + u_j^* \frac{\partial u_i^*}{\partial x_j^*} = -\frac{\partial \Pi^*}{\partial x_i^*} + g^* \beta^* \left(T^* - T_r^* \right) \lambda_i + \nu^* \frac{\partial^2 u_i^*}{\partial x_j^* \partial x_j^*} \tag{9}$$

In making the stability analysis a rest state will be assumed to exist: that is, no fluid motion. The response of this rest state to perturbations will then be examined. The "static" state equations are

$$\overline{u}_i^* = 0 \tag{10}$$

$$\frac{\partial \overline{\Pi}^*}{\partial z^*} = g^* \beta^* \left(\overline{T}^* - T_r^* \right) \tag{11}$$

$$\frac{\partial \overline{T}^*}{\partial t^*} = \kappa^* \frac{\partial^2 \overline{T}^*}{\partial z^{*2}} \tag{12}$$

with

$$\overline{T}^*(0^*, t^*) = T_0^*(t^*) + \Delta T^*(t^*)$$

$$\overline{T}^*(d^*, t^*) = T_0^*(t^*)$$

where the bar denotes a rest state quantity.

The following perturbation quantities are introduced, using a prime to denote a perturbed quantity:

$$\begin{aligned} u_i^* &= u_i^{*\prime} \\ \pi^* &= \overline{\Pi}^* + \Pi^{*\prime} \\ T^* &= \overline{T}^* + T^{*\prime} \end{aligned} \tag{13}$$

Substituting the perturbation expressions, (13), into the equations of motion, (4), (9) and (6), and then subtracting out the rest state equations, (10), (11) and (12), the resulting expressions are

$$\frac{\partial u_j^{*\prime}}{\partial x_j^*} = 0 \tag{14}$$

$$\frac{\partial u_i^{*\prime}}{\partial t^*} + u_j^{*\prime} \frac{\partial u_j^{*\prime}}{\partial x_j^*} = -\frac{\partial \Pi^{*\prime}}{\partial x_i^*} + g^* \beta^* T^{*\prime} \lambda_i + \nu^* \frac{\partial^2 u_i^{*\prime}}{\partial x_j^* \partial x_j^*} \tag{15}$$

$$\frac{\partial T^{*\prime}}{\partial t^*} + u_j^{*\prime} \frac{\partial T^{*\prime}}{\partial x_j^*} + w^{*\prime} \frac{\partial \overline{T}^*}{\partial z^*} = \varkappa^* \frac{\partial^2 T^{*\prime}}{\partial x_j^* \partial x_j^*} \tag{16}$$

In examining the stability of the system, the perturbation quantities are assumed to be "infinitesimal". This means that the squares of the quantities are very small in comparison to their absolute values. Thus, the second terms on the left hand side of Eqs. (15) and (16) can be neglected. The linearized equations are

$$\frac{\partial u_j^{*\prime}}{\partial x_j^*} = 0 \tag{17}$$

$$\left(\frac{\partial}{\partial t^*} - \nu^* \frac{\partial^2}{\partial x_j^* \partial x_j^*} \right) u_i^{*\prime} = -\frac{\partial \Pi^{*\prime}}{\partial x_i^*} + g^* \beta^* T^{*\prime} \lambda_1 \tag{18}$$

$$\left(\frac{\partial}{\partial t^*} - \varkappa^* \frac{\partial^2}{\partial x_j^* \partial x_j^*} \right) T^{*\prime} = w^{*\prime} \left(-\frac{\partial \overline{T}^*}{\partial z^*} \right) \tag{19}$$

The momentum equation can be cast into one involving only $w^{*\prime}$ and $T^{*\prime}$ by taking the curl of Equation (18) twice and using the z-omponent of the result. The resulting equations of motion are

$$\left(\frac{\partial}{\partial t^*} - \nu^* \frac{\partial^2}{\partial x_j^* \partial x_j^*}\right) \frac{\partial^2 w^{*\prime}}{\partial x_j^* \partial x_j^*} = g^* \beta^* \left(\frac{\partial^2}{\partial x^{*2}} + \frac{\partial^2}{\partial y^{*2}}\right) T^{*\prime} \tag{20}$$

$$\left(\frac{\partial}{\partial t^*} - \varkappa^* \frac{\partial^2}{\partial x_j^* \partial x_j}\right) T^{*\prime} = w^{*\prime} \left(-\frac{\partial \overline{T}^*}{\partial z^*}\right) \tag{21}$$

Along with the above equations some boundary conditions must be specified. In the problem to be analyzed the bounding surfaces are assumed to be of infinite thermal conductivity and diffusivity. This means that any small perturbation in temperature would be instantaneously dispersed into the bounding material. This leads to the thermal boundary condition that

$$T^{*\prime} = 0, \text{ at the boundary.}$$

For the velocity components, either the free (stress free) or the rigid (no slip) boundary condition is used in analytical work. In both cases the boundary is assumed to be impermeable and nondeformable. Thus,

$$w^{*\prime} = 0, \text{ at the boundary.}$$

The free boundary is one with zero shear, that is,

$$\frac{\partial u^{*\prime}}{\partial z^*} = \frac{\partial v^{*\prime}}{\partial z^*} = 0.$$

Examining the continuity equation (17) shows that this zero shear condition can be converted into the following boundary condition:

$$\frac{\partial^2 w^{*\prime}}{\partial z^{*2}} = 0, \text{ at the free boundary.}$$

For the rigid boundary there is zero slip, that is, $u^{*\prime} = v^{*\prime} = 0$. Again,

from the continuity equation the boundary condition in terms of $w^{*\prime}$ is

$$\frac{\partial w^{*\prime}}{\partial z^*} = 0, \text{ at the rigid boundary.}$$

Many of the analyses that have been carried out, particularly the more difficult ones, have used the free-free case because the resulting solutions are much simpler and the results should bear qualitative similarity to the usual experimental setup of rigid-rigid boundaries. In the present analysis, however, the rigid-rigid case will be examined. Thus, in summary, the boundary conditions to be used are

$$w^{*\prime} = \frac{\partial w^{*\prime}}{\partial z^*} = T^{*\prime} = 0 \quad \text{at} \quad z^* = 0, d^* \tag{22}$$

Equations (20) and (21), along with the boundary conditions (22), have a solution in which the horizontal dependence can be characterized by a single wave number. That is, let

$$\begin{aligned} w^{*\prime}(x^*, y^*, z^*, t^*) &= f(x^*, y^*)w^*(z^*, t^*) \\ T^{*\prime}(x^*, y^*, z^*, t^*) &= f(x^*, y^*)\theta^*(z^*, t^*) \end{aligned} \tag{23}$$

where

$$\left(\frac{\partial^2}{\partial x^{*2}} + \frac{\partial^2}{\partial y^{*2}}\right) f = -a^{*2} f$$

Substituting (23) into (20) and (21) yields

$$\begin{aligned} \left[\nu^*\left(\frac{\partial^2}{\partial z^{*2}} - a^{*2}\right) - \frac{\partial}{\partial t^*}\right]\left(\frac{\partial^2}{\partial z^{*2}} - a^{*2}\right)w^* &= g^*\beta^* a^{*2}\theta^* \\ \left[\kappa^*\left(\frac{\partial^2}{\partial z^{*2}} - a^{*2}\right) - \frac{\partial}{\partial t^*}\right]\theta^* &= -w^*\left(-\frac{\partial \overline{T}^*}{\partial z^*}\right) \end{aligned} \tag{24}$$

For convenience cast (24) into dimensionless form by using the following transformations:

$$z^* = d^* z \quad , \quad a^* = \frac{1}{d^*} a \quad , \quad t^* = \frac{d^{*2}}{\kappa^*} t \quad , \quad \omega^* = \frac{\kappa^*}{d^*} \omega \tag{25}$$

$$\theta^* = \frac{\kappa^* \nu^*}{g^* \beta^* d^{*3}} \quad , \quad \overline{T}^* = \Delta\Theta^* \overline{T}$$

where $\Delta\Theta^*$ is some "temperature" characteristic of the given conduction problem. Using (25), Equations (24) can be written in dimensionless form as

$$\left[\left(\frac{\partial^2}{\partial z^2} - a^2\right) - \frac{1}{Pr} \frac{\partial}{\partial t}\right]\left(\frac{\partial^2}{\partial z^2} - a^2\right)\omega = a^2 \theta$$

$$\left[\left(\frac{\partial^2}{\partial z^2} - a^2\right) - \frac{\partial}{\partial t}\right]\theta = -\omega R\left(-\frac{\partial \overline{T}}{\partial z}\right) \tag{26}$$

where R, a characteristic Rayleigh number, is given by

$$R = \frac{g^* \beta^* d^{*3} \Delta\Theta^*}{\kappa^* \nu^*}$$

The thermal and kinematic boundary conditions are

$$\omega = \frac{\partial \omega}{\partial z} = \theta = 0 \quad \text{at} \quad z = 0, 1 \tag{27}$$

Before proceeding with the transient analysis, it should be pointed out that Equations (26) are just the steady-state perturbation equations when $\Delta\Theta^*$ is chosen as the actual temperature difference ΔT^* and $-\partial\overline{T}/\partial z$ is replaced by its steady-state value of one.

Equations (26) form the starting point for three different approaches to the problem of transient heating. Two use different

methods of attack, but are essentially the same, while the third approach starts with an essential difference in philosophy.

The first method to be discussed was developed by Foster (1965 a). The main feature of this approach is the treatment of the equations as an initial value problem. For a given conduction profile [given $-\partial\overline{T}/\partial z\,(z,t)$] and with a specified initial disturbance $\omega(z,0)$ and $\theta(z,0)$, the time behavior of ω and θ is examined. As was pointed out in the previous chapter, this approach leads to the time required for the initial disturbance to reach a certain magnitude. The effects of the form and rate of heating and fluid properties (the Prandtl number) can be examined. This method seems the most appropriate one in tackling transient convection in the Bénard problem. Difficulty arises in comparing the results with experiments because the linear analysis does not yield the size of the disturbance which would be first noticed by an observer, only the size relative to some initial, "infinitesimal" perturbation. However, curves of constant growth rates can be plotted; and a comparison can be made with the experimental data. A second technical difficulty arises from the need to specify an initial disturbance. What is the best choice? Foster, after some trial and error, chose "white noise" distribution as the one that generally yielded the fastest growing disturbances and the one that seemed the most physically realistic.

The remaining two methods examine the behavior of the fluid layer, but time only appears parametrically in the calculations. The first of the two, the "quasi-static" approximation, was developed by

Lick (1965) and Currie (1966, 1967). The basic assumption is that the growth rates of the disturbances in the rest state are very large in comparison to the times characteristic of changes in the temperature profile. Making an asymptotic expansion, such as that performed by Lick, it is possible to show that to a first approximation, time derivatives of ω and θ do not appear in (26). Thus, time only appears parametrically in the term $-\partial\overline{T}/\partial z$. Using this technique, the time and space variables can be separated as in the steady-state case. This separation is not strictly possible in (26). If the stability boundary is to be determined, as was done by Currie, the growth rate is set equal to zero; and the resulting eigenvalue equation is solved for the Rayleigh number. This procedure, however, is in direct violation of the "quasi-static" assumption on which the method is based. The hope is that the growth rate will increase rapidly enough so that the results will at least be qualitatively similar to the actual case.

The last method, and the one which will be used in the present analysis, was developed by Goldstein (1959). The key to this method is the definition of criticality. Initially, and for a certain time thereafter, any disturbance will decay because the temperature profile will be stable. However, a time will be reached when the disturbance becomes unstable and will start growing with time. Somewhere between these two conditions is a stationary state for the disturbance. This behavior can be seen in the plots in Foster's work (1965 a). In the definition of the stationary state used by Goldstein, both the

temperature and velocity perturbations pass through the stationary state at the same time. That is,

$$\frac{\partial \omega}{\partial t} = \frac{\partial \theta}{\partial t} = 0, \text{ at the critical time.} \tag{28}$$

Following Goldstein, Galerkin's method will be used to solve Equations (26) approximately. A series expansion with time-dependent coefficients is made for $\omega(z, t)$ and $\theta(z, t)$ in the form

$$\begin{aligned} \omega(z, t) &= \sum_{n=1}^{\infty} \omega_n(t) W_n(z) \\ \theta(z, t) &= \sum_{n=1}^{\infty} \theta_n(t)\, \Theta_n(z) \end{aligned} \tag{29}$$

The $\Theta_n(z)$ and $W_n(z)$ are chosen to satisfy the boundary conditions (27). Several sets of trial functions have been developed. Two of the more commonly used ones were first proposed by Reid and Harris (1958). Another set has been recently used by Gresho and Sani (1971). In the present analysis a Fourier series will be used similar to that developed by Reid and Harris. Following Goldstein, the highest order spatial derivatives of ω and θ are expanded in sine series. Thus,

$$\begin{aligned} \left(\frac{d^2}{dz^2} - a^2\right)\Theta_n &= -(n^2\pi^2 + a^2) \sin n\pi z \\ \left(\frac{d^2}{dz^2} - a^2\right)^2 W_n &= (n^2\pi^2 \partial\, a^2)^2 \sin n\pi z \end{aligned} \tag{30}$$

Integrating Equations (30), the general solutions can be written as

$$\Theta_n(z) = \sin n\pi z + a_n e^{az} + b_n e^{-az}$$

$$W_n(z) = \sin n\pi z + c_n[(1-z)\sinh az + z\sinh a(1-z)] \qquad (31)$$
$$+ d_n[(1-z)\sinh az - z\sinh a(1-z)]$$

Applying the boundary conditions, the coefficients are

$$a_n = b_n = 0$$

$$c_n = -\frac{n\pi[1-(-1)^n]}{2(\sinh a + a)} \quad , \quad d_n = \frac{n\pi[1+(-1)^n]}{2(\sinh a - a)} \qquad (32)$$

In summary, the Fourier expansion terms are

$$\Theta_n(z) = \sin n\pi z$$

$$W_n(z) = \sin n\pi z - \frac{n\pi[1-(-1)^n]}{2(\sinh a + a)}[(1-z)\sinh az + z\sinh a(1-z)] \qquad (33)$$
$$+ \frac{n\pi[1+(-1)^n]}{2(\sinh a - a)}[(1-z)\sinh az - z\sinh a(1-z)]$$

Substituting the expansions (29) into the governing equations (26), the result is

$$\sum_{n=1}^{\infty}(n^2\pi^2 + a^2)^2 \omega_n \sin n\pi z - \frac{1}{Pr}\sum_{n=1}^{\infty}\dot{\omega}_r\left(\frac{d^2}{dz^2} - a^2\right)W_n = a^2\sum_{n=1}^{\infty}\theta_n \sin n\pi z$$

$$\sum_{n=1}^{\infty}(n^2\pi^2 + a^2)\theta_n \sin n\pi z + \sum_{n=1}^{\infty}\dot{\theta}_r \sin n\pi z = R\left(-\frac{\partial\overline{T}}{\partial z}\right)\sum_{n=1}^{\infty}\omega_n W_n \qquad (34)$$

If (34) is multiplied by $\sin r\pi z$ and the resulting expressions integrated over the depth of the fluid layer, the equations become

$$\frac{1}{2}(r^2\pi^2 + a^2)^2 \omega_r + \frac{(r^2\pi^2 + a^2)}{Pr}\sum_{n=1}^{\infty}\dot{\omega}_n K_{rn} = \frac{1}{2}a^2\theta_r \qquad r = 1, 2, \cdots \qquad (35a)$$

$$\frac{1}{2}(r^2\pi^2 + a^2)\theta_r + \frac{1}{2}\dot{\theta}_r = R\sum_{n=1}^{\infty} \omega_n E_{rn} \qquad r = 1, 2, \cdots \tag{35b}$$

where

$$\int_0^1 \sin r\pi z \sin n\pi z \, dz = \frac{1}{2}\delta_{rn}$$

$$K_{rn} \equiv \int_0^1 \sin r\pi z \, W_n(z) \, dz = -\frac{1}{(r^2\pi^2 + a^2)} \int_0^1 \sin r\pi z \left(\frac{d^2}{dz^2} - a^2\right) W_n(z) \, dz \tag{36}$$

$$E_{rn}(t) \equiv \int_0^1 \left(-\frac{\partial \overline{T}}{\partial z}(z, t)\right) \sin r\pi z \, W_n(z) \, dz$$

From Goldstein's definition of criticality (28), the time-dependent coefficients must satisfy the following conditions:

$$\dot{\omega}_n(t) = \dot{\theta}_n(t) = 0 \quad \text{at} \quad t = t_{cr} \qquad n = 1, 2, \cdots \tag{37}$$

The criticality condition (37) requires that

$$a^2\theta_r = (r^2\pi^2 + a^2)^2 \omega_r$$

$$\text{at} \quad t = t_{cr} \tag{38}$$

$$\frac{1}{2}(r^2\pi^2 + a^2)\theta_r = R\sum_{n=1}^{\infty} \omega_n E_{rn}$$

Eliminating $\theta_n(t_{cr})$ from Equations (38) and rearranging slightly, the equations at the critical time can be written as

$$\sum_{n=1}^{\infty} \omega_n \left[\frac{2a^2 E_{rn}}{(r^2\pi^2 + a^2)^3} - \frac{1}{R}\delta_{rn}\right] = 0 \quad \text{at} \quad t = t_{cr} \qquad r = 1, 2, \cdots \tag{39}$$

For a non-trivial solution of (39), the coefficients of the $\omega_n(t_{cr})$ must satisfy the following condition:

$$\det\left|\frac{2a^2 E_{rn}}{(r^2\pi^2 + a^2)^3} - \frac{1}{R}\delta_{rn}\right| = 0 \quad \text{at} \quad t = t_{cr} \tag{40}$$

Equation (40) is the required stability condition, where the effect of time-dependency is contained in $E_{rn}(t_{cr})$.

In principle, for a given conduction profile, a stability boundary can be obtained for some characteristic Rayleigh number as a function of, say, the critical time. However, because only the profile at $t = t_{cr}$ is of importance in Equation (40), it would be possible to construct an approximate profile, parametric in time, to determine the basic qualitative features of the stability boundary.

The first problem is to determine what parameter "best" characterizes a large group of conduction profiles. The one used by Lick (1965) and Currie (1966, 1967) is the "thermal thickness", ϵ, which is defined as

$$\epsilon(t) \equiv \frac{2}{\overline{T}(0,t) - \overline{T}(1,t)} \int_0^1 [\overline{T}(z,t) - \overline{T}(1,t)]\, dz \tag{41}$$

The thermal thickness is a measure of the energy content of the fluid relative to the steady-state case and, hence, indicative of the rate of heating. Fast heating rates imply that the heat has not had time to penetrate very far, that the temperature profile is highly non-linear and, correspondingly, that ϵ is small. Slow heating rates imply nearly linear temperature profiles; and, thus, the thermal thickness approaches one.

An alternate parameter that could be used to characterize the conduction problem is the heat flux at the lower surface, H, which is

defined as

$$H(t) \equiv \frac{g^* \beta^* d^{*3}}{\kappa^* \nu^*} \left(-d^* \frac{\partial \overline{T}^*}{\partial z^*} (0, t^*) \right)$$
$$= R \left(-\frac{\partial \overline{T}}{\partial z} (0, t) \right) \qquad (42)$$

where R is the characteristic Rayleigh number. This heat flux parameter should be important because, for the types of heating considered in the present analysis, the profile is the steepest at the lower boundary and would, hence, be the region where the fluid is least stable. Large values of the heat flux, H, would correspond to rapid heating, while steady-state conduction heating would correspond to H = Ra.

Using an approximate temperature profile that depends in some manner on the thermal thickness or heat flux at the lower surface, a stability boundary of the Rayleigh number as a function of the thickness or heat flux can be determined from Equation (40). To make use of the stability boundary for an actual conduction problem, the Rayleigh number, Ra(t), and the thermal thickness, $\epsilon(t)$, or the heat flux at the lower surface, H(t), are determined as a function of time for the actual case. The point of intersection of this functional relationship with the stability boundary would determine the critical time, t_{cr}. By varying the characteristic Rayleigh number, R, of the problem, the dependence of the critical time on the critical Rayleigh number can be determined. If the thermal thickness is used as the characteristic measure, the intersection of the Rayleigh number, Ra(t), as determined by the conduction problem, with the stability boundary corresponds to a matching

of the energy contents of the fluid layers. If the heat flux at the lower surface is used, the match is between the slopes of the temperature profiles at the lower boundary. The use of the heat flux gives a detailed match of the two profiles, while use of the thermal thickness requires an average match.

The next problem is the selection of an approximate profile to carry out the necessary calculations. The only profile that has been developed to date is the "two-step" or "kink" profile (see Figure 2), which was used by Lick and later by Currie. The profile consists of two straight line segments. Lick assumed the slope of the upper segment was a small fraction of the lower segment, which covered the region of large temperature change. For his calculation Lick assumed the upper slope was one tenth of the lower slope. Currie used the particular case of zero slope for the upper segment. Following Currie, the approximate temperature profile is given by

$$\overline{T}_a(z; t_{cr}) = \begin{cases} 1 - \frac{z}{\delta} & 0 \le z \le \delta \\ 0 & \delta \le z \le 1 \end{cases}$$

$$\epsilon(t_{cr}) = \delta \tag{43}$$

$$-\frac{d\overline{T}_a}{dz}(0; t_{cr}) = \frac{H(t_{cr})}{Ra_{cr}} = \frac{1}{\delta}$$

where the characteristic temperature difference is chosen as

$$\Delta\Theta^* \equiv T^*(0, t^*_{cr}) - T^*(d^*, t^*_{cr})$$

Using this profile and the "quasi-static" approximation, Currie calculated the stability boundary of the critical Rayleigh number as a

function of the critical thermal thickness. Utilizing the method of Goldstein, similar calculations were conducted with the two-step profile, details of which are contained in Appendix B. The results of the calculations are shown in Figures 3, 4, 5 and 6.

The results of the critical Rayleigh number versus the thermal thickness (Figure 3) or versus the heat flux at the lower surface (Figure 4) have a stationary character. The minimum critical Rayleigh number is 1350. This minimum occurs at a thermal thickness of 0.69 and a heat flux of 1950. The results of the critical wave number, shown in Figure 5 as a function of the thermal thickness and as a function of the heat flux in Figure 6, do not show a minimal character. In the limit of zero δ, corresponding to an infinite rate of heating or an infinitely deep layer of fluid, the calculations indicate that the critical Rayleigh number and the critical wave number satisfy the relationships $Ra_{cr}\delta^3 = 32$ and $a_{cr} = 13$. Similar results were found by Currie.

The existence of a minimum critical Rayleigh number indicates that for a certain range of heating rates it would be possible to initiate convection at temperature differences smaller than that required in the steady-state case. As seen in Figure 4, the range of heating rates over which lower than steady-state Rayleigh numbers can be obtained, according to this analysis, is not very large, with the bulk of the results showing Rayleigh numbers larger than the classical, steady-state value of 1708.

A conceptual difficulty with the two-step profile is the discontinuity at $z = \delta$. This, along with a desire to examine the effect of

profile shape on the stability boundary, led to the development of an alternate approximate profile which is shown below:

$$\overline{T}_a(z;t_{cr}) = (1-z)e^{-\alpha z}$$

$$\epsilon(t_{cr}) = \frac{2}{\alpha}\left(1-\frac{1-e^{-\alpha}}{\alpha}\right) \tag{44}$$

$$-\frac{d\overline{T}_a}{dz}(0;t_{cr}) = \frac{H(t_{cr})}{Ra_{cr}} = 1+\alpha$$

with

$$\Delta\Theta^* = T^*(0, t^*_{cr}) - T^*(d^*, t^*_{cr})$$

The "exponential" profile, seen in Figure 2, consists of the steady-state linear profile multiplied by an exponential weighting function. As seen in Equations (44), the weighting factor, α, can be related to the thermal thickness and the heat flux at the lower surface, with $\alpha = 0$ corresponding to $\epsilon = 1$ and $H = Ra$, while $\alpha = \infty$ is the same as $\epsilon = 0$ and $H = \infty$.

Details of the calculations using the exponential profile are contained in Appendix B. The critical Rayleigh number is shown as a function of the thermal thickness in Figure 3 and as a function of the heat flux at the lower surface in Figure 4. The critical wave number is shown as a function of the thickness and heat flux in Figures 5 and 6 respectively.

As was true with the two-step profile results, the critical wave number is a monotonically increasing function with decreasing thermal thickness and increasing lower surface heat flux. However, this

function of the critical Rayleigh number does not have a stationary character, which is in contrast to the kink profile case. The critical Rayleigh number simply increases monotonically with decreasing thermal thickness and increasing heat flux.

For the exponential profile the limiting case of infinite α yields the results that the critical Rayleigh number $Ra_{cr}/\alpha^3 = 1.3$ and that the critical wave number $a_{cr} = 13$. The limiting results for infinite heating or infinite depth for the exponential and two-step profiles allows a comparison to be made of the two cases. If the thermal thickness is the matching quantity, the critical Rayleigh number predicted from the two-step profile is three times the value obtained from the exponential profile in the limit of infinite heating or infinite depth. If the heat flux at the lower surface is used as the significant parameter, the ratio of the critical Rayleigh numbers for the two profiles is twenty-four.

A comparison of the results for the two-step and exponential profiles shows that the predicted stability boundary is sensitive to the chosen profile. The prediction of critical Rayleigh numbers with values smaller than the steady-state value of 1708 is dependent on the shape of the temperature profile used in the calculations. Nevertheless, the qualitative trends of the two cases are very similar. Over most of the heating range the critical Rayleigh number is larger than 1708. Also, the results for the two profiles indicate that rapid heating will excite larger wave number (smaller wavelength) disturbances to instability. Thus, except for a possibly small range of heating rates, the effect of time-dependent heating is to raise the temperature

difference at which instability will occur and to decrease the size of motion that will be seen once the disturbance has grown sufficiently to be observed.

IV. EXPERIMENTAL APPARATUS

A. Chamber Design

The experiments performed as part of this research were designed to determine and catalogue the effects of time-dependent heating on Bénard convection. Important information to be determined included the temperatures of the two bounding surfaces, the amount of heat conducted through the lower boundary into the fluid layer, an optical determination of the onset of convection and the patterns of motion once convection was initiated.

A wide range of heating rates were to be examined. To maximize the effectiveness of any heater system used, the heating surface would have to be as close as possible to the lower surface of the fluid layer and the surroundings of the fluid layer should have relatively poor thermal characteristics. The chamber design would have to incorporate some independent means of measuring the heat flux to determine that fraction of the total heat generated that was transferred to the fluid.

It was decided to make the optical studies using the shadowgraph technique from above, instead of the side. This required the upper boundary of the fluid layer to be a transparent material.

Using these considerations, the final chamber design is shown in cross-section in Figure 7. The bottom of the box was formed by a piece of 0.2318 m (9 1/8") square by 0.0381 m (1 1/2") thick piece of a laminated phenolic plastic. Lying on this base was

a 0.2286 m (9") square by 0.00635 m (1/4") thick piece of No. 7740 Pyrex glass, manufactured by the Corning Glass Works. The upper surface of the glass had a metallic oxide coating bonded to it. This coating was used as the heater. The upper surface of the fluid layer was formed by an identical piece of Pyrex glass in which the lower surface had the special coating.

The fluid layer was formed by three phenolic plastic posts, 0.0127 m (1/2") in diameter. They rested on the lower glass surface and were the support for the upper surface. Three heights of post were used in the experiments, 0.00635 m (1/4"), 0.01270 m (1/2") and 0.01905 m (3/4"). To minimize the effect of the posts on the flow patterns, a guard ring of phenolic plastic was inserted between the posts and the rest of the fluid layer. The ring was slightly smaller than the posts so that the upper glass surface did not rest on it. The ring was approximately 0.0032 m (1/8") thick with inside dimensions of 0.1968 m (7 3/4") square.

Sidewalls for the chamber were made of 0.0127 m (1/2") thick pieces of phenolic plastic, which were epoxied to the sides of the base piece. The chamber was supported by three cap screws that were attached to the chamber base. The screws were used as leveling devices for the apparatus. Further insulation was provided by an insulating blanket of styrofoam. For the sidewalls a 0.0508 m (2") layer was used, while the bottom insulation was formed by a dead air space approximately 0.00635 (1/4") thick followed by a 0.0254 m (1") thick piece of styrofoam.

Heating of the fluid layer was obtained by running a direct current through the metallic oxide coating on the lower glass plate. The current was brought to the plate by two flexible mesh wires, which were mechanically clamped to adjacent corners of the glass. From these wires the current was evenly distributed by two "busbars" consisting of 0.00953 m (3/8") strips of Silver Print, a paint used to patch printed circuit boards. The strips were run from the wires along opposite sides of the surface. Similar electrical connections were made on the coating of the upper glass plate.

To measure the net amount of heat being transferred through the fluid, a heat flux meter, Model CCH-1R, manufactured by Hy-Cal Engineering, was located in a depression in the phenolic base just below the glass surface. The meter was situated in the middle of the lower right quadrant of the chamber as seen in the photographs of motion.

The temperatures of the bounding surfaces were determined by measuring the change of resistance of the two glass coatings. The change in resistance was converted to a change in temperature by a calibration constant that had been determined from constant temperature bath measurements.

Because of the intimate contact with electrical currents, the choice of fluids was limited to electrical insulators. Even distilled water would have required the use of some sort of electrical insulation. Also, because the shadowgraph technique was selected for the optical studies, a fluid was desired which had a large change in its index of

refraction with temperature. This ruled out gases and narrowed the consideration to organic liquids, particularly oils. The last criteria, a desire to use a fluid which had a minimum change of physical properties with temperature, narrowed the choice to silicone oil. The oil was obtained from Dow Corning.

To increase the range of effective heating rates without changing the physical apparatus drastically, three different viscosity grades of the 200 series oils were chosen. The grades were 5 centistoke (cs), batch AA8198; 100 cs, batch AA8141; 500 cs, batch AA8150. The other physical properties of the oil remained essentially constant from viscosity grade to viscosity grade.

B. Controls and Instrumentation

The change in resistance with temperature of the two glass coatings was small. The values were 0.00575 $\Omega/^{\circ}K$ and 0.00436 $\Omega/^{\circ}K$ for the upper and lower surfaces, respectively. To measure these changes, the plates were made to form legs of separate Wheatstone bridges. The remaining legs of the bridges were constructed from Manganin wire, which possesses an extremely small change of resistance with temperature coefficient. Each leg was approximately one meter in length to ensure a large heat transfer area to dissipate the Joule heating. The wire was coiled to reduce the effective length of the bridge leg and allow the wires to be immersed in a bath of transformer oil. These precautions were taken to minimize resistance changes in the bridge legs, thus ensuring accurate measurements of the change of resistance for the two plates. Further details of the bridge setup are given in Appendix D.

For the upper plate a small voltage, 1.000 V, was maintained across the bridge using a Model VR-607 Secondary Standard Voltage Reference Source, manufactured by Epsco. The voltage imbalance of the bridge was measured using a Hewlett-Packard Model 412A DC Vacuum Tube Voltmeter. The voltage source for the lower plate was a 125 V direct current line available in the laboratory. Voltage across the bridge was adjusted by use of three rheostats of maximum values 100 Ω, 25 Ω and 25Ω. To obtain initial imbalance readings, a small voltage of approximately 0.8 V was used across the bridge. This low voltage was obtained by adding two 1000 Ω resistors in series with

the rheostats. The voltage across the bridge was measured directly on a Brush Mark 220 Recorder, manufactured by Clevite. The voltage imbalance of the lower surface bridge was measured with a Hewlett-Packard Model 425A DC Micro Volt-Ammeter. Both the upper and lower surface bridge imbalances were amplified in the Hewlett-Packard instruments before being recorded on the Brush recorders. The heat flux meter signal was measured on a Hewlett-Packard Model 412A DC Vacuum Tube Voltmeter. This signal was also amplified before being recorded by the Brush.

Time was measured on the recorders by a built in timing device that would automatically make tick marks on the sides of the recording paper at one second intervals. An electric clock was used to keep track of the time at which photographs were taken and the point at which motion started.

Ambient temperature was measured with a thermometer that was located near the apparatus.

C. Optical System

As mentioned previously, the flow was made visible by means of shadowgraph technique. A schematic layout of the system is shown in Figure 8.

The light source was an Osram 100 W mercury vapor arc lamp. This was enclosed in a protective housing with the light passing through a small hole approximately 0.006 m in diameter. From the source the light was reflected from a front surface mirror located above the chamber through the fluid layer to a mirror which was located on the backside of the lower glass surface. From this mirror the light was again reflected through the fluid layer to the front surface mirror. Because the light source was slightly off axis, an image was formed on a screen of flashed opal glass located adjacent to the lamp.

No attempt was made to collimate the light because of the large field of view desired. This resulted in a slight distortion of the vertical length scale as is seen in Figure 9, which is a drawing of the chamber with 0.02 m marks indicated to show the scale changes. All measurements taken from the photographic results took into account this distortion.

The shadowgraph method detects point to point differences in the second derivative of the index of refraction. The light intensity at a certain point on the screen will be inversely proportional to the curvature of the index of refraction at the corresponding point in the fluid layer. The warm bands that appear in the flow patterns would be regions of larger curvature than the surrounding fluid and, hence,

would appear as dark regions on the screen. The brighter regions would represent relatively cooler sections of the fluid layer.

A good review of the shadowgraph technique, as well as the schlieren and interferometer methods, is given by Holder and North (1963).

The photographs shown in this thesis were taken with a Model 360 Polaroid Land Pack camera, which was located on the far side of the opal glass. Because of the low intensity of the light at the screen, 3000 speed Polaroid film was used with an approximately two-second time exposure.

V. EXPERIMENTAL PROCEDURE

A. Initial Preparation

When starting a series of experimental runs with a different oil, the apparatus was completely disassembled. The phenolic box was washed with benzene to remove any traces of the previous oil. The glass surfaces, excluding the mirror and busbars, were also washed with benzene. The entire apparatus was then given a light covering of the new grade of oil to be used. This coating was wiped off, and the unit was reassembled with the new oil as the working fluid. The heat flux meter and lower glass surface were replaced. Then the posts and guard ring, which had also been cleaned, were inserted. The oil was poured in the chamber to a level slightly higher than the posts. The upper glass surface was then lowered into place. Finally, any excess oil was cleaned from the upper surface using benzene.

When changing from one depth to another for the same oil, the upper surface was lifted, and the phenolic posts and guard ring were replaced. Additional oil was added as needed to reach the desired level, and benzene was used for any cleanup work. Periodically, when the upper glass plate would become oily and dusty due to evaporation of the silicone oil from the chamber, the surface was again cleaned with benzene.

To ensure the fact that any disturbances had dissipated due to the changing of the oil and/or depth, a day was allowed to pass before

the new experimental series was started. The viscous time constant based on the inside chamber dimension and the 5 centistoke oil (the worst case) was about 1×10^4 seconds, while the thermal time constant based on the thickness of the phenolic base and using the thermal properties of the plastic was about 2×10^4 seconds. A twenty four hour period would thus correspond to about four to eight characteristic times.

The final check that was made before a new experimental series was started, was a measurement of the voltage imbalance of the two bridges. Sometimes an imbalance would occur because of changes in contact resistance during assembly of the apparatus. To compensate for this effect, the resistance of the remaining legs of the bridge would be adjusted accordingly.

B. Test Procedure

Approximately one half hour before the experiment was to start, the upper plate voltage source, the Hewlett-Packard instruments and the Brush recorders were turned on to allow the units to warm up. At this time the ambient temperature was recorded from the thermometer located next to the apparatus. This reading was needed to determine the values of the properties to be used in the calculations.

Immediately preceding the start of the experimental run, the light source was turned on; and if photographs were to be taken, the camera was set up. Initial voltage imbalance and voltage drops were noted on the Brush recorders from the readings taken from the Hewlett-Packard instruments.

The experimental run was started with the closing of a switch in the lower plate electrical circuit. At the same time the electric clock was started. The time of starting was indicated in the log book, where pertinent information about the run, including the ambient temperature, external resistance for the lower surface and starting time of the run, was kept. When the shadowgraph image indicated that the onset of motion had occurred, the time of onset was noted in the log. Whenever any pictures were taken, the time at which they occurred was also recorded.

At the end of the run, which lasted between 500 s and 2000 s, the current was shut off. Approximately twenty-four hours were allowed to pass before the next run was undertaken. This was to allow the motion and the heat that had soaked into the apparatus to dissipate.

Part of a typical chart record is shown in Figure 10, where ΔV_L is the lower surface imbalance, V_L is the total voltage drop across the lower surface bridge, ΔV_U is the upper surface imbalance and HFM is the heat flux meter signal. The tick marks on the sides of the charts are at one-second intervals.

C. Data Reduction

With the completion of a run, the major task of data reduction was the conversion of the voltage information on the chart recordings to temperature differences and heat fluxes. The first stage of data reduction was accomplished with the use of a Benson & Lehner digitizing analyzer. The chart record was taped to a table (a 099D Data-reducer), and a cross hair system was located on the ink trace. From a preset origin the machine (a Type 282E Telecordex) converted the position to units of two-hundreths of an inch. These coordinates, the x-axis being the time line and the y-axis the voltage reading, were then transferred to an IBM 029 Keypunch machine through a footpedal device. Data were taken for the two voltage imbalances and the heat flux meter signal at ten-second intervals for the length of the run. The time interval was a compromise between a desire to know as accurately as possible the voltages as a function of time and a need to keep the amount of data to manageable levels. For a typical run of 1000 s, three hundred data points were needed.

Digital values of the instrument signals that had been noted on the chart recordings were determined. These values were used to evaluate the correction factors that should be applied to the data. The total voltage across the lower surface bridge was also noted. Because of the small change in resistances involved in the run, the experiments were performed at constant voltage. Thus, a record of the trace of the voltage drop was not needed. Actually, this reading was only used as a check. More accurate readings were obtained from a set of

calibration experiments, where a Hewlett-Packard instrument was used to determine the voltage drop for the same external resistance.

The punched cards, with the necessary scale factors and any needed corrections, were submitted with a computer program to convert the voltage information to temperatures and heat fluxes as well as the total heat generated at the lower surface due to Joule heating. All data analysis was done on an IBM 360/75.

The conduction problem of constant heat generation at a surface in a semi-infinite composite solid had previously been solved for the various combinations of depths and fluids that had been used in the experiments. Details of the calculations are given in Appendix C. This result was subtracted from the experimental values to indicate more clearly the onset of motion. The results were then normalized by the total rate of heat generation to make the data uniform. These values were plotted and punched onto new cards. The plot served as a very useful indication of when motion occurred.

The new cards, with any needed correction factors, were included in a second computer program which first smoothed the data using a fifith order orthogonal polynomial fit by the least squares technique. A comparison between the normalized temperatures and heat fluxes, along with the smoothed curves, is shown in Figure 11. The vertical axis functions are DTL, the normalized difference of the lower surface temperature and the conduction result; DTU, the normalized temperature difference for the upper surface; and QHFM, the normalized difference between the actual heat flux meter reading

and the conduction result.

Using the simple forward step finite difference scheme, the various desired quantities were calculated as a function of time. Stability of the scheme required a one-second time interval to be used. This time step was obtained by a quadratic interpolation of the temperature and heat flux data. Two separate calculations were carried out simultaneously. The first was for the conduction problem of the lower glass plate. For this problem the given boundary conditions were the temperature of the glass surface at the fluid layer boundary and the heat flux passing through the lower glass surface. For the second problem, the heat transfer through the fluid layer, it was assumed that the layer was always conducting. Thus, in comparing the results of the two calculations, which should be identical when the fluid layer is conducting, any deviations in the results would indicate the presence of motion. To carry out the fluid layer conduction problem, the temperatures of the two bounding glass surfaces were used as boundary conditions.

After adding the analytical conduction profile that had been subtracted from the results in the first computer program, the various quantities were listed as a function of time. The parameters included the dimensionless time, the average temperature between the upper and lower surface (the temperature at which the properties were evaluated), the temperature difference, the thermal thickness, the Rayleigh numbers based on depth and thermal thickness, the dimensionless total heat generation rate, the dimensionless heat flux through the

lower surface into the fluid layer and the Prandtl number. To help determine the onset of motion, the ratio of the heat flux through the lower surface determined by an assumed conducting fluid layer to that determined from the glass conduction problem was also listed. These data were then used to determine the values of the various quantities at the onset of motion as well as the transient heat transfer results which are presented in the subsequent chapters.

A discussion of the physical properties used in the calculations is contained in Appendix E.

D. Test Conditions

Seventy-five experimental runs, comprising eight different series, were performed using three grades of silicone oil and three fluid layer depths. Each run was carried out at one of thirteen different external resistance settings. These settings gave a range of voltage drops across the lower surface Wheatstone bridge from 10.4 V to 55.8 V. The voltage drops corresponded to total rates of heat generation at the lower surface ranging from 35.8 W/m^2 to 1032. W/m^2.

Series A involved twelve separate runs and was performed with 100 cs oil, using the 0.01905 m depth. A total of eight runs, comprising series B, were performed with 100 cs oil at 0.01270 m. The six runs of series G used 100 cs oil at 0.00635 m. A 0.01905 m layer of 500 cs oil was used for the nine runs of series F. Fourteen runs were performed for series C, which utilized a 0.00635 m layer of 5 cs oil. The nine runs of series D were carried out with 5 cs oil at a 0.01270 m depth. Series H used the same oil and depth as series D and involved five runs. Finally, the twelve runs of series E used a 0.01905 m layer of 5 cs oil.

Experimental runs lasted from 500 to 2000 seconds, with the bulk of the runs being 1000 s in length. The onset of motion occurred in all the runs except GC, which operated in the conduction phase for the entire monitoring time of 2000 s. For the other runs the time for the onset of motion, as determined from visual observations, ranged from 15 to 1800 seconds. In terms of dimensionless times, the range

of critical times for the onset of motion was 0.006 to 3.861.

The heat flux at the lower surface, expressed in dimensionless form spanned four decades of values, from 9.2×10^{2} to 1.9×10^{7}. Because the experiments started with an initially isothermal layer, the minimum temperature difference and corresponding Rayleigh number were zero. The range of values at the onset of motion was for the temperature difference 0.3 K to 11.2 K and for the Rayleigh number 1.4×10^{3} to 7.0×10^{5}.

In addition to the heat transfer measurements, photographic studies were performed for fifty-five of the runs. Of these photographic runs forty were selected for presentation in this thesis. The range of heating rates was the same as given above for the heat transfer results.

VI. EXPERIMENTAL RESULTS

A. General Considerations

The experimental results presented in this dissertation are separated into three sections. The first of these sections presents the heat transfer data pertinent to the onset of motion as determined from visual observations. The heat transfer data relating to the transient period, covering both the conduction and convection regimes, are presented in the second section. The last part is devoted to the photographic results.

Figures 12 through 21 present the heat transfer results at the time of onset of convection. The first four figures show the variables, dimensionless critical time, Rayleigh number at the critical time, dimensionless heat flux at the lower surface at the critical time and the thermal thickness at the critical time, as functions of the dimensionless total heat generation rate. Included on the plots are the least squares correlations. In Figures 16 and 17 the Rayleigh number and the lower surface heat flux are plotted as functions of the thermal thickness. The next figure is a plot of the Rayleigh number versus the heat flux at the lower surface, while the subsequent figure shows the Nusselt number and the Rayleigh number plotted against each other. (The Nusselt number in this work is defined as the lower surface heat flux divided by the Rayleigh number.) Figure 20 presents lower surface heat flux versus Rayleigh number correlation with the correlation for the critical time superimposed. The last figure of this series compares the present

results with those of Soberman (1959).

The transient data are presented in Figures 22 to 40. All the plots, except 37, 39 and 40 are in the form of the Rayleigh number versus the heat flux at the lower surface for the particular time in question. The first three plots present the data when the dimensionless time, τ, is some fixed multiple of the critical time. The multiples used were 2, 4 and 10. Figures 25 through 35 present the data for constant dimensionless time where the following values were chosen: 0.01, 0.05, 0.10, 0.20, 0.40, 0.70, 1.00, 1.30, 1.60, 2.00 and 2.50. Again the least squares correlations have been plotted on these figures. These correlations are used in the composite plots of Figures 37, 39 and 40, where the Nusselt number is plotted as a function of the Rayleigh number to help distinguish the correlations more clearly. The first figure shows the results dimensionless times that are fixed multiples of the critical time, while the last two figures present the data for constant dimensionless time. For clarity the results for dimensionless times 1.30, 1.60, 2.00 and 2.50 are shown as one correlation, ≥ 1.30. On the figures the correlation for the heat transfer results at the critical time have been included for reference. Also plotted on Figures 37 and 40, for comparison purposes, is the curve recommended by Rossby (1966, 1969) for a layer of 20 centistoke silicone oil operating in a steady-state. Figure 39 shows lines of constant lower surface heat flux to indicate the trend of the results with time.

The last series of figures (41 to 50) present the photographic

results. The experiments are grouped by depth, and within each group the runs are arranged in order of increasing total heat generation rate. Each photograph is identified by the time at which the picture was taken, in the form of dimensional time, dimensionless time and fraction above the critical time. Also listed is the Rayleigh number at the time the picture was taken. Figures 41 and 42 are the results for a 0.00635 m layer of fluid (series G and C). The 0.01270 m depth (series B, D and H) results are presented in Figures 43 through 45. Figures 46 through 49 are for a depth of 0.01905 m (series F, A and E). Figure 50 is a plot of the dimensionless wave number versus the heat flux at the lower surface at the critical time. The wave number data were taken from the photograph taken nearest to the onset of motion from which the pertinent information could be extracted.

B. Critical Time Studies

As the heat flux at the lower surface is increased, the Rayleigh number at which instability occurs increases. Thus, all things being the same, a larger temperature difference is required to initiate convection for an increased heat flux. But as can be seen from Figure 18, the necessary temperature difference does not increase in proportion to changes in the heat flux at the lower boundary, but more nearly as the 0.65 power over the range of data gathered from the experiments. Consequently, when comparing the critical time temperature difference to the characteristic, steady-state temperature difference, Qd/k, the ratio decreases with increasing heat flux at the lower surface, Q; or inversely, the Nusselt number at the critical time, $Qd/k\Delta T_{cr}$, increases with increasing heat flux or correspondingly increasing Rayleigh number. This result is seen in Figure 19.

For very rapid heating the onset of motion should occur before the heating has penetrated very far into the fluid layer. The system for these large heat fluxes will behave as if it is infinitely deep. The overall depth, d, will then lose its significance as a length scale of the problem. Thus, in a correlation between the critical time Rayleigh number and the critical time heat flux at the lower surface, the result should be such that it is independent of depth. Since the Rayleigh number is proportional to the depth cubed and the heat flux at the lower surface goes as the fourth power of the depth, this requires the Rayleigh number to be proportional to the 0.75 power of the heat flux, H. At a heat flux of $H = 1 \times 10^7$ the experimental correlation yields a

power of 0.67. Over the heat flux range of the experiments, 2×10^3 to 1×10^7, the exponent increases from 0.63 to 0.67. This power implies that the temperature difference at the onset of motion is proportional to the -0.4 power of the depth.

For the lowest of the heat fluxes (series G) some of the critical Rayleigh numbers were below the classical, steady-state value of 1708. The smallest value was for run GE (heat flux at the lower boundary, $H_{cr} = 1.74 \times 10^3$), with a value of the critical Rayleigh number of $Ra_{cr} = 1.43 \times 10^3$. Other sub steady-state values were 1.50×10^3 for run GD ($H_{cr} = 2.23 \times 10^3$) and 1.54×10^3 for run GB ($H_{cr} = 2.12 \times 10^3$). All the other heating rates had Rayleigh numbers at the onset of convection that were greater than the steady-state value. The three sub steady-state results were obtained for runs with the lowest values of the total heat generation rate for which motion was observed.

An examination of Figure 20 shows that as the heat flux at the lower surface is increased, the time required for instability to occur decreases. This is also somewhat more dramatically seen in Figure 12, where the dimensionless time for the onset of motion is plotted against the total heat generation rate. This behavior of the critical time is entirely consistent with the other results. As was pointed out earlier, the Nusselt number at the onset of motion increases with increasing heat flux at the lower surface. This was also stated in terms of the effective temperature difference, the inverse of the Nusselt number, which would decrease with increasing heat flux. Thus, in dimensionless terms, it would take a shorter time to reach a

smaller temperature difference, which is just the result that is observed.

For very high heat fluxes, using the same arguments that were used above, it would be expected that the dimensionless time at the onset of motion be proportional to the -0.50 power of the total heat generation rate. The experimental power is -0.531.

For lower heat fluxes there will be some minimum heat flux below which the system will always be stable. As this heat flux is approached from above, longer and longer times will be required before the initiation of convection, until at the minimum heat flux an infinite time will be required. As can be seen from Figure 12, the experiments bear out this trend. The least squares fit indicates that the minimum total heat generation rate is approximately 5.09×10^3. Substituting this value into the Rayleigh number correlation yields a steady-state, critical Rayleigh number of 1.45×10^3.

At these lower heat fluxes very small changes produce major changes in the time for the onset of motion. This is seen in Figure 20, where changing the heat flux at the lower surface from 2.5×10^3 to 1.8×10^3 changes the critical time from one unit to an infinite time.

The dimensionless thermal thickness is plotted against the Rayleigh number and the heat flux at the lower surface in Figures 16 and 17, respectively. As can be seen, for decreasing thermal thicknesses the heating rate increases. The rate of increase also increases with larger heat fluxes and Rayleigh numbers.

For the highest heating rates the thermal thickness goes as the

-0.193 power of the total heat generation rate. Very rapid heating or very deep fluid layers would have a power relationship of -0.250.

Using the same least squares fit line, the value of the steady-state, critical Rayleigh number, corresponding to a thermal thickness of one, is 1.63×10^3.

C. Transient Data

For any given time, whether measured in multiples of the time required for the onset of motion or some fixed value, the Rayleigh number increases as the heat flux at the lower boundary increases. As was true for the relationship at the onset of motion, however, the increase in Rayleigh number is not proportionate to increases in the heat flux. Thus as the Rayleigh number increases, the Nusselt number also increases. This fact is seen in Figures 37, 39 and 40 where the least squares fit lines are plotted for various times in the form of Nusselt number versus Rayleigh number.

Also to be seen from the figures is the fact that for a given heat flux at the lower surface, as time increases, the temperature difference (which is proportional to the Rayleigh number) increases. This temperature difference approaches an asymptotic value as time increases. That is, the Rayleigh number increases more slowly at a given heat flux as time increases, finally approaching some steady-state value.

In Figure 37, where time is measured in multiples of the onset of motion time, it is seen that for Rayleigh numbers greater than about 1×10^4, the decrease in the Nusselt number for each doubling of the time is less as time increases. For example, considering a fixed Rayleigh number of 1×10^5, the Nusselt number decreases from 7.8 to 6.4 as time increases from its onset of motion value to twice that much. This is a decrease in 1.4 units or 18 percent. Going from two units to four units of the critical time, the decrease is 1.1 units or a 14 percent

further reduction. If the rate of decrease were constant over this time range, there would have been a 52 percent decrease. Finally, in going from four units to ten units of the onset of motion time, the decrease is 0.6 units or a further 8 percent.

For a Rayleigh number less than about 6×10^3 the Nusselt number is larger for times greater than the critical time, although the value at four multiples of the time to onset of motion is less than the value for two multiples.

When time is some fixed value, the qualitative behavior of the Rayleigh number for a fixed heat flux at the lower boundary is the same as the fixed multiples of the critical time results. As time increases, so does the Rayleigh number but at ever decreasing rates. The new feature that can be seen here is that it takes longer times for an asymptotic value of the Rayleigh number to be reached when heat fluxes at the lower boundary is decreased. Although the data are sketchy, for Rayleigh numbers greater than about 1×10^5, a time of about 0.20 units will give approximately steady-state results. That is, 0.20 units corresponds roughly to infinite time as far as heat transfer is concerned for these Rayleigh numbers. For values of the Rayleigh number less than the 1×10^5 value, steady-state heat transfer results are approximately reached for times on the order of 0.70 to 1.00 units.

D. Photographic Results

Before starting the description of the photographic results, a brief discussion of the terms used to describe the various flow patterns is needed. When looking down at the fluid layer, the motion is found to occur in a relatively regular array, except possibly for the very large Rayleigh number flows. In examining the photographs in Figures 41 to 49, distinct regions in which hot fluid rises from the lower surface (shown as the dark bands in the photographs) are seen. Along with the cold descending bands of fluid, these flow structures for the lower Rayleigh number range form various polygonal patterns when viewed from above.

The term "closed cell" will refer to a flow pattern in which the sides of the polygonal structure that outline the flow unit are all of approximately the same size. The term "roll" or "roll-like" will be applied to flows in which the polygons are approximately rectangular in shape and the long sides are much greater in length than the width. In the theoretical analyses the roll is supposed to be strictly two-dimensional, but in actual experimental situations the axis of the roll will have a curvature. To characterize this feature, Avsec (1939) described the pattern as "vermiculated rolls" after its worm-like appearance.

A cursory examination of the photographic results indicates that at any given depth, as the total heat generation rate is increased, the initial flow pattern consists of an increasing number of small closed cells as opposed to rolls.

In the 0.00635m depth series (Figures 41 and 42) runs GB, GA, CK, CI, CH and CM display qualitatively similar pattern development. Starting from a system of small wavelength, closed cell motion, the pattern changes to a larger wavelength, predominantly roll-like pattern. Runs GB and GA have planforms showing a strong orientation with the boundary; this feature is less pronounced in the C runs. This transition from a small closed cell to a roll pattern appears to occur in two distinct ways. The first method is for adjacent cells to merge together to form a single roll cell. This process is very clearly seen in the photographs of run GA. As the rolls continue to increase in wavelength, some merging of rolls occurs to allow for the growth in the finite size chamber. The second method of transition comes from the "destruction" of a small closed cell located between two existing rolls. This phenomenon will be described more fully in the description of the 0.01270 m results.

Runs CC, CD and CA (Figure 42) exhibit a behavior that is qualitatively different from the previous runs. Starting from the closed cells, the pattern changes toward a longer wavelength, roll-like pattern, but with dark lines or hot bands running locally perpendicular to the main warm cell boundaries. The pattern is again one of closed cells, although for these photographs the first impression is that motion is in a roll-like pattern. This superimposed or extra pattern increases in intensity with increasing heat generation rate. The time development of the motion for the three runs does not seem to pass through the strictly roll-like stage that is characteristic of lower

heating rate runs. This observation somewhat depends on the interpretation of the photographs of run CC, particularly pictures 3 and 4.

For the 0.01270 m series (Figures 43 through 45) the noticeable new feature is the strong orientation of the motion with the boundaries. This is particularly true for the B series. With increasing heat generation rates the B series shows increasing initial pattern disorganization with an increasing number of small closed cells. All of this series, except run BA, evolves to a roll pattern as time progresses. In run BA the final pattern contains a large fraction of "nodules" superimposed on the dark bands with very faint connections between opposing nodules in a manner very similar to run CC. Run BA also does not appear to pass through the strictly roll-like pattern of the lower heating rate runs.

As mentioned above, one method of pattern transition was the elimination of a small closed cell surrounded by two rolls. This phenomenon is clearly seen in the photographs of the B series. For example, in the second picture of run BC (Figure 43), two small closed cells are seen in the middle of the photograph with a roll on either side. The lower cell has made a "connection" with the two rolls in the form of hot rising fluid bands shown as the dark regions in the photos. In the next picture the lower cell boundaries (bright lines) have disappeared, and a connection has been made with the upper cell. In picture 4 the lower cell connection has been broken and the boundary between the two rolls "patched." In the meantime, the upper cell has had its boundaries "destroyed." Picture 5 shows the boundary between

the two rolls being patched up, with the horizontal dark band having decreased in intensity. The last picture shows the final result in which it is impossible to tell that the original cells existed.

The remainder of the 0.01270 m series, the D and H runs, exhibit a much more disorganized pattern development. Two of the runs, DB and DA, have quite anomalous behavior and will be discussed separately with some anomalous runs in the E series. Runs DI and DG were duplication runs which showed the more "consistent" initial pattern.

The initial pattern consisted of small closed cells, with a larger number of cells appearing for an increasing heat generation rate. The boundary orientation appears to be very strong, with the least influence seen in run HE, which is a duplicate of run HA.

Runs DD and DC have a qualitatively similar pattern development. Starting from a rectangular array, the pattern changes to a closed cell motion in which the characteristic size of the motion is larger than the initial pattern.

The remaining runs are also very three-dimensional, but with an extra feature that cannot be seen from a still photograph. The best example of the phenomenon is seen in the last picture of run DB (Figure 44). In the photograph the large three-dimensional closed cells are seen along with hot blobs that are in various stages of connection with the cell boundaries. These blobs would appear in a periodic fashion in the central regions of the cells and then drift to the cell boundaries. This periodic time dependence was different from the previous aperiodic

time development of the overall pattern.

The last feature to be noted about the D and H series is the appearance of a large boundary affected area surrounding the pattern area. This zone of influence was not nearly as prevalent in the lower heating rate runs.

For the final depth series of 0.01905 m (Figures 46 through 49) the F series and run AJ exhibit very similar time development of the patterns of motion. Here the initial pattern is predominantly a roll, with any closed cells being eliminated as time progresses. The flow patterns also show a strong boundary alignment. For these runs cell elimination is only through the merger technique.

Runs AL and AH follow slightly different time development. Both runs are still strongly orientated with the boundaries, but both include the appearance of the "nodules" along with the interconnections between them. Although somewhat difficult to determine, it does appear that these two runs do not pass through the strictly roll-like pattern in the same manner as the similar runs at the smaller depths.

In the E series there are two anomalous runs, EI and EJ, which will be discussed separately. For the other runs in the series the initial pattern is very similar to the patterns seen in series D and H, with an increasing number of small closed cells with an increasing heat generation rate. The strong boundary orientation is also apparent.

All of the runs appear to go through a similar initial time development, except possibly run EA. Starting from a basically rectangular planform, the pattern changes to one of isolated hot spots with

some interconnecting dark bands. The hot spots are then reconnected, but with a more disorganized orientation of cell boundaries. With higher heat generation rates this time development is followed with the appearance of time dependent hot blobs in the interior of the cells in a manner very similar to that described for run DB. The rather strong region of boundary influence can also be seen in these flow patterns.

For the highest heating rates used, runs EK and EA (Figure 49), the entire pattern was highly time dependent, although an overall view of the flow indicated a pattern that was cellular in character. The boundaries of these cells would shift and move; but the general feature was still cellular, as can be seen from an examination of the pictures. The detailed flow was, however, highly energetic.

In the course of the experiments four runs were conducted in which the initial pattern was quite different from the "normal" beginning motion. These were runs DA and DB and EI and EJ (Figures 44, 45, 48 and 49). As can be seen from the second letter of the run, the pairs were performed on subsequent days, although they were for different heat generation rates. The four rates ranged from 1.9×10^6 to 7.6×10^6.

The characteristic feature of these anomalous runs was that the initial pattern had a scale of motion that was substantially larger than the regular scale at the same heat generation rate. These anomalous patterns would also appear at an earlier time than the normal pattern. As can clearly be seen from runs DB and EJ, the regular planform would start appearing subsequent to the initial motion. The flow would continue to develop until the pattern was substantially similar to the

duplicate run at a comparable time. This is seen, for example, in a comparison of picture 4 of run DA and picture 3 of the duplication run DG, where the patterns are very similar.

An examination of Figure 50, a plot of the dimensionless wave number versus the heat flux at the lower surface at the onset of motion, shows that for increasing heat flux the wave number increases. This means that the scale of motion gets smaller as the heating is increased, a feature of the flow that was noted in the study of the photographs.

The data points were determined from the photographs by a measurement of the width and length of the cells. Because of the generally strong boundary orientation, the cells were at least locally assumed to be rectangular in shape. This assumption allowed an easy determination of the wave number. The wave number was then scaled with the depth of the fluid layer to give the values plotted in the figure. For a given run four separate measurements were taken. An attempt was made to choose several different cells that would give a range of wave number that was characteristic of that run.

Although the scatter of the wave number was relatively large compared to the precision of the other results, the trend of the data is very clearly an increase in wave number with increasing heat flux. Also, the mean values of the wave number at the lower heating rates is larger than the steady-state, theoretical result of 3.117.

VII. COMPARISON AND DISCUSSION OF THE RESULTS

A. General Comments.

All of the information presented in the figures described in the previous chapter were in the form of plots between dimensionless variables. The amount of scatter in the data was normally very small for these figures. The least scatter is probably seen in Figure 14, a plot of the dimensionless heat flux at the lower surface versus the total heat generation rate. The largest amount of scatter is in the plot of the wave number versus the heat flux at the lower surface, Figure 50.

A somewhat subtle, though obvious, conclusion that can be drawn from the fact that the data does exhibit very definite correlations when plotted in dimensionless form is that the choice of dimensionless variables was an appropriate one. In other words, the small scatter of the data indicates that there are probably no other significant parameters than those used in the figures. Over the many different dimensional conditions that determine the experiments, the resulting data can be collapsed to simple relationships between the dimensionless variables.

All of the data appears to be expressible in terms of two independent variables: the total heat generation rate and the dimensionless time from the start of heating. For given times the various variables, such as the Rayleigh number, the heat flux at the lower

surface, the Nusselt number and the thermal thickness, can be expressed in terms of the total heat generation rate alone. This fact allows direct crossplotting of the dependent variables for a given time.

Two dimensionless variables which should be checked to see if they are important correlating parameters in the problem are the aspect ratio and the Prandtl number. The aspect ratio, which compares the characteristic horizontal length scale of the chamber (in this case the length of the side of the square guard ring) to the depth of the fluid layer, does not have any noticeable effect on the heat transfer results, nor on the wave number at the onset of motion. This ratio, with values 10.3, 15.5 and 31.0, is a parameter in the detailed flow pattern; and its effect will be discussed in the section dealing with the photographic results.

The Prandtl number, which ranged from 45 to 8770, also appears to have an insignificant effect on the heat transfer results. For extremely large Prandtl numbers the effect on heat transfer results should be negligible. In accord with other experimental investigations, the range of Prandtl numbers in the present experiments are in the "large" Prandtl number region. This would lead to the supposition that the effect of this property parameter should be small, as is the case. The only data which appear to show some slight systematic Prandtl number dependence are the onset of motion times. A discussion of this feature will be found in the subsequent section on the onset of motion.

B. Onset of Motion Results.

In the present experimental research the critical time, the time for the onset of motion, was that time at which motion was observed to occur from an examination of the shadowgraph image of the fluid layer. An alternate definition that could have been used in the experiments was that motion was occurring when there was a change in the heat transfer rate from that predicted on the basis of pure conduction. This experimental technique has been used many times to determine the steady-state critical Rayleigh number. A check was made of all the experimental results to determine if the second definition would give different results for the critical time. It was found, essentially uniformly, that the time determined from the heat transfer results was slightly longer than the one determined from shadowgraph observations. All of the data presented in connection with the onset of motion is based on the shorter of the two times, the optically determined one. This choice was made because the visual indication was more sensitive than the deviation of the heat transfer rate.

There remains the question of how to compare this experimentally determined time to the ones calculated from the theoretical results of Currie (1966, 1967). Currie carried out an analysis of a constant heat flux problem to compare his analytical results to the experimental ones of Soberman (1959). When a comparison is made with the present experimental times and the times calculated by Currie the obvious feature is that the experimental times are much longer. Using, for example, a critical Rayleigh number of 1×10^5, the

experimental time is ten times longer than the theoretical one. This apparently large discrepancy is explained by an examination of the definitions of the critical times for the two cases. For the analytical case the critical time is the time required for an initially decaying disturbance to reach a stationary state and thereafter to grow in size. This is to be contrasted with the experimental time, which is the time required for this same disturbance to be seen, that is, to be of finite size. There will be some finite amount of time required for the disturbance to grow from an infinitesimal size to one that can be seen. The work of Foster (1965 a), which treated the theory as an initial value problem, indicates that the time required for a disturbance to grow about one hundred times its original size is approximately an order of magnitude larger than the time required to reach a stationary state. This is certainly a qualitative verification of the growth factor given above for the present experiments and the work of Currie.

Another question that can be raised about time to the onset of motion is whether there is any systematic effect of the Prandtl number on the time, a point noted in Section A of this chapter. A detailed examination of the experimental results, particularly Figure 12, indicates that the critical time is affected by the Prandtl number, but only slightly. As mentioned in Section A, the results for the critical time will become independent of the Prandtl number when the Prandtl number is large enough. The analytical work of Foster (1965 a) indicates that "large enough" is somewhere in the range of 100 to 1000, depending on the conduction problem considered. The experimental work of

Onat and Grigull (1970), which approximates the case of constant heat flux at the lower surface of a semi-infinite medium, indicates that for Prandtl numbers larger than 200 the time at the onset of motion is independent of Prandtl number. Both works also indicate that the smaller the Prandtl number, the larger the critical time. As applied to the present experiments, the results for the 100 cs and 500 cs oils should be the same, while the 5 cs oil results should give slightly longer times. The data shown in the plot of the critical time versus the total heat generation rate, Figure 12, verifies this conclusion. An examination of the region of overlap of the various oil data indicates that the times to instability for the 5 cs oil are approximately thirty to forty percent longer than the corresponding times for the 100 cs oil and 500 cs oil. The results of Foster and Onat and Grigull would indicate less of an increase in this time. The discrepancy, however, is within the bounds explainable by the differences in the boundary conditions and the experimental errors inherent in the experiments. In any case, the effect of the Prandtl number on the critical time is small; and it may be neglected in the relation between the heat generation rate and the critical time. For engineering purposes certainly a single time would be sufficient in this Prandtl number range.

The experimental data also allow the computation of the thermal thickness, a measure of the rapidity of the heating (see Equation (41) for its definition); and this thickness, based on measurements, may then be compared to the present theoretical work as well as to the work of Currie (1966, 1967). When this comparison is made, the

experimental thicknesses are much larger than the theoretical ones. The discrepancy is again resolved when it is remembered that the experimental and theoretical results are based on different critical times. With a longer time the Rayleigh number and the thermal thickness will have a chance to increase over their values when the infinitesimal disturbance has reached a stationary state. This is in agreement with the findings.

One question raised by earlier research was whether certain types of transient heating could induce instabilities at Rayleigh numbers lower than the steady-state value of 1708. In the present series of experiments three such cases were found, all occurring at the low end of the heating rates studied (Figure 18). The number and accuracy of data points, however, was not believed to be sufficient to determine conclusively whether for this case of nearly constant heat flux there are heating rates for which the critical Rayleigh number is lower than the steady-state value of 1708.

The only experiments which have been carried out to date which cover a similar range of heating rates and which approximate the case of constant heat flux were performed by Soberman (1959). He used mercury and 500 cs silicone oil to determine the relationship between the Rayleigh number and the heat flux at the lower surface at the onset of convection. A comparison of the present data and Soberman's results is shown in Figure 21. As can be seen, there is a major disagreement in the two series of data, which the following discussion clarifies.

Currie (1966, 1967), who also studied Soberman's data for comparison with his analytical work, determined that discrepancies of the results were probably due to the method of temperature measurement used by Soberman. In his apparatus two thermopiles were located at a distance of 0.00318 m (1/8") on each side of the centerline of the fluid layer, which was either 0.0127 m (1/2") or 0.0254 m (1") deep. Soberman claimed that the times required for the onset of convection were not short compared to the thermal time scale, d^2/κ. No times were listed, but three figures give dimensionless times of 0.17, 0.29 and 2.6. If it is assumed that the times are not short, the temperature profile will be "close" to its steady-state configuration. The gradient measured by the thermopiles can then be used for the overall gradient. The temperature difference between the two surfaces at the onset of convection is then just the measured temperature gradient multiplied by the overall depth, which was Soberman's procedure. Although the times given by Soberman are not small, the critical times in the present work, seen in Figure 20, are indeed small for the rapid heating rates. It then could be that the times in Soberman's experiments were artificially long because of a defect in the test apparatus and the method of heating. A time lag, not present in the current experiments, was involved because the energy from the heater had to pass through a "small" air gap and a 0.00635 m (1/4") thick piece of copper before entering the fluid layer. Because the onset of motion times was actually short, the heat flux at the lower surface would be larger than predicted by the thermopiles; and hence, the temperature difference

would be larger than calculated, Consequently, the Rayleigh number at the onset of convection would be underestimated, and the error would increase as the heat flux at the lower surface is increased. This is in agreement with the results shown in Figure 21.

C. Time-Dependent Results.

The present experiments are concerned with the time-dependent behavior of the Bénard convection system during the transient period while the steady-state conditions are being established. The heat transfer results of the experimental runs are effectively summarized in Figures 39 and 40 in which the Nusselt number (based on the heat transfer rate at the lower surface) is plotted as a function of the Rayleigh number for several values of the dimensionless time. On both of the plots the time required for the onset of motion to occur is shown as a dashed line. In Figure 39 lines of constant heat flux at the lower surface are also marked. Each of the experiments of the present series essentially proceeds along one of these lines in the direction of increasing Rayleigh numbers. In Figure 40 a steady-state line is plotted to show the limiting behavior of the free convection layer. The correlation was taken from the experimental results of Rossby (1966, 1969) for 20 cs silicone oil. The results of long duration in the present experiments agree well with his steady-state findings. The graphs (Figures 39 and 40) clearly indicate the following: (a) the regions in which heat is transferred solely by unsteady conduction; (b) the time at which convection is initiated; (c) the response of the Nusselt number and the Rayleigh number in the region of transient convection; and finally, (d) the times required for the Rayleigh number to approach a steady-state value. The "fifteen percent line" indicates when the Rayleigh number is within fifteen percent of its steady-state

value for a given constant heat flux at the lower surface. The line also represents the point at which the Nusselt number is within eighteen percent (1/0.85 -1) of its steady-state value.

In Figure 37 the Nusselt number is plotted as a function of the Rayleigh number for several different dimensionless times, using time measured in multiples of the critical time. This figure shows that the data for ten multiples are within fifteen percent of the steady-state value for all Rayleigh numbers. If the Rayleigh numbers are less than 5×10^5, it requires only four multiples; for Rayleigh numbers less than 1.5×10^4, only two multiples are needed. Finally, when the Rayleigh numbers are less than 8×10^3, the fifteen percent limit is reached at the onset of motion.

Similarly, referring to Figure 40, for dimensionless time of 0.01 none of the results are within the fifteen precent limit over the range of data presented, and this remains true for times up to about 0.05. For Rayleigh numbers greater than 3×10^4 the results are within the fifteen percent line when the time is 0.10. At a time 0.20 the results are within fifteen percent for a Rayleigh number greater than 9×10^3. For times between 0.40 and 2.50 the results are within fifteen percent for Rayleigh numbers between 1.5×10^3 and 2.2×10^3, the higher number corresponding to a shorter time.

The apparatus used in the experiments requires approximately a day to reach truly steady-state conditions in the heat transfer and the flow patterns. It was found, however, that it takes only a comparatively short time (normally less than one dimensionless unit) to reach

the steady-state temperature difference and, therefore, the steady-state Rayleigh number. Once this Rayleigh number is reached, the main change in the fluid layer is an increase in the mean temperature of the oil. During this time the Rayleigh number changes only slightly, mainly due to changing property values and small changes in the amount of heat transferred. The mechanism involved appears to be the following: once motion occurs, the fluid layer is able through rapidly changing flow conditions to adjust the amount of heat transferred to an approximately steady value. The flow pattern adjusts from an initial, generally small closed cell motion to a pattern that is qualitatively similar to the final steady-state motion in a few dimensionless times. With the heat transfer rate near the steady-state value, only the temperature level changes gradually.

D. Flow Conditions.

The photographic survey of the experimental runs presents some striking patterns of motion. For each of the three depths the lower heating rate runs have initial patterns that are predominantly roll-like in character. The deeper the fluid layer, the more strongly the rolls are aligned with the vertical boundaries.

This influence of the vertical boundaries in orienting the pattern was first shown to exist by Koschmieder (1966). He used a square frame with an aspect ratio of approximately 12, using the side of the square as the characteristic length; he also used a circular ring with an aspect ratio of 20, in which the diameter of the ring is the characteristic length. (The aspect ratio is defined as the characteristic horizontal length of the chamber divided by the depth of the fluid layer.) For the present experiments, in which only square frames were used, the aspect ratios were 10.3, 15.5 and 31.0.

In confirmation of Koschmieder's work the present results also indicate this boundary influence. The largest aspect ratio experiments (0.00635 m depth) show the least orientation with the sidewalls. The influence does increase as the heating rate is lowered. For runs GB, GA, CK, CI, CH and CM in Figure 41, the effect of the boundaries appears to increase as time progresses.

Even though the boundaries exert an influence on the orientation of the pattern of motion, apparently they do not strongly influence the total wave number of the system, as can be seen in Figure 50. The data does not show any systematic deviation of the dimensionless wave

number with depth. A similar observation can be made about the heat transfer results. This independence of aspect ratio of the heat transfer results had been anticipated because of the extensive experiments by Catton and Edwards (1967) on the influence of sidewalls on steady Bénard convection. Their results indicated that for aspect ratios larger than about five the heat transfer would be essentially independent of sidewall influence.

Returning to Figure 50, one of the obvious features of the graph is the relatively large band spread of the wave number data as, for example, compared to the heat transfer results. In the analytical work of Foster (1965 a) it was found that although there was a wave number that was most unstable, there was a band of wave numbers about this fastest growing one that had only slightly smaller growth rates. This means that as convection is initiated, there can easily be a range of wave numbers that will be visible simultaneously.

Foster (1965 b, 1969 b) reported experimental wave number results for the case of constant increase of the lower surface temperature, using comparatively thick layers (greater than 0.02 m) of water. His results give wave numbers ranging from 6 to 120. The present data yield wave numbers between 3 and 17 over a generally lower heating range. No direct comparison can be made with his data due to the different forms of heating. A check with the theoretical results of Foster (1965 a) does indicate that the wave numbers at least follow the expected trend of increasing with rising heating rates. A comparison with the present theoretical results and those of Currie (1966, 1967)

does show a large discrepancy, however. For these analytical results the wave number has a maximum value of approximately 13, which corresponds to the fastest heating rate. This behavior is not confirmed by the present experiments.

In Chapter I some questions were posed as to the nature of the flow patterns. These included how the transient results compared to the steady-state planforms of motion. Krishnamurti (1968 c, 1969, 1970 a, 1970 b, 1970 c) has performed very complete experiments on the forms of motion to be expected for steady-state heat transfer; comparisons will be made with her results.

Starting with a pattern of vermiculated rolls, Krishnamurti found that there was a transition to a three-dimensional cross instability for Rayleigh numbers greater than about 2×10^4. It was noted in Chapter VI that this type of flow pattern was seen in runs CC, CD, CA, BA, AL and AH (Figures 42, 44 and 47). These runs exhibited this flow pattern at Rayleigh numbers greater than the transition value.

Krishnamurti found that the next change in flow conditions occurred at a Rayleigh number of approximately 6×10^4. The motion changed from the steady three-dimensional flow to one exhibiting a time periodic nature. This behavior was only noticed in the present experiments for Rayleigh numbers larger than roughly 10^5 (see run DB, picture 4 in Figure 44, for example). Above this approximate Rayleigh number, periodic bursts of warm fluid could be observed.

The last major transition was to "turbulence", which Krishnamurti found to occur at a Rayleigh number of approximately

1×10^6. Runs EK and EA (Figure 49) have Rayleigh numbers greater than this value. A comparison with runs *EJ* and *EC* (*Figure* 49), indicates that the flows with Rayleigh numbers above the turbulence transition value are at least qualitatively more "chaotic" than the flows at lower Rayleigh numbers. The flows were definitely not steady and were subject to bursts of hot fluid from the lower surface.

An additional extra planform of motion that has not been observed in the steady-state situation, but which has been observed in the transient phases, is the small closed cell flow seen as the initial pattern for many of the runs. The pattern can be seen in runs CC, CD and CA of Figure 42, runs BA, DD, DC and DI of Figure 44, runs HE HA and DG of Figure 45, runs EG, EF, EE and ED of Figure 48 and runs EC, EK and EA of Figure 49. In making a linear analysis of the stability problem, the flow pattern only appears as the total wave number. The actual form of motion cannot be determined, except in principle through a full non-linear analysis. Apparently, the flow chooses the small closed cell over, say, a series of closely packed rolls as the most efficient means of transferring the heat from the lower surface. As time progresses, the flow adjusts itself to optimize in some manner the configuration at a given time. A similar ability to adjust the flow and cell structure was found by Chen and Whitehead (1968), who experimentally studied the time evolution of an initial, arbitrarily sized, two-dimensional roll pattern for Rayleigh numbers somewhat greater than critical.

The development of the fluid motion as a function of time for a given heating rate can be described in terms of the basic planforms cited above. A description of the time evolution of the patterns for several different heating rates was given in Section D of Chapter VI.

Four runs, DB, DA, EI and EJ (Figures 44, 45, 48 and 49), started with initial convection patterns that were substantially different from the rest of the experiments. All the patterns had characteristic sizes that were much larger than the "normal" series, and the patterns appeared at earlier times than the duplicate runs which exhibited the "regular" pattern.

Two explanations of the abnormal form of motion are possible. The first is that the pattern was due to an initial, finite amplitude disturbance: that is, there was some residual motion in the chamber. This disturbance could have been more unstable to the heating than the infinitesimal disturbances that were normally excited. This view is also supported by the fact that these patterns were not reproducible, whereas the normal pattern was a reproducible one. Series H was performed in an attempt to reproduce these anomalous patterns.

The second explanation is that the patterns were of the "streaming" type described by Berg, Acrivos and Boudart (1966) in their morphology of cellular patterns found in evaporative convection. The pattern is characterized as one containing warm bands of rising fluid with the cold fluid descending slowly downward in the regions between the streamers. For the evaporative convection case the streamers were observed for depths greater than 0.007 m. In the

present experiments the anomalous runs had depths greater than this value, and the flows appear at least qualitatively similar to the evaporation patterns.

As was pointed out in the description of the flow patterns, after a sufficient time had elapsed, the planform of motion was essentially independent of the initial motion, so that the anomalous patterns were eventually "washed" away. This characteristic points out another major feature of the flow field: as the fluid layer proceeds towards a steady-state system, the pattern of motion is not dependent on its initial history.

VIII. SUMMARY AND CONCLUSIONS

The subject matter of this thesis, heat transfer in a fluid layer heated from below, is a classical one. Accordingly, a great number of studies had been devoted to this subject, the principal results of which were described and discussed in Chapter II. However, despite the attention which many investigators have given to this problem, several aspects could be clarified. Among these areas, the transient phases of the problem are of importance. Of particular interest would be an experimental study of the heat transfer and flow characteristics during this phase.

For these reasons, a series of experiments has been performed which study the effect of time-dependent heating on a horizontal fluid layer heated from below. Three silicone oils of 5 centistoke (cs), 100 cs and 500 cs viscosities were the working fluids with fluid layer depths ranging from 0.00635 m to 0.01905 m. Experiments were carried out in which the heat flux at the lower surface was maintained approximately constant for each run. The rates ranged from 9.2×10^2 to 1.9×10^7. The effect of different heat transfer rates on the initiation of convection, the increase of the Rayleigh number with time and the development of motion were examined. Visual observations were made from shadowgraph images, which were recorded photographically.

The primary effect of increasing the heat flux at the lower surface was to decrease the time to the onset of motion, to increase the critical Rayleigh number, to decrease the scale of initial motion

and to increase the Rayleigh number of the fluid layer for any specific dimensionless time.

Although the boundaries influence the orientation of the pattern, the principal feature of the larger heating rates is the appearance of small closed cell motion shortly after the initiation of convection. This pattern, which is present only during the earliest transient stages of motion, evolves into a variety of steady-state patterns, depending on the heating rate.

For the Prandtl number range of the present experiments (45 to 8770) the condition of the fluid layer for a given dimensionless time is effectively determined by the heat flux at the lower surface. The orientation and "two-dimensionality" of the fluid motion are also influenced by the vertical sidewalls; but the horizontal scale of motion, the total wave number, is dependent only on the heat transfer rate at a given time.

The quantitative heat transfer data during the transient phase indicate that over most of the experimentally studied range of heating rates essentially steady-state temperature differences (Rayleigh numbers) are reached in dimensionless times less than approximately one unit. This observation is borne out by the photographic results, which indicate that nearly steady-state fluid patterns are set up in a comparable time period.

A supplementary analytical analysis of the onset of motion was performed. The results of this work support the trends of the critical time data found in the experiments, although the quantitative agreement

is not substantial. This disagreement of results is largely due to the different definitions of critical time used in the two cases, which was discussed in Section B of Chapter VII.

Based on the experimental results, the conclusions about the effect of time-dependent heating on Bénard convection can be summarized as follows: (a) the temperature difference required for the initiation of convection increases as the heat transfer rate is increased; (b) an increase in the heat flux at the lower surface leads to shorter times to the onset of motion; (c) for the higher heating rates the initiation of convection is accompanied with the appearance of a "new" small closed cell motion that is not observed when the fluid layer is in a steady-state condition; and (d) specifying the dimensionless time and the heat flux at the lower surface is sufficient for "large" Prandtl number flows to characterize the state of the fluid layer.

Future research using the present results as a reference point could be carried out on at least three fronts. First, studies could be performed on the effect of different initial temperature profiles on Bénard convection. These studies would be useful in determining the sensitivity of the onset of motion and the development of the fluid planform to changes in the manner of heating. Second, the effects of spatially non-uniform heating of the lower surface, and of heat generation throughout the fluid have not been studied extensively and may be of importance in several applications. Third, a challenge is presented by the problem of free convection in a fluid which is subject to large property variations. Such cases occur for fluids near their

thermodynamic critical point, for fluids with large temperature differences and for "fluids" of the type found in the mantle of the earth.

The results which have been presented, as well as the additional studies which have been suggested, may contribute to the understanding of many applied problems ranging from the spreading of fires, the heating of food products in containers, the motion of the atmosphere and even to the drift of the continents.

BIBLIOGRAPHY

AVSEC, D. 1939. Tourbillons thermoconvectifs dans l'air application à la météorologie. Publ. Sci. et Techn. du Ministère de l'Air Nr. 155. Paris.

BATES, O. K. 1949. Thermal conductivity of liquid silicones. Ind. Eng. Chem. 41, 1966-1968.

BÉNARD, H. 1900. Les tourbillons cellulaires dans une nappe liquide. Revue générale des Sciences pures et appliquées. 11, 1261-1271 and 1309-1328.

BÉNARD, H. 1901. Les tourbillons cellulaires dans une nappe liquide transportant de la chaleur par convection en régime permanent. Ann. Chim. Phys. 23, 62-144.

BERG, J. C., ACRIVOS, A. and BOUDART, M. 1966. Evaporative convection. Advances in Chemical Engineering, eds. T. Drew, J. Hoopes and T. Vermeulen. 6, 61-123. New York: Academic Press.

BLAIR, L. M. and QUINN, J. A. 1969. The onset of cellular convection in a fluid layer with time-dependent density gradients. J. Fluid Mech. 36, 385-400.

BLOCK, M. J. 1956. Surface tension as the cause of Bénard cells and surface deformation in a liquid film. Nature. 178, 650-651.

BOUSSINESQ, J. 1903. Théorie Analytique de la Chaleur. 2, 172. Paris: Gauthier-Villars.

BRINDLEY, J. 1967. Thermal convection in horizontal fluid layers. J. Inst. Maths Applics. 3, 313-343.

BUSSE, F. H. 1962. Das stabilitätsverhalten der zellularkonvektion bei endlicher amplitude. Inaugural dissertation, Ludwig-Maximilians-Universität, Munich, Germany.

BUSSE, F. H. 1967a. The stability of finite amplitude cellular convection and its relation to an extremum principle. J. Fluid Mech. 30, 625-649.

BUSSE, F. H. 1967b. On the stability of two-dimensional convection in a layer heated from below. J. Math. Phys. 46, 140-150.

BUSSE, F. H. 1969. On Howard's upper bound for heat transport by turbulent convection. J. Fluid Mech. 37, 457-477.

BUSSE, F. H. 1970. Instabilities of convection rolls in a high Prandtl number fluid. Summer Study Program in Geophysical Fluid Dynamics. 1, 71-73. Woods Hole Oceanographic Institution.

CATTON, I. 1966. Natural convection in horizontal liquid layers. Phys. Fluids. 9, 2521-2522.

CATTON, I. 1970. Convection in a closed rectangular region: the onset of motion. J. Heat Transfer. 92, 186-188.

CATTON, I. and EDWARDS, D. K. 1967. Effect of side walls on natural convection between horizontal plates heated from below. J. Heat Transfer. 89, 295-299.

CHANDRA, K. 1938. Instability of fluids heated from below. Proc. Roy. Soc. A. 164, 231-242.

CHANDRASEKHAR, S. 1961. Hydrodynamic and Hydromagnetic Stability. Oxford: Oxford University Press.

CHARLSON, G. S. and SANI, R. L. 1970. Thermoconvective instability in a bounded cylindrical fluid layer. Int. J. Heat Mass Transfer. 13, 1479-1496.

CHEN, M. M. and WHITEHEAD, J. A. 1968. Evolution of two-dimensional periodic Rayleigh convection cells of arbitrary wave-numbers. J. Fluid Mech. 31, 1-15.

CHORIN, A. J. 1967. A numerical method for solving incompressible viscous flow problems. J. Comp. Phys. 2, 12-26.

CURRIE, I. G. 1966. The instability of fluids with time dependent heating. Ph.D. dissertation, California Institute of Technology, Pasadena, California.

CURRIE, I. G. 1967. The effect of heating rate on the stability of stationary fluids. J. Fluid Mech. 29, 337-347.

DASSANAYAKE, D. T. E. 1950. Unpublished dissertation cited in SUTTON, O. G. 1950.

DAVIS, S. H. 1967. Convection in a box: linear theory. J. Fluid Mech. 30, 465-478.

DAVIS, S. H. 1968. Convection in a box—on the dependence of preferred wave-number upon the Rayleigh number at finite amplitude. J. Fluid Mech. 32, 619-624.

DAVIS, S. H. 1970. Finite amplitude instability of time-dependent flows. J. Fluid Mech. 45, 33-48.

DAVIS, S. H. and SEGEL, L. A. 1965. The effects of surface curvature and property variation on cellular convection. Memorandum RM-4709-PR. Santa Monica: The Rand Corporation.

DAVIS, S. H. and SEGEL, L. A. 1968. Effects of surface curvature and property variation on cellular convection. Phys. Fluids. 11, 470-476.

DEARDORFF, J. W. 1964. A numerical study of two-dimensional parallel-plate convection. J. Atmos. Sci. 21, 419-438.

DEARDORFF, J. W. 1965. A numerical study of pseudo three-dimensional parallel-plate convection. J. Atmos. Sci. 22, 419-435.

DEARDORFF, J. W. 1968. Examination of numerically calculated heat fluxes for evidence of a supercritical transition. Phys. Fluids. 11, 1254-1256.

DEARDORFF, J. W. and WILLIS, G. E. 1965. The effect of two-dimensionality on the suppression of thermal turbulence. J. Fluid Mech. 23, 337-353.

DEARDORFF, J. W. and WILLIS, G. E. 1967a. Investigation of turbulent thermal convection between horizontal plates. J. Fluid Mech. 28, 675-704.

DEARDORFF, J. W. and WILLIS, G. E. 1967b. The free convection temperature profile. Quart. J. Roy. Meteor. Soc. 93, 166-175.

DE GRAAF, J. G. A. and VAN DER HELD, E. F. M. 1953. The relation between the heat transfer and the convection phenomena in enclosed plane air layers. App. Sci. Res. A. 3, 393-409.

DI FEDERICO, I. and FORABOSCHI, F. P. 1966. A contribution to the study of free convection in a fluid layer heated from below. Int. J. Heat Mass Transfer. 9, 1351-1360.

DOW CORNING 1952. Silicone notebook. Reference No. 2003. Midland, Michigan: Dow Corning Corp.

DOW CORNING 1957. Silicone notes. Reference No. 3-106. Midland, Michigan: Dow Corning Corp.

DOW CORNING 1967. Information about electronic materials. Bulletin 05-172. Midland, Michigan: Dow Corning Corp.

DROPKIN, D. and SOMERSCALES, E. F. C. 1965. Heat transfer by natural convection in liquids confined by two parallel plates which are inclined at various angles with respect to the horizontal. J. Heat Transfer. 87, 77-84.

EDWARDS, D. K. 1969. Suppression of cellular convection by lateral walls. J. Heat Transfer. 91, 145-150.

EDWARDS, D. K. and CATTON, I. 1969. Prediction of heat transfer by natural convection in closed cylinders heated from below. Int. J. Heat Mass Transfer. 12, 23-30.

ELDER, J. W. 1966. Thermal turbulence. Proc. Second Australasian Conf. Hyd. Fluid Mech. B289-B311. University of Auckland.

ELDER, J. W. 1967. Thermal turbulence and its role in the earth's mantle. Mantles of the Earth and Terrestrial Planets, ed. S. K. Runcorn. 525-547. New York: Interscience Publishers.

ELDER, J. W. 1969. The temporal development of a model of high Rayleigh number convection. J. Fluid Mech. 35, 417-437.

FOSTER, T. D. 1965a. Stability of a homogeneous fluid cooled uniformly from above. Phys. Fluids. 8, 1249-1257.

FOSTER, T. D. 1965b. Onset of convection in a layer of fluid cooled from above. Phys. Fluids. 8, 1770-1774.

FOSTER, T. D. 1968. Effect of boundary conditions on the onset of convection. Phys. Fluids. 11, 1257-1262.

FOSTER, T. D. 1969a. The effect of initial conditions and lateral boundaries on convection. J. Fluid Mech. 37, 81-94.

FOSTER, T. D. 1969b. Onset of manifest convection in a layer of fluid with a time-dependent surface temperature. Phys. Fluids. 12, 2482-2487.

FROMM, J. E. 1965. Numerical solutions of the nonlinear equations for a heated fluid layer. Phys. Fluids. 8, 1757-1769.

GERSHUNI, G. Z. and ZHUKHOVITSKII, E. M. 1963. On parametric excitation of convective instability. Appl. Math. Mech., P. M. M. 27, 1197-1204.

GILLE, J. 1967. Interferometric measurement of temperature gradient reversal in a layer of convection air. J. Fluid Mech. 30, 371-384.

GILLE, J. and GOODY, R. 1964. Convection in a radiating gas. J. Fluid Mech. 20, 47-79.

GLOBE, S. and DROPKIN, D. 1959. Natural-convection heat transfer in liquids confined by two horizontal plates and heated from below. J. Heat Transfer. 81, 24-28.

GOLDSTEIN, A. W. 1959. Stability of a horizontal fluid layer with unsteady heating from below and time-dependent body force. NASA Tech. Rep. R-4.

GOLDSTEIN, R. J. and CHU, T. Y. 1966. Study of heat transfer through convection layers. NASA CR81740.

GOLDSTEIN, R. J. and CHU, T. Y. 1968. Thermal convection in a horizontal layer of air. Mechanical Engineering Department Institute of Technology HTL TR No. 81. Minneapolis: University of Minnesota.

GOLDSTEIN, R. J. and CHU, T. Y. 1969. Thermal convection in a horizontal layer of air. Progress in Heat and Mass Transfer, eds. T. F. Irvine, Jr., W. E. Ibele, J. P. Hartnett and R. J. Goldstein. 2, 55-75. Oxford: Pergamon Press.

GOLDSTEIN, R. J. and GRAHAM, D. J. 1969. Stability of a horizontal fluid layer with zero shear boundaries. Phys. Fluids. 12, 1133-1137.

GOR'KOV, L. P. 1958. Stationary convection in a plane liquid layer near the critical heat transfer point. Sov. Phys. JETP. 6, 311-315.

GOUGH, D. O. 1969. An approach to thermal convection. Summer Study Program in Geophysical Fluid Dynamics. 1, 108-109. Woods Hole Oceanographic Institution.

GRAHAM, A. 1933. Shear patterns in an unstable layer of air. Phil. Trans. A. 232, 285-296.

GRESHO, P. M. and SANI, R. L. 1970. The effects of gravity modulation on the stability of a heated fluid layer. J. Fluid Mech. 40, 783-806.

GRESHO, P. M. and SANI, R. L. 1971. The stability of a fluid layer subjected to a step change in temperature: transient vs. frozen time analyses. Int. J. Heat Mass Transfer. 14, 207-221.

HAHNE, E. W. P. 1968. Natural convection heat transfer through an enclosed horizontal layer of supercritical carbon dioxide. Wärme-und Stoffübertragung. 1, 190-196.

HAHNE, E. W. P. 1969. Heat transfer and natural convection patterns on a horizontal circular plate. Int. J. Heat Mass Transfer. 12, 651-652.

HERRING, J. R. 1963. Investigation of problems in thermal convection. J. Atmos. Sci. 20, 325-338.

HERRING, J. R. 1964. Investigation of problems in thermal convection: rigid boundaries. J. Atmos. Sci. 21, 277-290.

HERRING, J. R. 1966. Some analytic results in the theory of thermal convection. J. Atmos. Sci. 23, 672-677.

HERRING, J. R. 1969. Statistical theory of thermal convection at large Prandtl number. Phys. Fluids. 12, 39-52.

HOARD, C. Q., ROBERTSON, C. R. and ACRIVOS, A. 1970. Experiments on the cellular structure in Bénard convection. Int. J. Heat Mass Transfer. 13, 849-856.

HOLDER, D. W. and NORTH, R. J. 1963. Schlieren Methods. Notes on Applied Science No. 31. London: Her Majesty's Stationery Office.

HOWARD, L. N. 1963. Heat transport by turbulent convection. J. Fluid Mech. 17, 405-432.

HOWARD, L. N. 1965. Boundary layer treatment of the mean field equations. Summer Study Program in Geophysical Fluid Dynamics. 1, 124-126. Woods Hole Oceanographic Institution.

HOWARD, L. N. 1966. Convection at high Rayleigh number. Proc. Eleventh Int. Cong. Appl. Mech., Munich, ed. H. Görtler. 1109-1115. Berlin: Springer-Verlag.

HURLE, D. T. J., JAKEMAN, E. and PIKE, E. R. 1967. On the solution of the Bénard problem with boundaries of finite conductivity. Proc. Roy. Soc. A. 296, 469-475.

INGERSOLL, A. P. 1966. Thermal convection with shear at high Rayleigh number. J. Fluid Mech. 25, 209-228.

JAKEMAN, E. 1968. Convective instability in fluids of high thermal diffusivity. Phys. Fluids. 11, 10-14.

JEFFREYS, H. 1926. The stability of a layer of fluid heated below. Phil. Mag. 2, Ser. 7, 833-844.

JEFFREYS, H. 1928. Some cases of instability in fluid motion. Proc. Roy. Soc. A. 118, 195-208.

JENSSEN, O. 1963. Note on the influence of variable viscosity on the critical Rayleigh number. ACTA Polytech. Scand. Ph. 24.

KOSCHMIEDER, E. L. 1966. On convection on a uniformly heated plane. Beitr. Phys. Atmos. 39, 1-11.

KOSCHMIEDER, E. L. 1967. On convection under an air surface. J. Fluid Mech. 30, 9-15.

KOSCHMIEDER, E. L. 1969. On the wavelength of convective motions. J. Fluid Mech. 35, 527-530.

KRAICHNAN, R. H. 1962. Turbulent thermal convection at arbitrary Prandtl number. Phys. Fluids. 5, 1374-1389.

KRAICHNAN, R. H. 1964a. Direct-interaction approximation for shear and thermally driven turbulence. Phys. Fluids. 7, 1048-1062.

KRAICHNAN, R. H. 1964b. Diagonalizing approximation for inhomogeneous turbulence. Phys. Fluids. 7, 1169-1177.

KRISHNAMURTI, R. E. 1967. Finite amplitude thermal convection with changing mean temperature: the stability of hexagonal flows and the possibility of finite amplitude instability. Ph. D. dissertation, University of California, Los Angeles, California.

KRISHNAMURTI, R. E. 1968a. Finite amplitude convection with changing mean temperature, part 1: theory. J. Fluid Mech. 33, 445-455.

KRISHNAMURTI, R. E. 1968b. Finite amplitude convection with changing mean temperature, part 2: an experimental test of the theory. J. Fluid Mech. 33, 457-463.

KRISHNAMURTI, R. E. 1968c. On the transition to turbulent convection, part 1: transition from two to three-dimensional flow. Geophysical Fluid Dynamics Institute Tech. Rep. No. 14. Tallahassee: Florida State University.

KRISHNAMURTI, R. E. 1969. On the transition to turbulent convection, part 2: the transition to time dependent flow. Geophysical Fluid Dynamics Institute Tech. Rep. No. 16. Tallahassee: Florida State University.

KRISHNAMURTI, R. E. 1970a. On the transition to turbulent convection, part 3. Geophysical Fluid Dynamics Institute Tech. Rep. No. 32. Tallahassee: Florida State University.

KRISHNAMURTI, R. E. 1970b. On the transition to turbulent convection, part 1: the transition from two- to three-dimensional flow. J. Fluid Mech. 42, 295-307.

KIRSHNAMURTI, R. E. 1970c. On the transition to turbulent convection, part 2: the transition to time-dependent flow. J. Fluid Mech. 42, 309-320.

KUO, H. L. 1961. Solution of the nonlinear equations of cellular convection and heat transport. J. Fluid Mech. 10, 611-634.

KUO, H. L. and PLATZMAN, G. W. 1961. A normal mode nonlinear solution of the Rayleigh convection problem. Beitr. Phys. Atmos. 33, 137-168.

LEDOUX, P., SCHWARZSCHILD, M. and SPIEGEL, E. A. 1961. On the spectrum of turbulent convection. Ap J. 133, 184-197.

LEONTIEV, A. I. and KIRDYASHKIN, A. G. 1965. Free convection heat transfer in horizontal channels and over a horizontal surface. J. Eng. Phys. 9, 5-9.

LEONTIEV, A. I. and KIRDYASHKIN, A. G. 1966. The theory of the convective heat transfer for the vertical flow of fluid. Proc. Third Int. Heat Transfer Conf., Chicago. 1, Paper 21, 216-224. New York: A. I. Ch. E.

LEONTIEV, A. I. and KIRDYASHKIN, A. G. 1968. Experimental study of flow patterns and temperature fields in horizontal free convection liquid layers. Int. J. Heat Mass Transfer. 11, 1461-1466.

LEONTIEV, A. I. and KIRDYASHKIN, A. G. 1969. Experimental study of free convection in horizontal and vertical fluid layers. Heat Transfer-Soviet Research. 1, 5-8.

LIANG, S. F., VIDAL, A. and ACRIVOS, A. 1969. Buoyancy-driven convection in cylindrical geometries. J. Fluid Mech. 36, 239-256.

LICK, W. 1965. The instability of a fluid layer with time-dependent heating. J. Fluid Mech. 21, 565-576.

LOW, A. R. 1929. On the criterion for stability of a layer of viscous fluid heated from below. Proc. Roy. Soc. A. 125, 180-195.

MAHLER, E. G. and SCHECHTER, R. S. 1970. The stability of a fluid layer with gas absorption. Chem. Engng Sci. 25, 955-968.

MAHLER, E. G., SCHECHTER, R. S. and WISSLER, E. H. 1968. Stability of a fluid layer with time-dependent density gradients. Phys. Fluids. 11, 1901-1912.

MALKUS, W. V. R. 1954a. Discrete transitions in turbulent convection. Proc. Roy. Soc. A. 225, 185-195.

MALKUS, W. V. R. 1954b. The heat transport and spectrum of thermal turbulence. Proc. Roy. Soc. A. 225, 196-212.

MALKUS, W. V. R. 1956. Outline of a theory of turbulent shear flow. J. Fluid Mech. 1, 521-539.

MALKUS, W. V. R. 1961. Similarity arguments for fully developed turbulence. Nuovo Cimento, Supplemento. 22, Ser. 10, 376-402.

MALKUS, W. V. R. 1963. Outline of a theory of turbulent convection. Theory and Fundamental Research in Heat Transfer, ed. J. A. Clark. 203-212. New York: Macmillan.

MALKUS, W. V. R. 1969. A scaling and expansion of equations of motion to yield the Boussinesq equations. Summer Study Program in Geophysical Fluid Dynamics. 1, 23-28. Woods Hole Oceanographic Institution.

MALKUS, W. V. R. and VERONIS, G. 1958. Finite amplitude cellular convection. J. Fluid Mech. 4, 225-260.

MIHALJAN, J. A. 1962. A rigorous exposition of the Boussinesq approximations applicable to a thin layer of fluid. Ap J. 136, 1126-1133.

MORTON, B. R. 1957. On the equilibrium of a stratified layer of fluid. Quart. J. Mech. App. Math. 10, 433-447.

MULL, W. and REIHER, H. 1930. Der Wärmeschutz von Luftschichten, seine experimentalle Bestimmung und graphishe Berechnung. Beih. Gesundh. -Ing. 28, Reihe 1, 1-28.

MULLER, G. J. 1966. Laminated plastics. Machine Design: Plastics Reference Issue. 38, No. 14, 31-35.

NAKAGAWA, Y. 1960. Heat transport by convection. Phys. Fluids 3, 82-86.

NEWELL, A. C., LANGE, C. G. and AUCOIN, P. J. 1970. Random convection. J. Fluid Mech. 40, 513-542.

NEWELL, A. C. and WHITEHEAD, J. A. 1969. Finite bandwidth, finite amplitude convection. J. Fluid Mech. 38, 279-303.

NIELD, D. A. 1968. The Rayleigh-Jeffreys problem with boundary slab of finite conductivity. J. Fluid Mech. 32, 393-398.

NOLL, W. 1968. Chemistry and Technology of Silicones. New York: Academic Press.

NAT, K. and GRIGULL, U. 1970. The onset of convection in a horizontal fluid layer heated from below. Wärme-und Stoffübertragung. 3, 103-113.

OSTRACH, S. 1957. Convection phenomena in fluids heated from below. Trans. ASME. 79, 299-305.

OSTRACH, S. 1964. Laminar flows with body forces. Theory of Laminar Flows, ed. F. K. Moore. Sec. F. Princeton: Princeton University Press.

OSTRACH, S. and PNUELI, D. 1963. The thermal instability of completely confined fluids inside some particular configurations. J. Heat Transfer. 85, 346-354.

O'TOOLE, J. L. and SILVESTON, P. L. 1961. Correlations of convective heat transfer in confined horizontal layers. Chem. Eng. Prog. Symp. Ser. 57, No. 32, 81-86.

PALM, E. 1960. On the tendency towards hexagonal cells in steady convection. J. Fluid Mech. 8, 183-192.

PALM, E., ELLINGSEN, T. and GJEVIK, B. 1967. On the occurrence of cellular motion in Bénard convection. J. Fluid Mech. 30, 651-661.

PALM, E. and ØIANN, H. 1964. Contribution to the theory of cellular thermal convection. J. Fluid Mech. 19, 353-365.

PEARSON, J. R. A. 1958. On convection cells induced by surface tension. J. Fluid Mech. 4, 489-500.

PELLEW, A. and SOUTHWELL, R. V. 1940. On maintained convective motion in a fluid heated from below. Proc. Roy. Soc. A. 176, 312-343.

PILLOW, A. F. 1952. The free convection cells in two dimensions. Aeronautical Research Laboratories Rep. A 79. Melbourne: Australia Department of Supply.

PLATZMAN, G. W. 1965. The spectral dynamics of laminar convection. J. Fluid Mech. 23, 481-510.

PLEVAN, R. E. and QUINN, J. A. 1966. The effect of monomolecular films on the rate of gas absorption into a quiescent liquid. A. I. Ch. E. J. 12, 894-902.

PLOWS, W. H. 1968. Some numerical results for two-dimensional steady laminar Bénard convection. Phys. Fluids. 11, 1593-1599.

PLUMMER, W. A., CAMPBELL, D. E. and COMSTOCK, A. A. 1962. Method of measurement of thermal diffusivity to 1000° C. J. Am. Ceram. Soc. 45, 310-316.

PNUELI, D. 1964. Lower bounds to thermal instability criteria of completely confined fluids inside cylinders of arbitrary cross section. J. Appl. Mech. 31, 376-379.

PNUELI, D. and ISCOVICI, S. 1968. The asymptotic thermal stability of confined fluids. J. Eng. Math. 2, 53-81.

RAYLEIGH, LORD 1916. On convective currents in a horizontal layer of fluid when the higher temperature is on the under side. Phil. Mag. 32, Ser. 6, 529-546.

REID, W. H. and HARRIS, D. L. 1958. Some further results on the Bénard problem. Phys. Fluids. 1, 102-110.

ROBERTS, P. H. 1966. On non-linear Bénard convection. Non-equilibrium Thermodynamics Variational Techniques and Stability, eds. R. J. Donnelly, R. Herman and I. Prigogine. 125-162. Chicago: University of Chicago Press.

ROBINSON, J. L. 1965. A boundary layer convection cell. Summer Study Program in Geophysical Fluid Dynamics. 2, 92-112. Woods Hole Oceanographic Institution.

ROBINSON, J. L. 1967a. A note on the stability of an infinite fluid heated from below. J. Fluid Mech. 29, 461-464.

ROBINSON, J. L. 1967b. Finite amplitude convection cells. J. Fluid Mech. 30, 577-600.

ROBINSON, J. L. 1969. The failure of a boundary layer model to describe certain cases of cellular convection. Int. J. Heat Mass Transfer. 12, 1257-1265.

ROSSBY, H. T. 1966. An experimental study of Bénard convection with and without rotation. Department of Geology and Geophysics Scient. Rep. HRF/SR 27. Cambridge: Massachusetts Institute of Technology.

ROSSBY, H. T. 1969. A study of Bénard convection with and without rotation. J. Fluid Mech. 36, 309-335.

SALTZMAN, B. 1962a. Selected Papers on the Theory of Thermal Convection: with special application to the earth's planetary atmosphere. New York: Dover Publications.

SALTZMAN, B. 1962b. Finite amplitude free convection as an initial value problem. J. Atmos. Sci. 19, 329-341.

SCHLÜTER, A., LORTZ, D. and BUSSE, F. H. 1965. On the stability of steady finite amplitude convection. J. Fluid Mech. 23, 129-144.

SCHMIDT, E. and SILVESTON, P. L. 1959. Natural convection in horizontal liquid layers. Chem. Eng. Prog. Symp. Ser. 55, No. 29, 163-169.

SCHMIDT, R. J. and MILVERTON, S. W. 1935. On the instability of a fluid when heated from below. Proc. Roy. Soc. A. 152, 586-594.

SCHMIDT, R. J. and SAUNDERS, O. A. 1938. On the motion of a fluid heated from below. Proc. Roy. Soc. A. 165, 216-228.

SCHNECK, P. and VERONIS, G. 1967. Comparison of some recent experimental and numerical results in Bénard convection. Phys. Fluids. 10, 927-930.

SEGEL, L. A. 1962. The non-linear interaction of two disturbances in the thermal convection problem. J. Fluid Mech. 14, 97-114.

SEGEL, L. A. 1963. The structure on nonlinear cellular solutions to the Boussinesq equations. RPI Math Rep. No. 60. New York: Rensselaer Polytechnic Institute.

SEGEL, L. A. 1964. The nonlinear interaction of a finite number of disturbances to a layer of fluid heated from below. RPI Math Rep. No. 64. New York: Rensselaer Polytechnic Institute.

SEGEL, L. A. 1965a. The structure of nonlinear cellular solutions to the Boussinesq equations. J. Fluid Mech. 21, 345-358.

SEGEL, L. A. 1965b. The non-linear interaction of a finite number of disturbances to a layer of fluid heated from below. J. Fluid Mech. 21, 359-384.

SEGEL, L. A. 1966. Non-linear hydrodynamic stability theory and its applications to thermal convection and curved flows. Non-equilibrium Thermodynamics Variational Techniques and Stability, eds. R. J. Donnelly, R. Herman and I. Prigogine. 165-197. Chicago: University of Chicago Press.

SEGEL, L. A. 1969. Distant side-walls cause slow amplitude modulation of cellular convection. J. Fluid Mech. 38, 203-224.

SEGEL, L. A. and STUART, J. T. 1962. On the question of the preferred mode in cellular thermal convection. J. Fluid Mech. 13, 289-306.

SILVESTON, P. L. 1958. Wärmedurchgang in waagerechten Flüssigkeitsschichten. Forsch. Ing.-Wes. 24, 29-32 and 59-69.

SOBERMAN, R. K. 1958. Effects of lateral boundaries on natural convection. J. Appl. Phys. 29, 872-873.

SOBERMAN, R. K. 1959. Onset of convection in liquids subjected to transient heating from below. Phys. Fluids. 2, 131-138.

SOMERSCALES, E. F. C. and DOUGHERTY, T. S. 1969. Observed flow patterns at the initiation of convection in a horizontal liquid layer heated from below. Fluid, Chemical and Thermal Processes Division Rep. No. FCT 69-1. New York: Rensselaer Polytechnic Institute.

SOMERSCALES, E. F. C. and DOUGHERTY, T. S. 1970. Observed flow patterns at the initiation of convection in a horizontal liquid layer heated from below. J. Fluid Mech. 42, 755-768.

SOMERSCALES, E. F. C. and DROPKIN, D. 1966. Experimental investigation of the temperature distribution in a horizontal layer of fluid heated from below. Int. J. Heat Mass Transfer. 9, 1189-1204.

SOMERSCALES, E. F. C. and GAZDA, I. W. 1968. Thermal convection in high Prandtl number liquids at high Rayleigh numbers. Mechanical Engineering Department Rep. No. HT-5. New York: Rensselaer Polytechnic Institute.

SOMERSCALES, E. F. C. and GAZDA, I. W. 1969. Thermal convection in high Prandtl number liquids at high Rayleigh numbers. Int. J. Heat Mass Transfer. 12, 1491-1511.

SOMERVILLE, R. C. J. 1970a. Heat transfer in steady two-dimensional Bénard convection. Summer Study Program in Geophysical Fluid Dynamics. 1, 87-89. Woods Hole Oceanographic Institution.

SOMERVILLE, R. C. J. 1970b. Preferred modes in convection. Summer Study Program in Geophysical Fluid Dynamics, 1, 89-91. Woods Hole Oceanographic Institution.

SPANGENBERG, W. G. and ROWLAND, W. R. 1961. Convective circulation in water induced by evaporative cooling. Phys. Fluids. 4, 743-750.

SPARROW, E. M., GOLDSTEIN, R. J. and JONSSON, V. K. 1964. Thermal instability in a horizontal fluid layer: effect of boundary conditions and non-linear temperature profile. J. Fluid Mech. 18, 513-528.

SPIEGEL, E. A. 1962. On the Malkus theory of turbulence. Mécanique de la Turbulence, Marseille, ed. A. Favre. 181-201. Paris: Editions du Centre National de la Recherche Scientifique.

SPIEGEL, E. A. 1966. Energy transport by turbulent convection. Stellar Evolution, Proc. Int. Conf., eds. R. F. Stein and A. G. W. Cameron. 143-173. New York: Plenum Press.

SPIEGEL, E. A. 1967. The theory of turbulent convection. Fifth Symp. Cosmical Gas Dyn., Aerodynamic Phenomena Stellar Atmos., ed. R. N. Thomas. 348-366. New York: Academic Press.

SPIEGEL, E. A. 1970. Estimate of convective transfer. Summer Study Program in Geophysical Fluid Dynamics. 1, 91-95. Woods Hole Oceanographic Institution.

SPIEGEL, E. A. and VERONIS, G. 1960. On the Boussinesq approximation for a compressible fluid. Ap J. 131, 442-447.

STEWARTSON, K. 1966. Appendix: asymptotic theory in the limit $R \to \infty$. Non-equilibrium Thermodynamics Variational Techniques and Stability, eds. R. J. Donnelly, R. Herman and I. Prigogine. 158-162. Chicago: University of Chicago Press.

STOMMEL, H. 1947. A summary of the theory of convection cells. Ann. N. Y. Acad. Sci. 48, 715-726.

STUART, J. T. 1960. Non-linear effects in hydrodynamic stability. Proc. Tenth Int. Cong. Appl. Mech., Stresa, eds. F. Rolla and W. T. Koiter. 63-97. Amsterdam: Elsevier.

STUART, J. T. 1964. On the cellular patterns in thermal convection. J. Fluid Mech. 18, 481-498.

SUN, W. M. and EDWARDS, D. K. 1970. Natural convection in cells with finite conducting side walls heated from below. Heat Transfer 1970: Fourth Int. Heat Transfer Conf., Paris, eds. U. Grigull and E. W. P. Hahne. 4, NC 2.3.1-NC 2.3.11. Amsterdam: Elsevier.

SUTTON, O. G. 1950. On the stability of a fluid heated from below. Proc. Roy. Soc. A. 204, 297-309.

THOMPSON, H. A. and SOGIN, H. H. 1966. Experiments on the onset of thermal convection in horizontal layers of gases. J. Fluid Mech. 24, 451-479.

THOMSON, J. 1882. On a changing tesselated structure in certain liquids. Proc. Phil. Soc. Glasgow. 13, 464-468.

TOOMRE, J. 1969. Time-dependent cellular convection. Summer Study Program in Geophysical Fluid Dynamics. 1, 126-128. Woods Hole Oceanographic Institution.

TORRANCE, K. E., ORLOFF, L. and ROCKETT, J. A. 1969. Experiments on natural convection in enclosures with localized heating from below. J. Fluid Mech. 36, 21-31.

TORRANCE, K. E. and ROCKETT, J. A. 1969. Numerical study of natural convection in an enclosure with localized heating from below—creeping flow to the onset of laminar instability. J. Fluid Mech. 36, 33-54.

TOULOUKIAN, Y. S., ed. 1967. Thermophysical Properties of High Temperature Solid Materials. 4, Part 2. 1693-1714. New York: Macmillan.

TOWNSEND, A. A. 1962. Remarks on the Malkus theory of turbulent flow. Mécanique de la Turbulence, Marseille, ed. A. Favre. 167-180. Paris: Editions du Centre National de la Recherche Scientifique.

TURCOTTE, D. L. 1967. A boundary-layer theory for cellular convection. Int. J. Heat Mass Transfer. 10, 1065-1074.

TURCOTTE, D. L. and OXBURGH, E. R. 1967. Finite amplitude convective cells and continental drift. J. Fluid Mech. 28, 29-42.

UNION CARBIDE 1970. L-45 Silicone Fluids, Product Information. New York: Union Carbide Corp.

VENEZIAN, G. 1968. Effect of modulation on the onset of thermal convection. Division of Engineering and Applied Science Rep. No. 97-15. Pasadena: California Institute of Technology.

VENEZIAN, G. 1969. Effect of modulation on the onset of thermal convection. J. Fluid Mech. 35, 243-254.

VERONIS, G. 1966. Large-amplitude Bénard convection. J. Fluid Mech. 26, 49-68.

VON TIPPELSKIRCH, H. 1956. Über Konvektionszel len insbesondere im flüssigen Schwefel. Beitr. Phys. Atmos. 29, 37-54.

WANTLAND, J. L. 1970. A numerical evaluation of the thermal and hydrodynamic characteristics of laminar cellular convection between rigid horizontal surfaces. Heat Transfer 1970: Fourth Int. Heat Transfer Conf., Paris, eds. U. Grigull and E. W. P. Hahne. 4, NC 2.5.1-NC 2.5.10. Amsterdam: Elsevier.

WESSELING, P. 1969. Laminar convection cells at high Rayleigh number. J. Fluid Mech. 36, 625-637.

WILLIS, G. E. and DEARDORFF, J. W. 1967a. Development of short-period temperature fluctuations in thermal convection. Phys. Fluids. 10, 931-937.

WILLIS, G. E. and DEARDORFF, J. W. 1967b. Confirmation and renumbering of the discrete heat flux transitions of Malkus. Phys. Fluids. 10, 1861-1866.

WILLIS, G. E. and DEARDORFF, J. W. 1970. The oscillatory motions of Rayleigh convection. J. Fluid Mech. 44, 661-672.

APPENDIX A

TABLES AND FIGURES

TABLE 1.

CRITICAL RAYLEIGH NUMBERS

1. Analytical predictions - Reid and Harris (1958)

Boundary condition	Ra_{cr}	a_{cr}
Free-Free	657.511	2.2214
Rigid-Free	1100.65	2.682
Rigid-Rigid	1707.762	3.117

2. Experimental results

Investigator	Ra_{cr}	Working fluid
a. Free-Free boundary condition		
Goldstein and Graham (1969)	596 ± 57	10000 cs silicone oil
b. Rigid-Rigid boundary condition		
Schmidt and Milverton (1935)	1770 ± 170	water
Schmidt and Saunders (1938)	1700 1800	water
Malkus (1954a)	1700 ± 80	water, acetone
Silveston (1958)	1700 ± 51	water, ethylene glycol, 3 cs and 350 cs silicone oil
Gille and Goody (1964)	1786 ± 16	air
Thompson and Sogin (1966)	1793 ± 80	air, argon, carbon dioxide
Rossby (1966, 1969)	1680 1760 1810	mercury water 20 cs silicone oil
Goldstein and Chu (1966, 1968, 1969)	1783 ± 60	air
Willis and Deardorff (1967a)	1750	air

TABLE 2.

THE NUSSELT NUMBER AS A FUNCTION OF THE RAYLEIGH NUMBER

1. Analytical predictions

Source	Correlation	Ra Range	Remarks
a. Free-Free boundary condition			
Malkus (1963)	$Nu = (Ra/1533)^{1/3}$		Maximum heat flux, smallest scale unstable
Herring (1963)	$Nu = .31\,Ra^{1/3}$	$Ra > 3 \times 10^3$	"Quasilinear" approximation
Fromm (1965) [from Robinson (1967)]	$Nu \approx .25\,Ra^{1/3}$ $Pr \sim 1$		2 d rolls - numerical integration
Howard (1965)	$Nu = .325\,Ra^{1/3}$		One wave number, maximum heat flux - large Ra
Robinson (1965)	$Nu \approx .25\,Ra^{1/3}$		2 d rolls - boundary layer approximation
Robinson (1967)	$Nu \approx .27\,Ra^{1/3}$ $Pr = 1$		2 d rolls - boundary layer approximation
Turcotte and Oxburgh (1967)	$Nu = .167\,Ra^{1/3}$ $Pr \gg 1$		2 d rolls - boundary layer approximation

(continued)

TABLE 2.

1. Analytical predictions (continued)

Source	Correlation	Ra Range	Remarks
b. Rigid-Rigid boundary condition			
Pillow (1952)	$Nu = .86\,Ra^{.25}Pr^{.125}$		2 d rolls - boundary layer approximation
Kraichnan (1962)	$Nu \approx \begin{cases} .089\,Ra^{1/3} & Pr \geq 0.1 \\ .17\,(Ra\,Pr)^{1/3} & Pr \leq 0.1 \end{cases}$		Mixing length approximation
Malkus (1963)	$Nu = (Ra/2533)^{1/3}$		Maximum heat flux, smallest scale unstable
Herring (1964)	$Nu = .135\,Ra^{1/3}$	$Ra \geq 10^4$	"Quasilinear" approximation
Fromm (1965) [from Robinson (1967)]	$Nu \approx .19\,Ra^{.28}$ $Pr \sim 1$		2 d rolls - numerical integration
Catton (1966)	$Nu = .157\,Ra^{.285}$	$Ra > 10^4$	Power integral technique
Leontiev and Kirdyashkin (1966)	$Nu = .206\,Ra^{1/4}$	$Ra < 1.5 \times 10^5$	Boundary layer approximation
	$Nu = .108\,Ra^{1/3}$	$Ra > 1.5 \times 10^5$	
Robinson (1967)	$Nu = .15\,Ra^{1/3}$ $Pr = 1$		2 d rolls - boundary layer approximation
Turcotte (1967)	$Nu = .304\,Ra^{1/4}$ $Pr \gg 1$		2 d rolls - boundary layer approximation

(continued)

TABLE 2.

2. Experimental results - Rigid-Rigid boundary condition

Source	Correlation	Ra Range	Working Fluid
de Graaf and van der Held (1953)	$Nu = .0595\,Ra^{.40}$	$1.3\times10^{3} < Ra < 3.3\times10^{4}$	air (Pr = 0.67)
	$Nu \approx 3.8$	$3.3\times10^{4} < Ra < 1.3\times10^{5}$	
	$Nu = .0494\,Ra^{.37}$	$Ra > 1.3\times10^{5}$	
Malkus (1954a)	$Nu = (Ra/650)^{.260}$	$Ra < 5\times10^{5}$	water and acetone
	$Nu = (Ra/2000)^{.325}$	$Ra > 5\times10^{5}$	
Silveston (1958)	$Nu = .0012\,Ra^{.90}$	$1700 < Ra < 3000$	water, ethylene glycol, heptane, 3 cs and 350 cs silicone oil
	$Nu = .24\,Ra^{.25}$	$3000 < Ra < 8000\,Pr^{.2}$	
	$Nu = .30\,Ra^{.16}\,Pr^{.05}$	$8000\,Pr^{.1} < Ra < 18000\,Pr^{.2}$	
	$Nu = .10\,Ra^{.31}\,Pr^{.05}$		
Globe and Dropkin (1959)	$Nu = .069\,Ra^{1/3}\,Pr^{.074}$	$1.51\times10^{5} < Ra < 6.76\times10^{8}$	water, mercury, 1.5 cs, 50 cs and 1000 cs silicone oil
		$0.02 < Pr < 8750$	
O'Toole and Silveston (1961)	$Nu = .00238\,Ra^{.816}$	$1700 < Ra < 3500$	used data from other works
	$Nu = .229\,Ra^{.251}$	$3500 < Ra < 10^{5}$	
	$Nu = .104\,Ra^{.305}\,Pr^{.084}$	$10^{5} < Ra < 10^{9}$	
Dropkin and Somerscales (1965)	$Nu = .069\,Ra^{1/3}\,Pr^{.074}$	$5\times10^{4} < Ra < 7.17\times10^{8}$	water, mercury, 2 cs and 1000 cs silicone oil
		$0.02 < Pr < 11560$	

(continued)

TABLE 2.

2. Experimental results (continued)

Source	Correlation	Ra Range	Working Fluid
Ingersoll (1966)	$Nu = .0784\,Ra^{1/3} + .77$	$8 \times 10^3 < Ra < 2.6 \times 10^7$	0.65 cs silicone oil
	$Nu = .0820\,Ra^{1/3} + .86$	$8 \times 10^3 < Ra < 8 \times 10^6$	1.5 cs silicone oil
	$Nu = .0827\,Ra^{1/3} + .82$	$8 \times 10^3 < Ra < 7 \times 10^6$	kerosene
Goldstein and Chu (1966, 1968, 1969)	$Nu = .123\,Ra^{.294}$	$6 \times 10^5 < Ra < 2 \times 10^8$	air
Rossby (1966, 1969)	$Nu = .184\,Ra^{.281}$	$Ra > 4 \times 10^3$	20 cs silicone oil
	$Nu = .131\,Ra^{.30}$	$Ra > 3.4 \times 10^4$	water
	$Nu = .147\,Ra^{.257}$	$Ra > 2.0 \times 10^4$	mercury
Somerscales and Gazda (1968, 1969)	$Nu = .196\,Ra^{.283}$	$7.4 \times 10^5 < Ra < 3.2 \times 10^8$	0.65 cs and 2 cs silicone oil

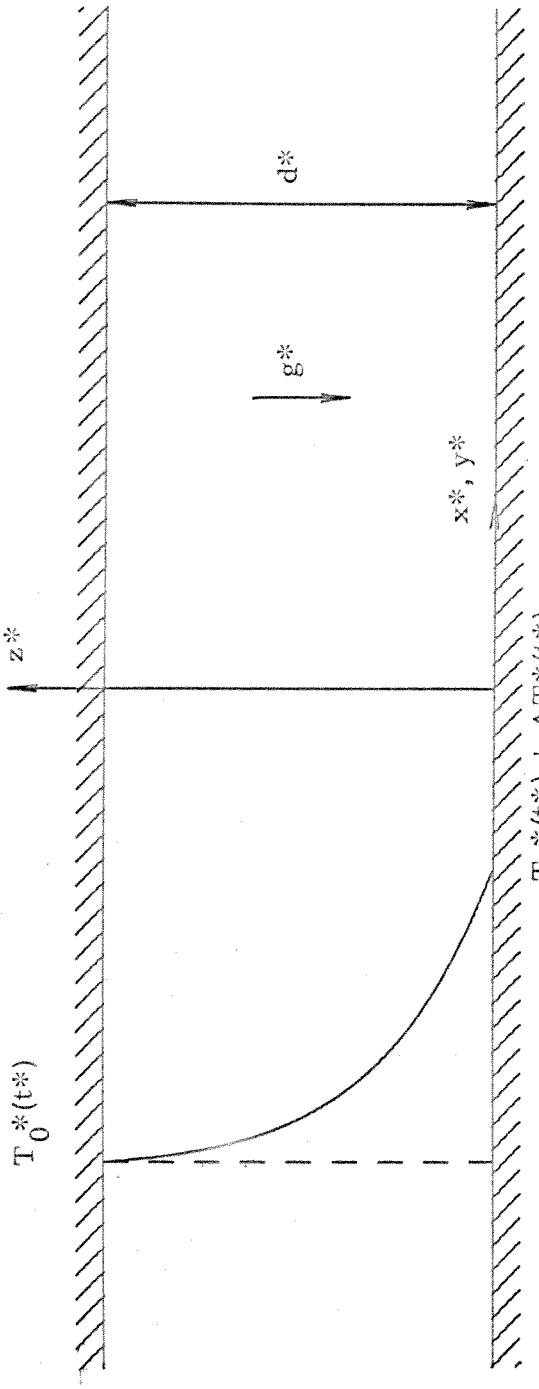

Figure 1. Fluid Layer with Nomenclature.

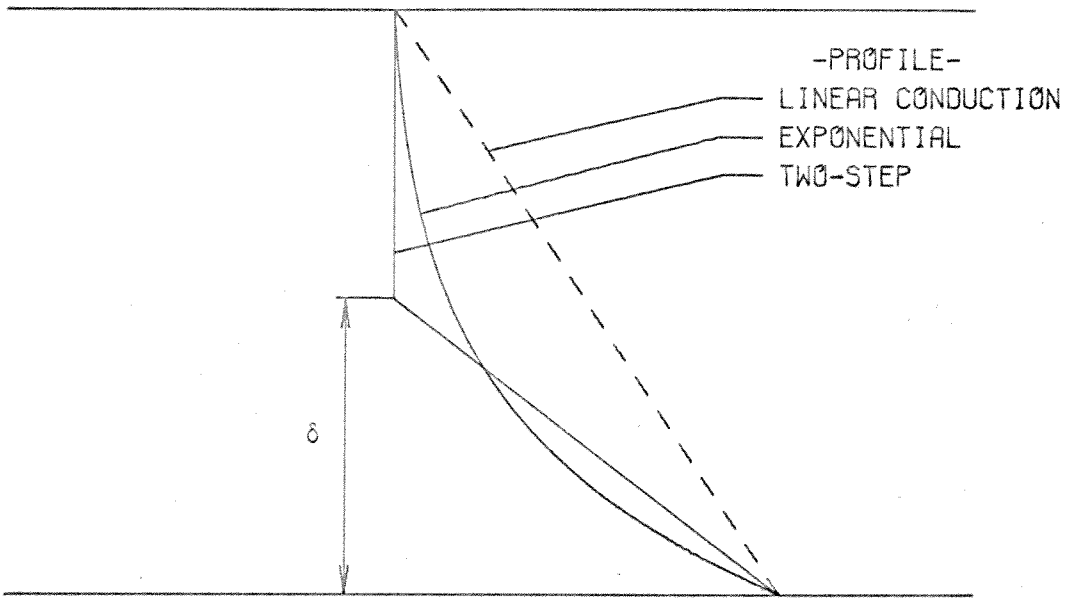

Figure 2. Approximate Temperature Profiles.

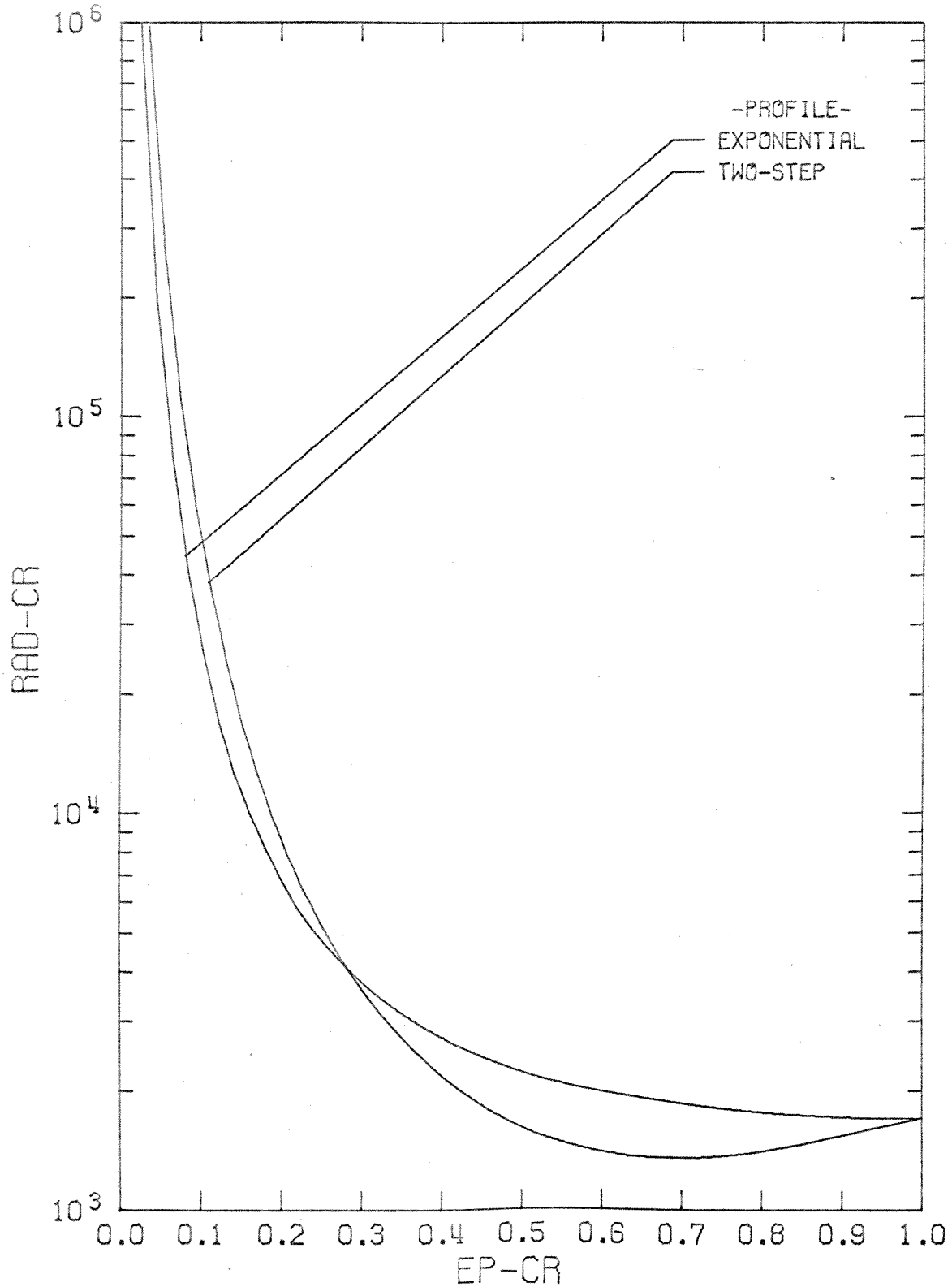

Figure 3. Critical Rayleigh Number versus Critical Thermal Thickness

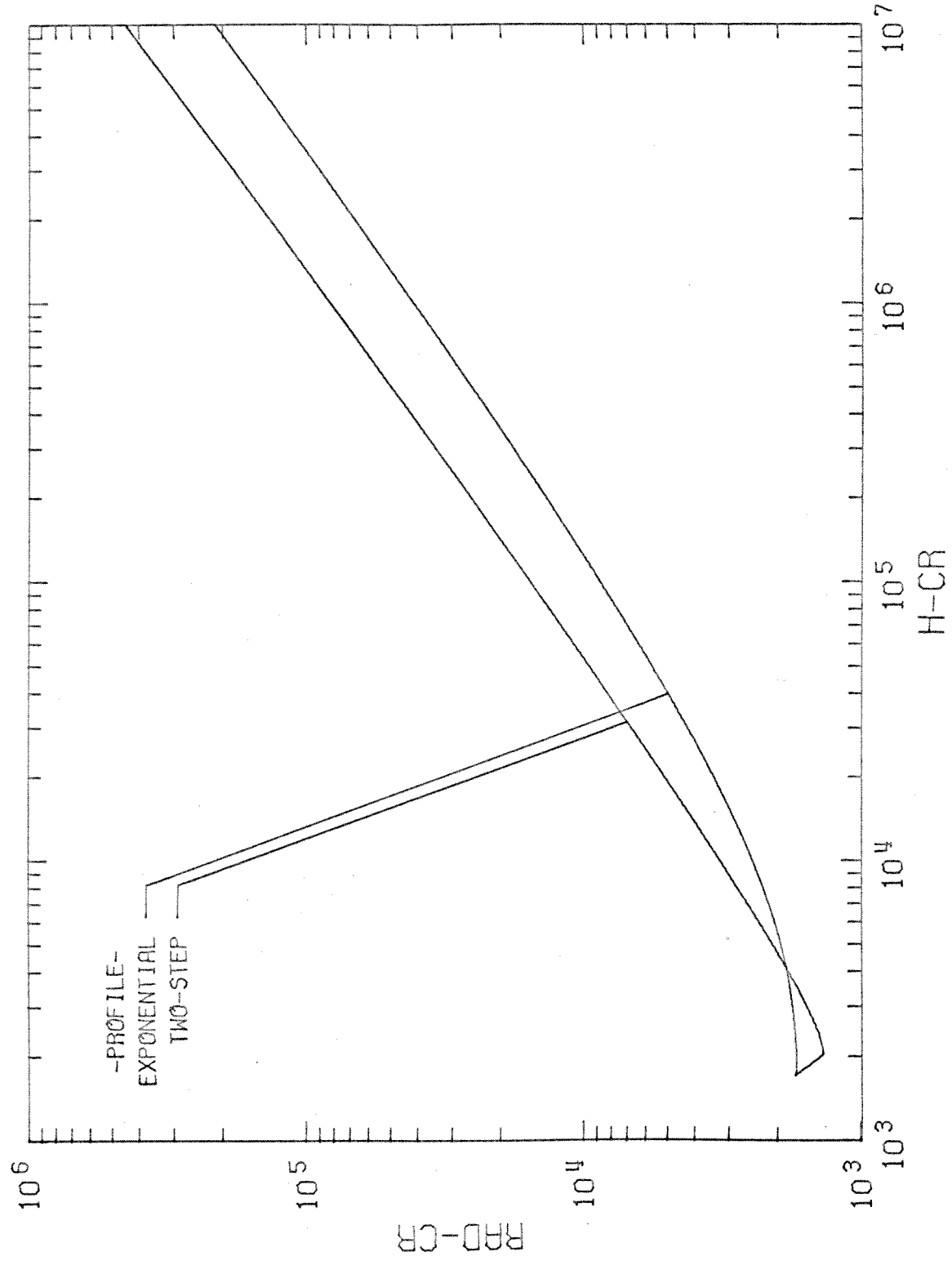

Figure 4. Critical Rayleigh Number versus Critical Lower Surface Heat Flux

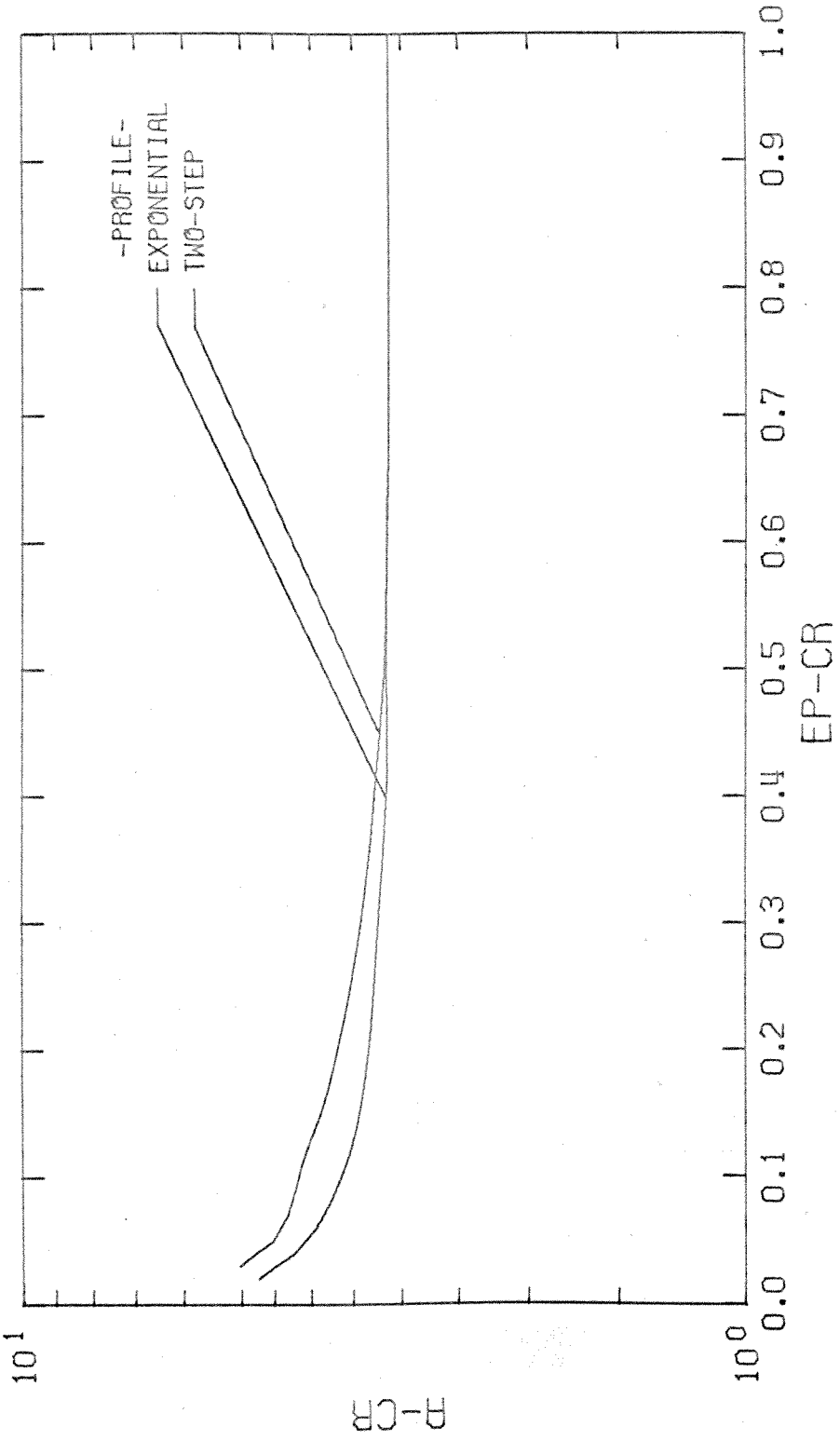

Figure 5. Critical Wave Number versus Critical Thermal Thickness

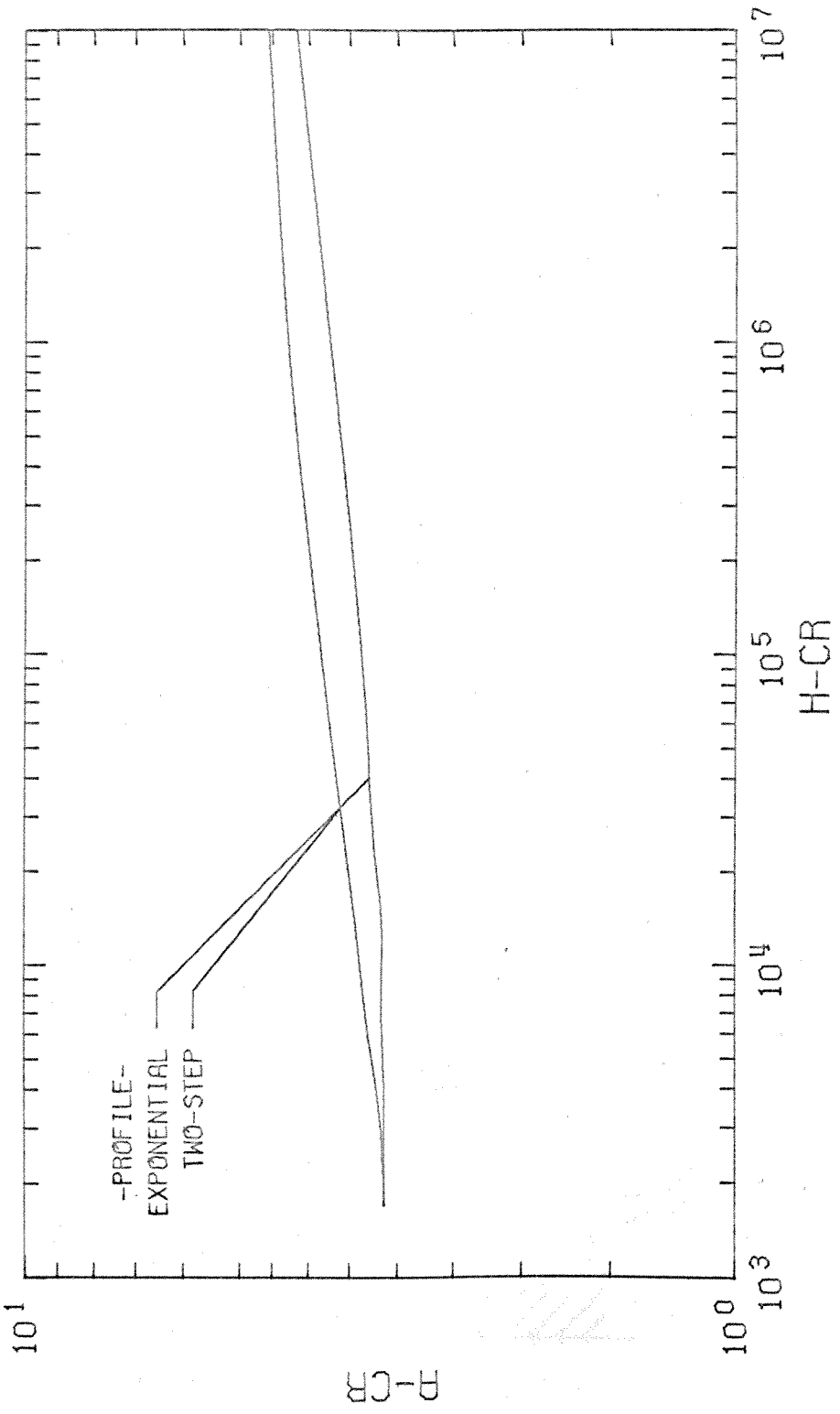

Figure 6. Critical Wave Number versus Critical Lower Surface Heat Flux

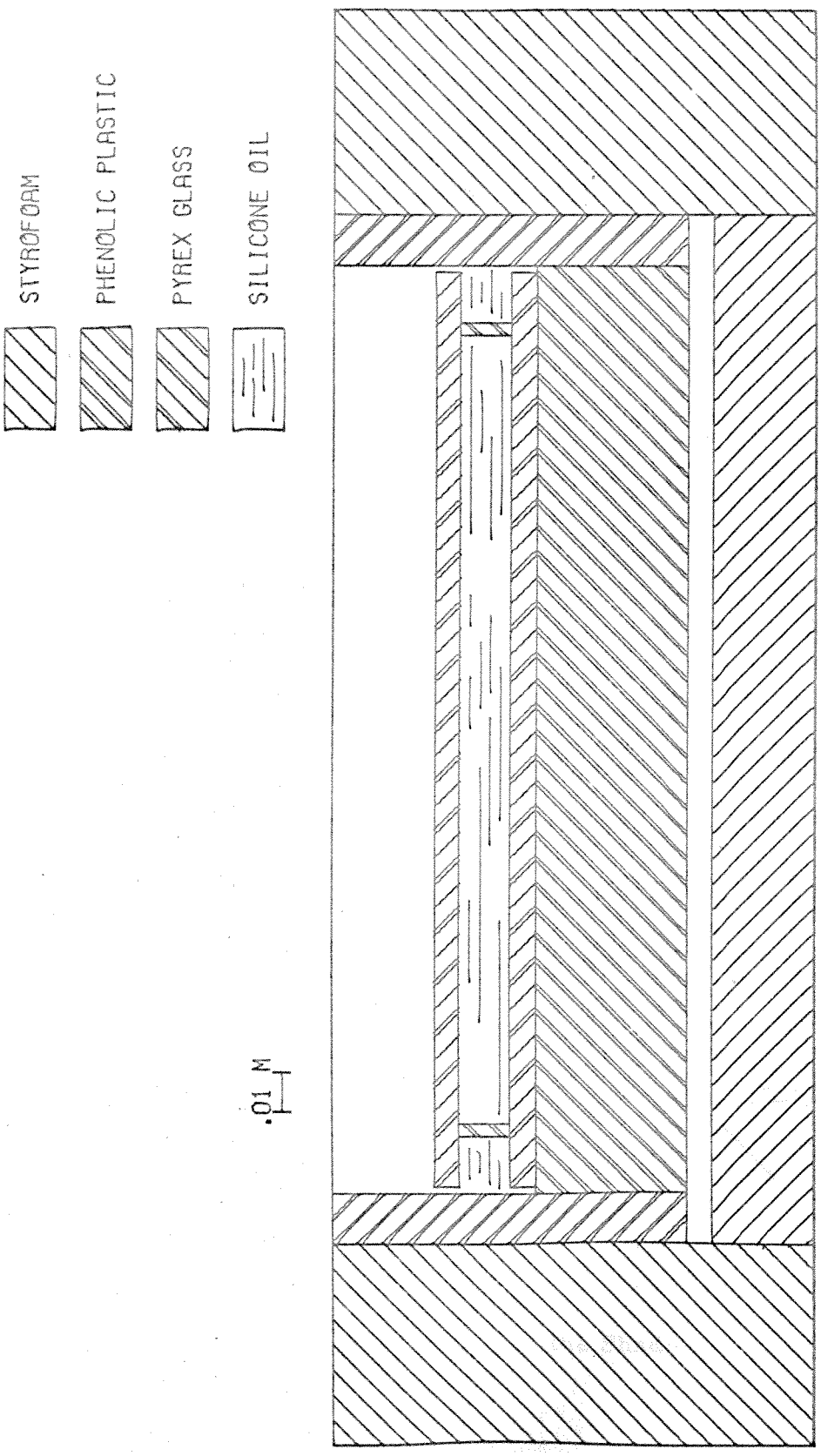

Figure 7. Experimental Apparatus in Cross-Section.

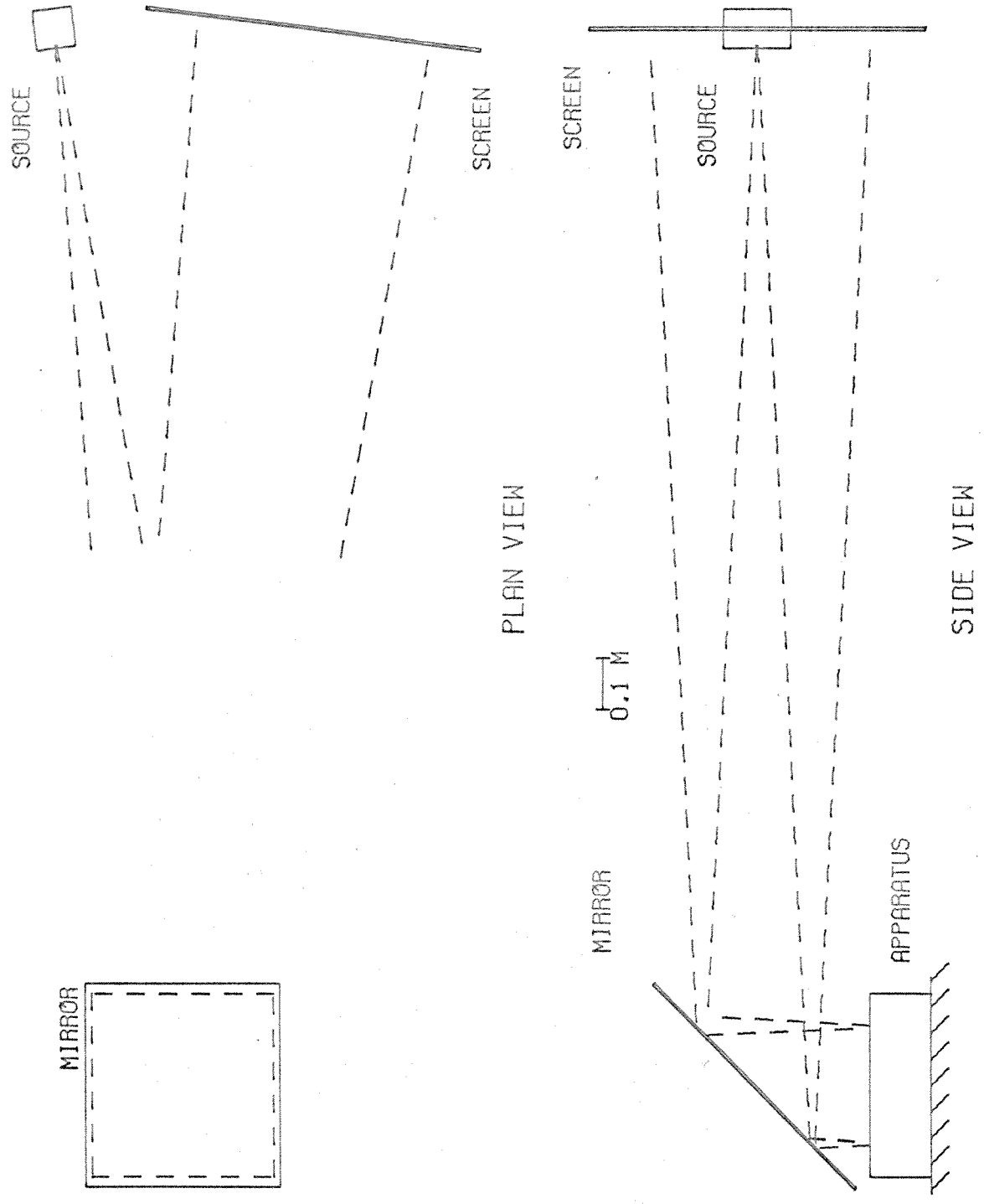

Figure 8. Schematic Drawing of the Shadowgraph Optics.

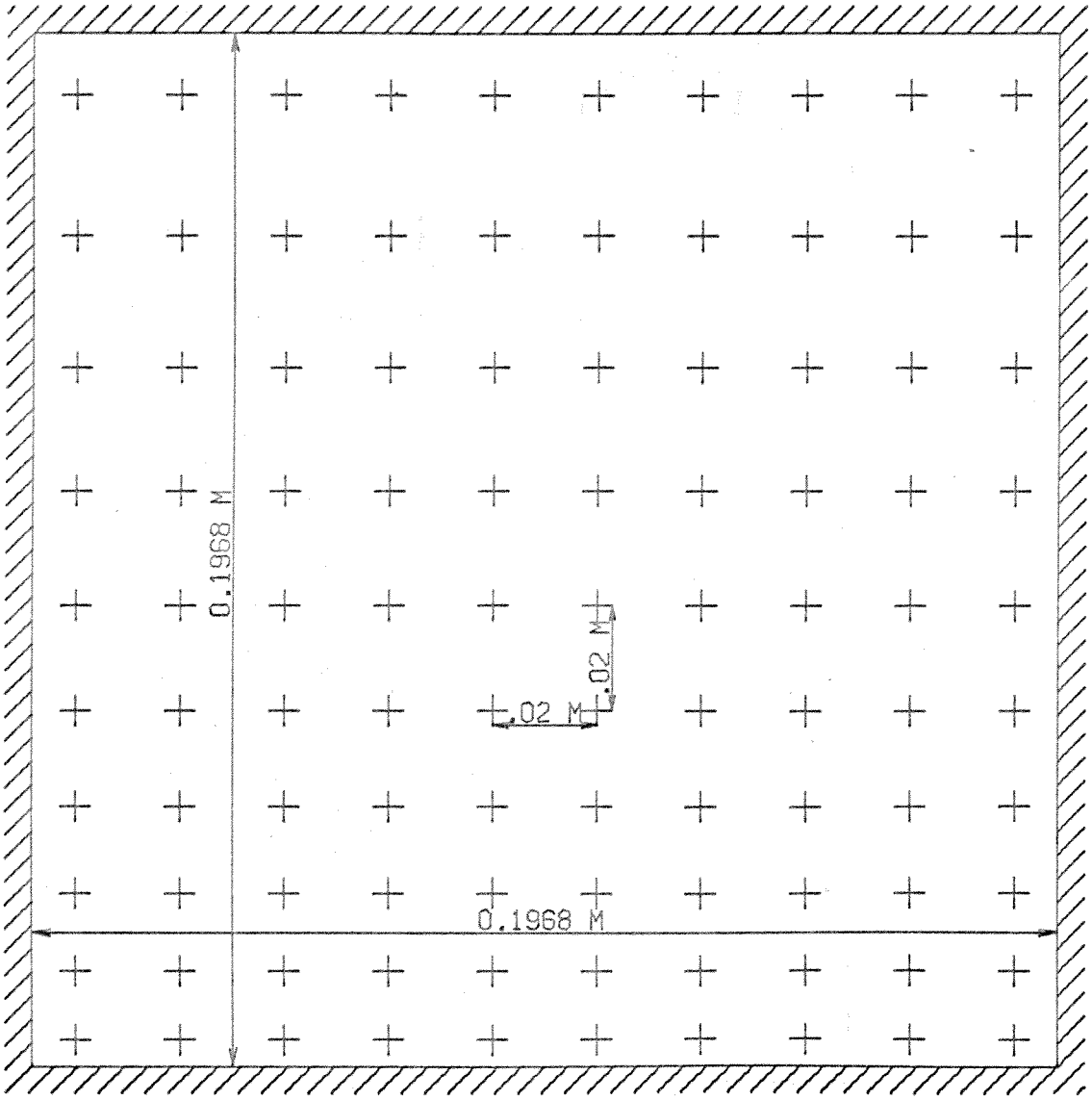

Figure 9. Distortion of Chamber Image due to Non-Parallel Optics.

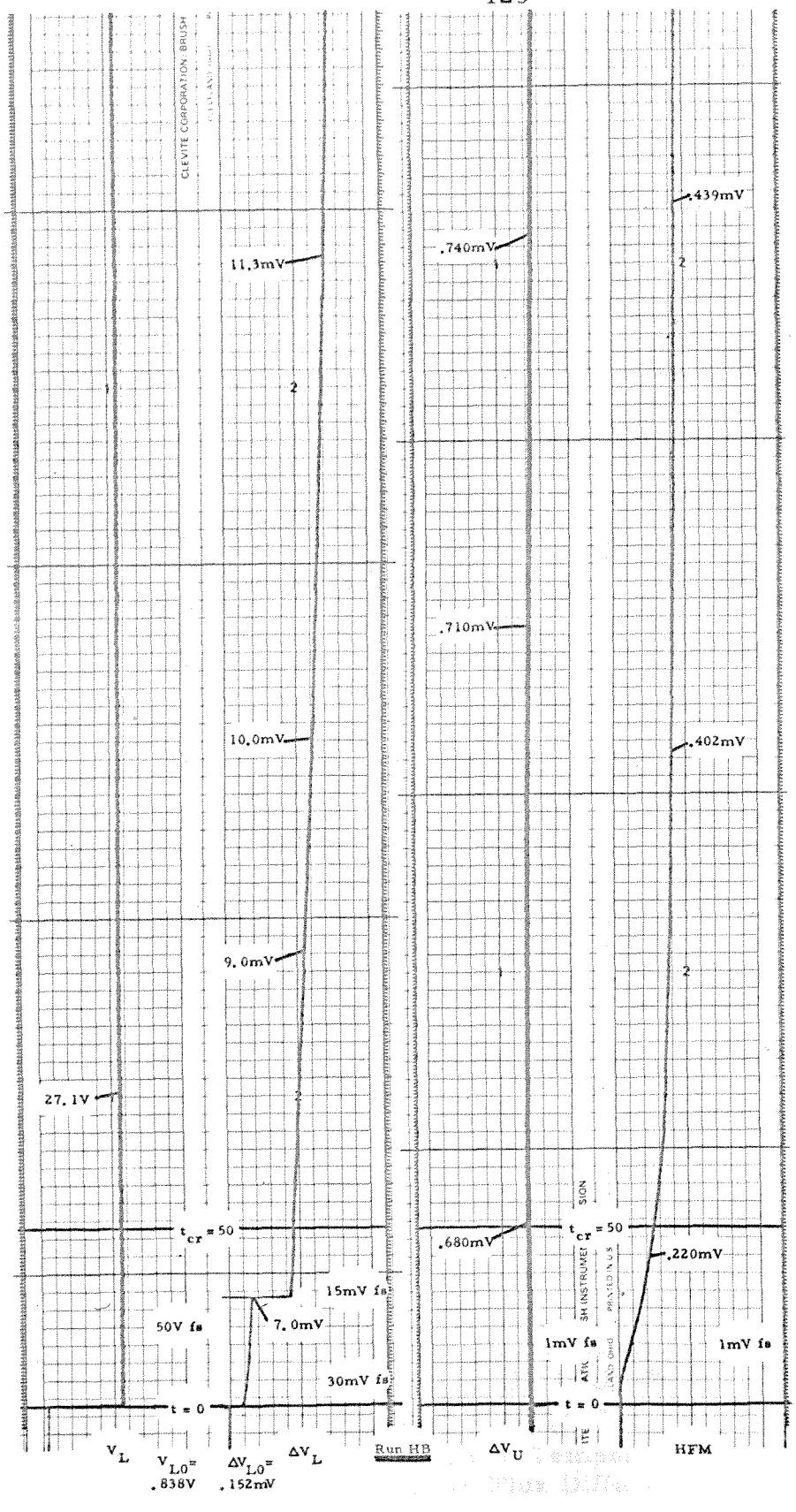

Figure 10. Typical Chart Recordings from an Experimental Run.

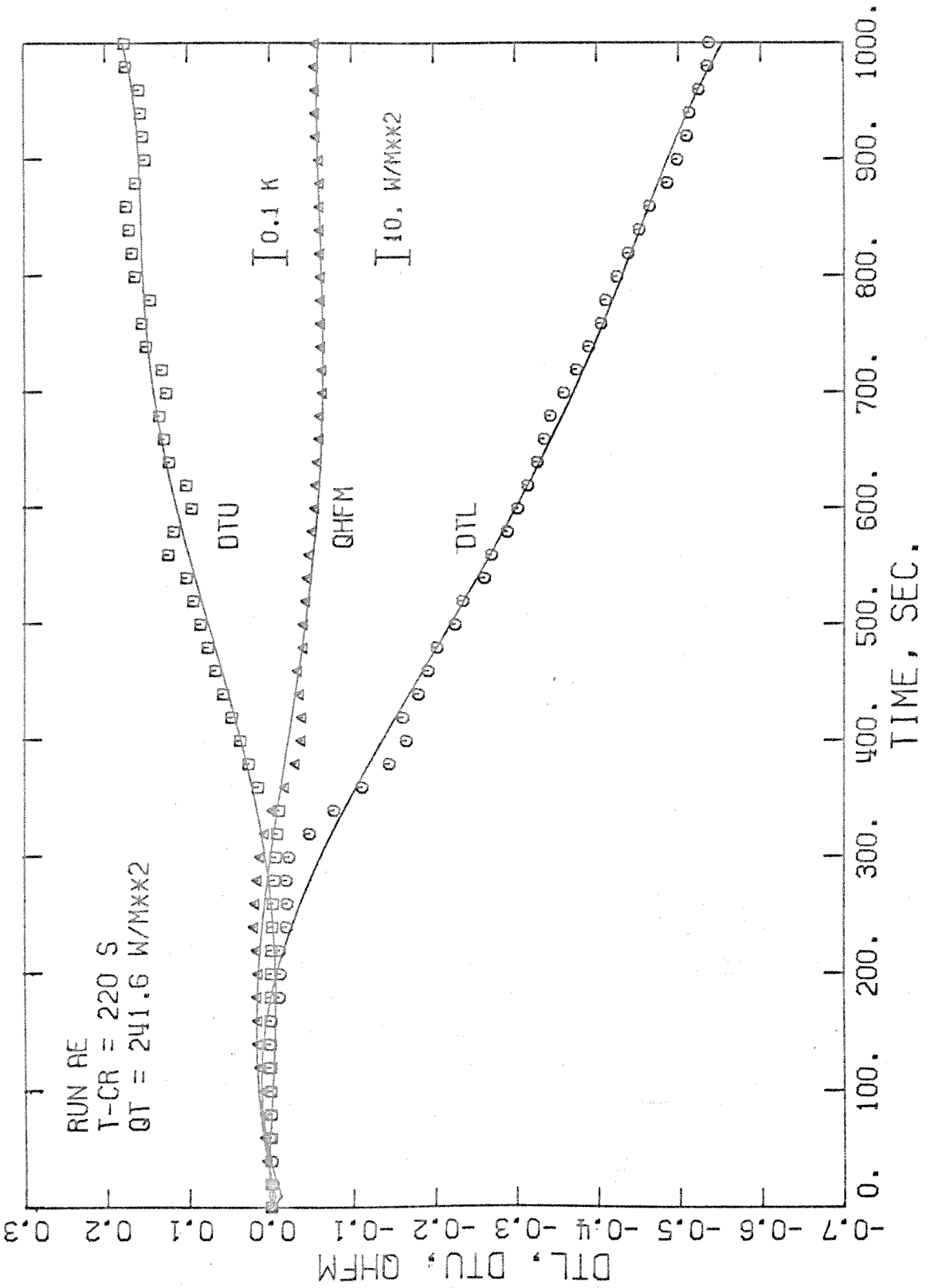

Figure 11. Typical Normalized Temperature Differences and Normalized Heat Flux Difference as a Funtion of Time

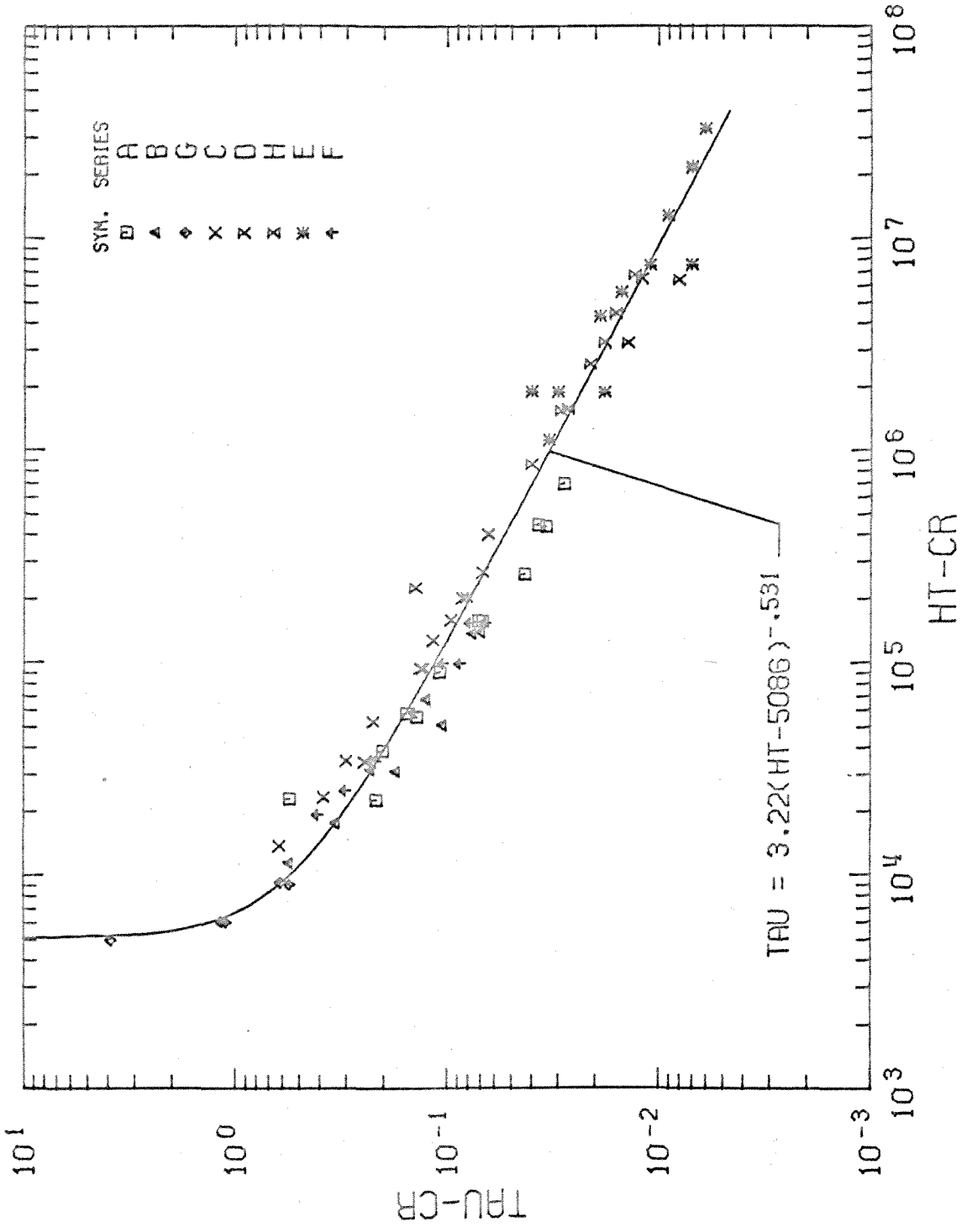

Figure 12. Critical Time versus Total Heat Generation Rate.

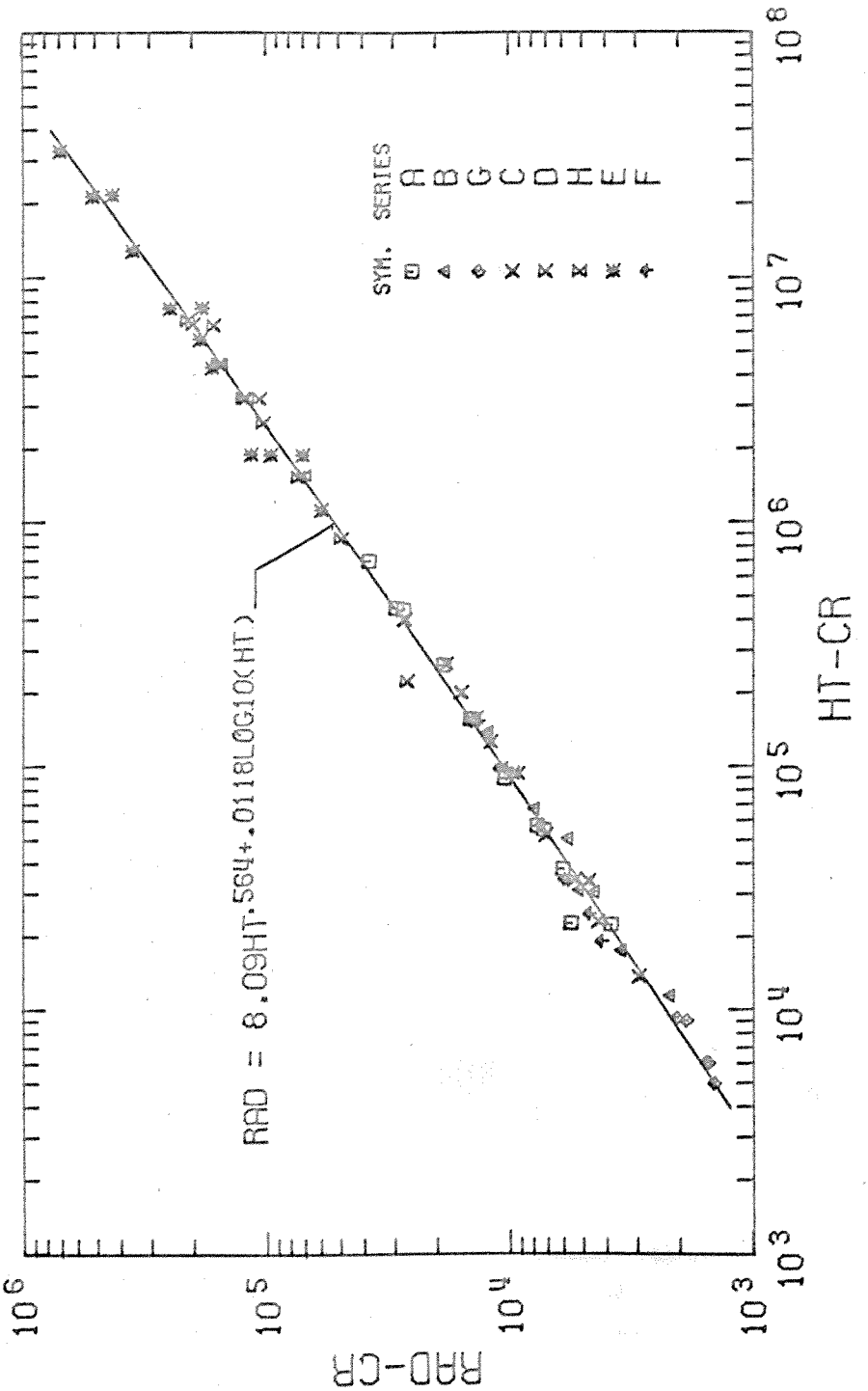

Figure 13. Critical Rayleigh Number versus Total Heat Generation Rate.

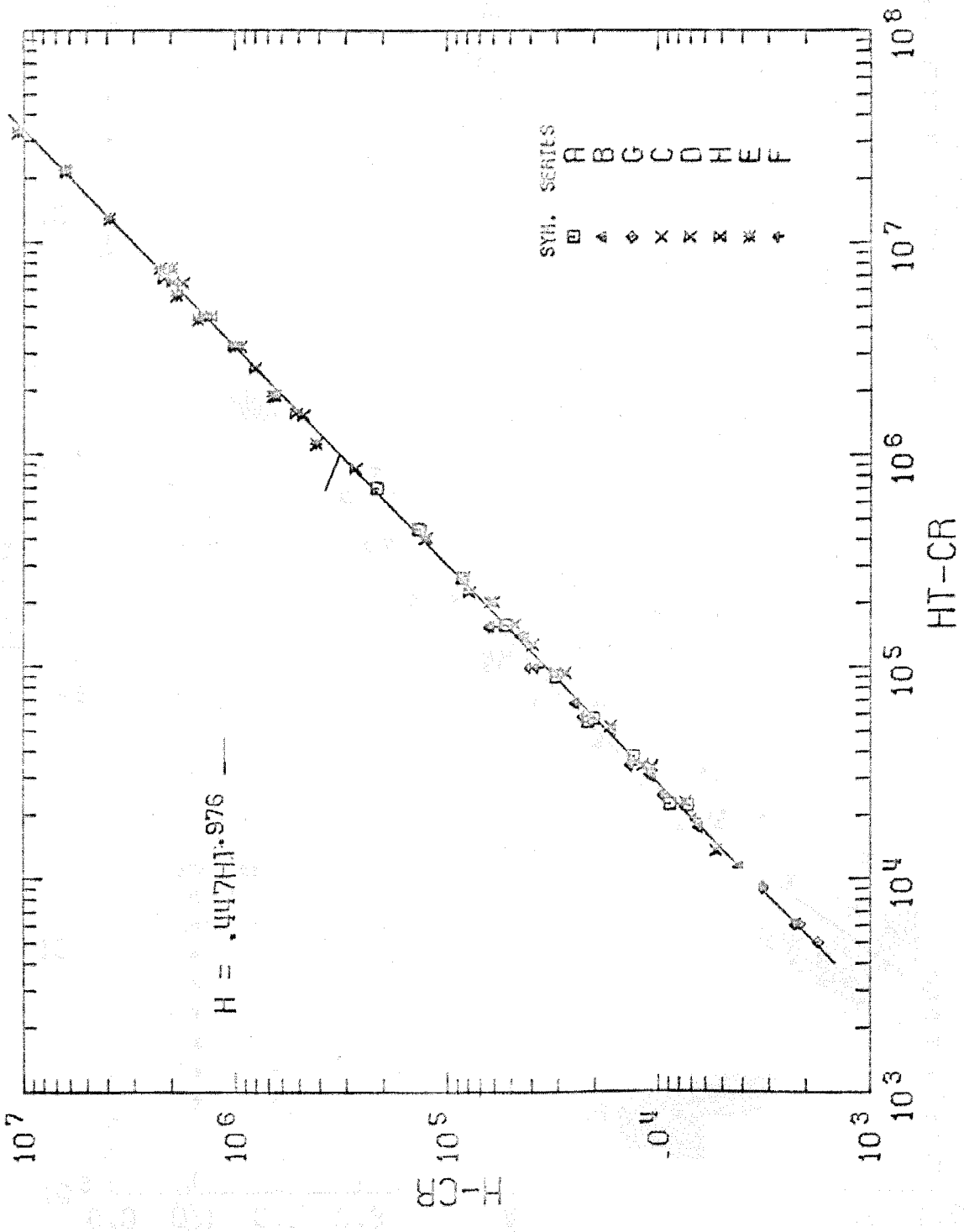

Figure 14. Critical Lower Surface Heat Flux versus Total Heat Generation Rate.

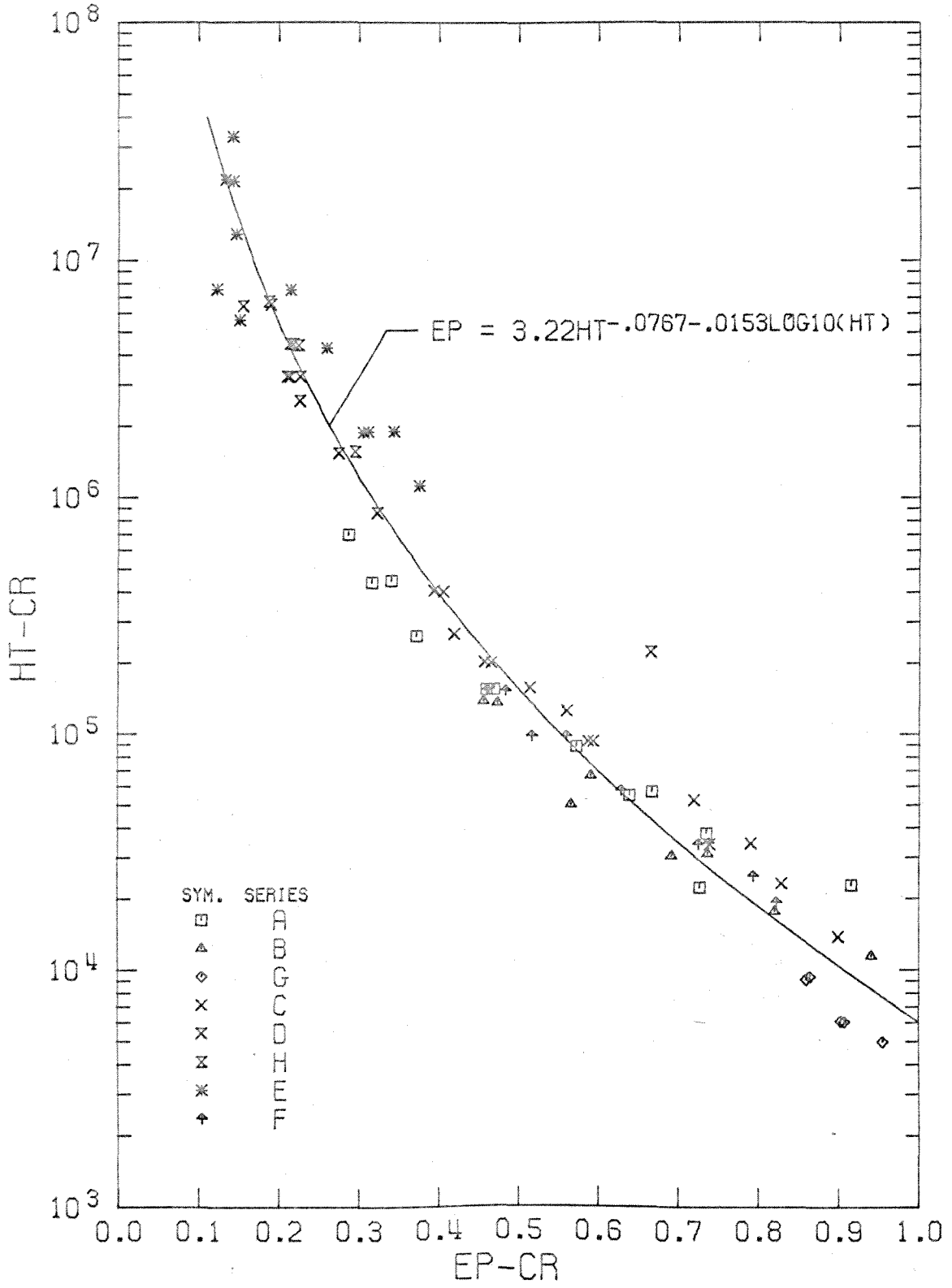

Figure 15. Critical Thermal Thickness versus Total Heat Generation Rate.

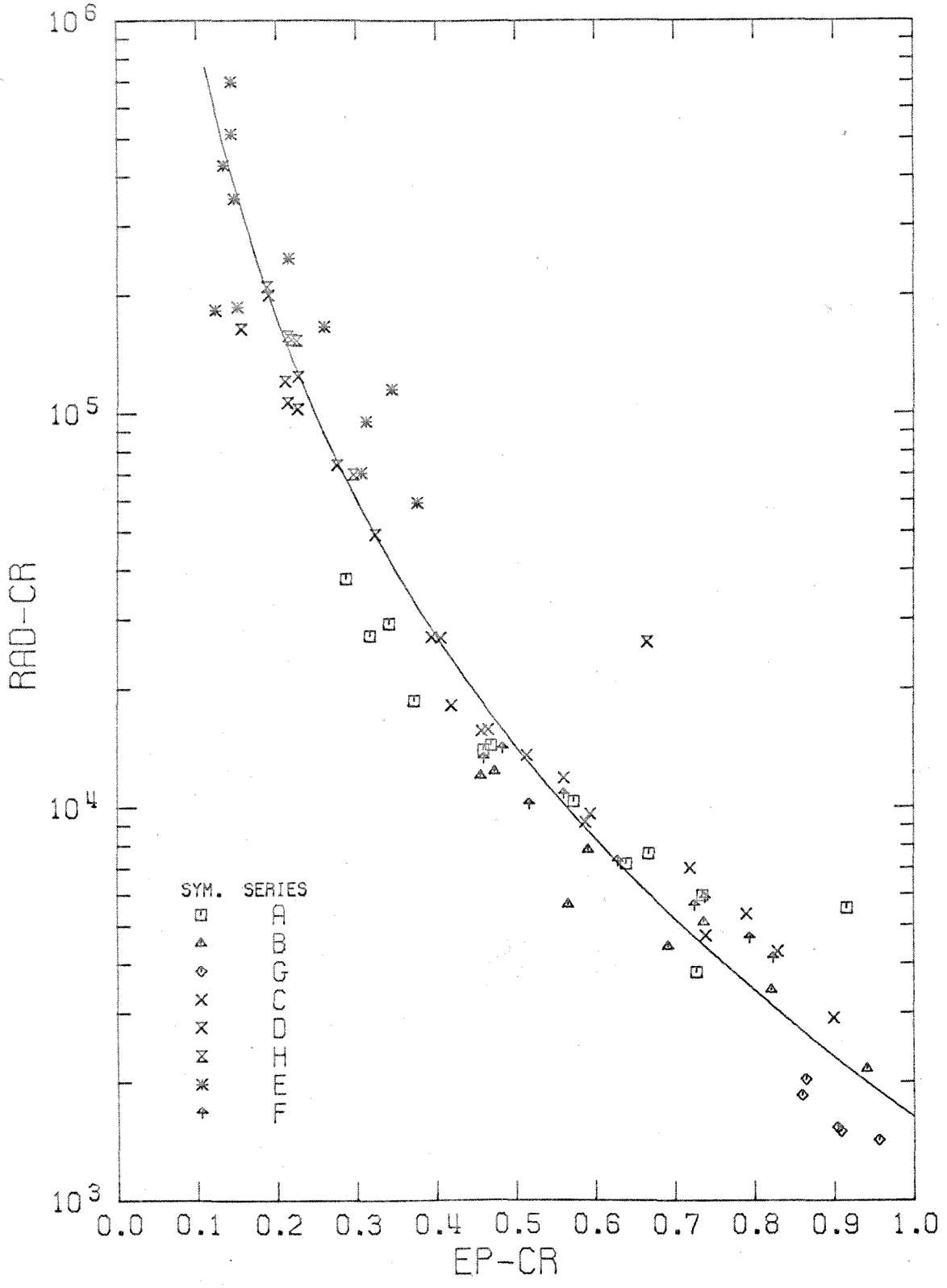

Figure 16. Critical Rayleigh Number versus Critical Thermal Thickness.

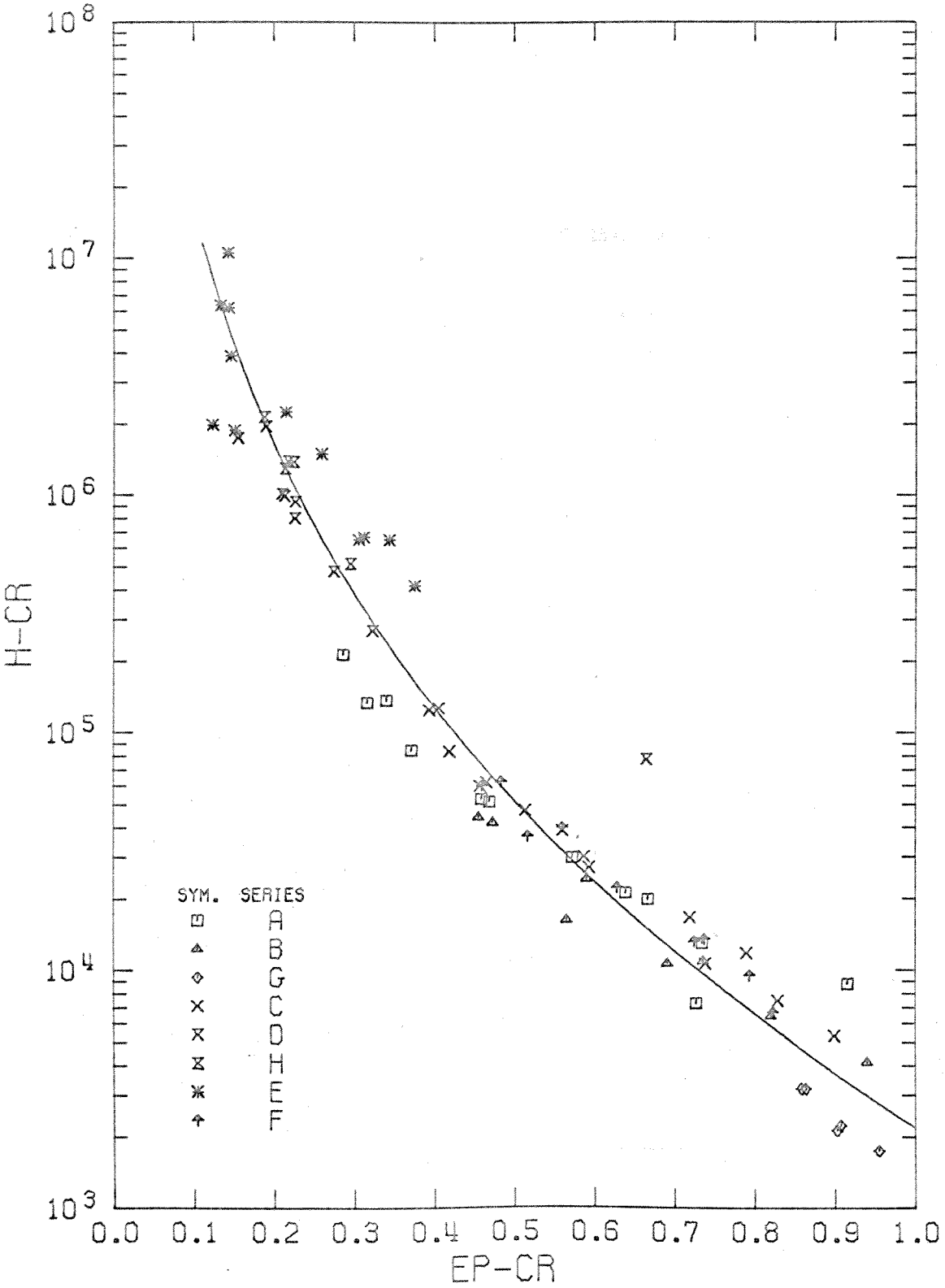

Figure 17. Critical Lower Surface Heat Flux versus Thermal Thickness.

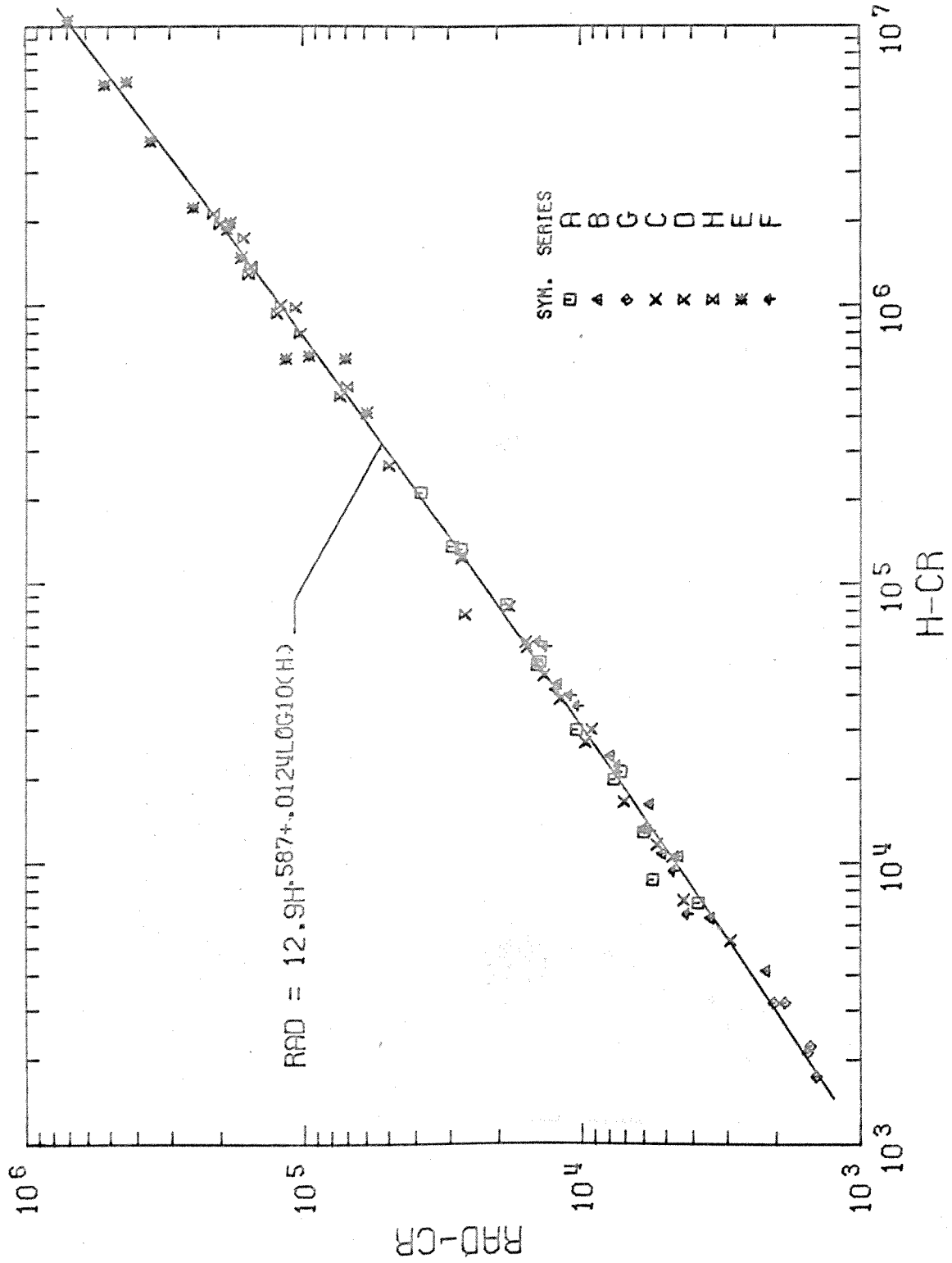

Figure 18. Critical Rayleigh Number versus Critical Lower Surface Heat Flux.

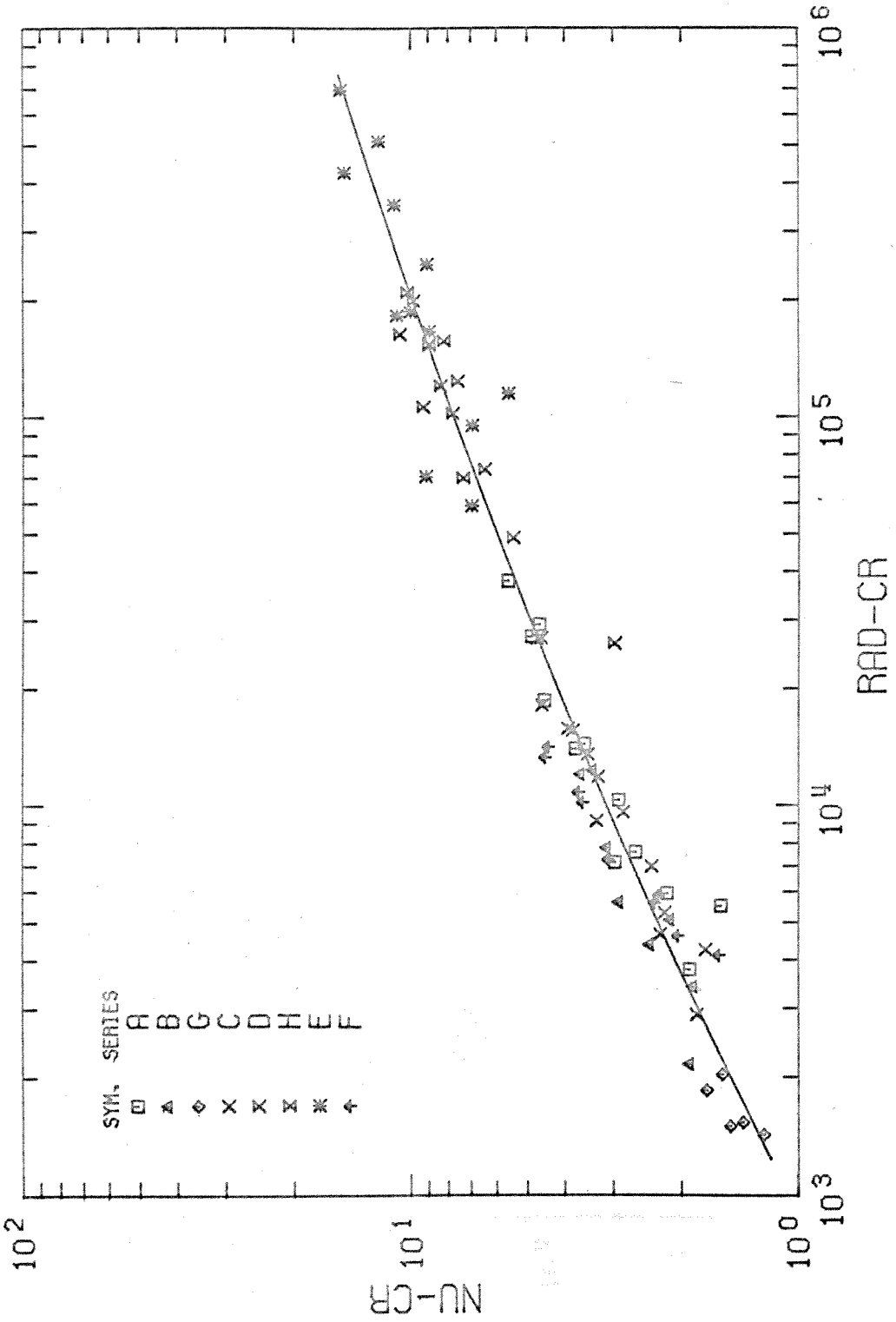

Figure 19. Critical Nusselt Number versus Critical Rayleigh Number.

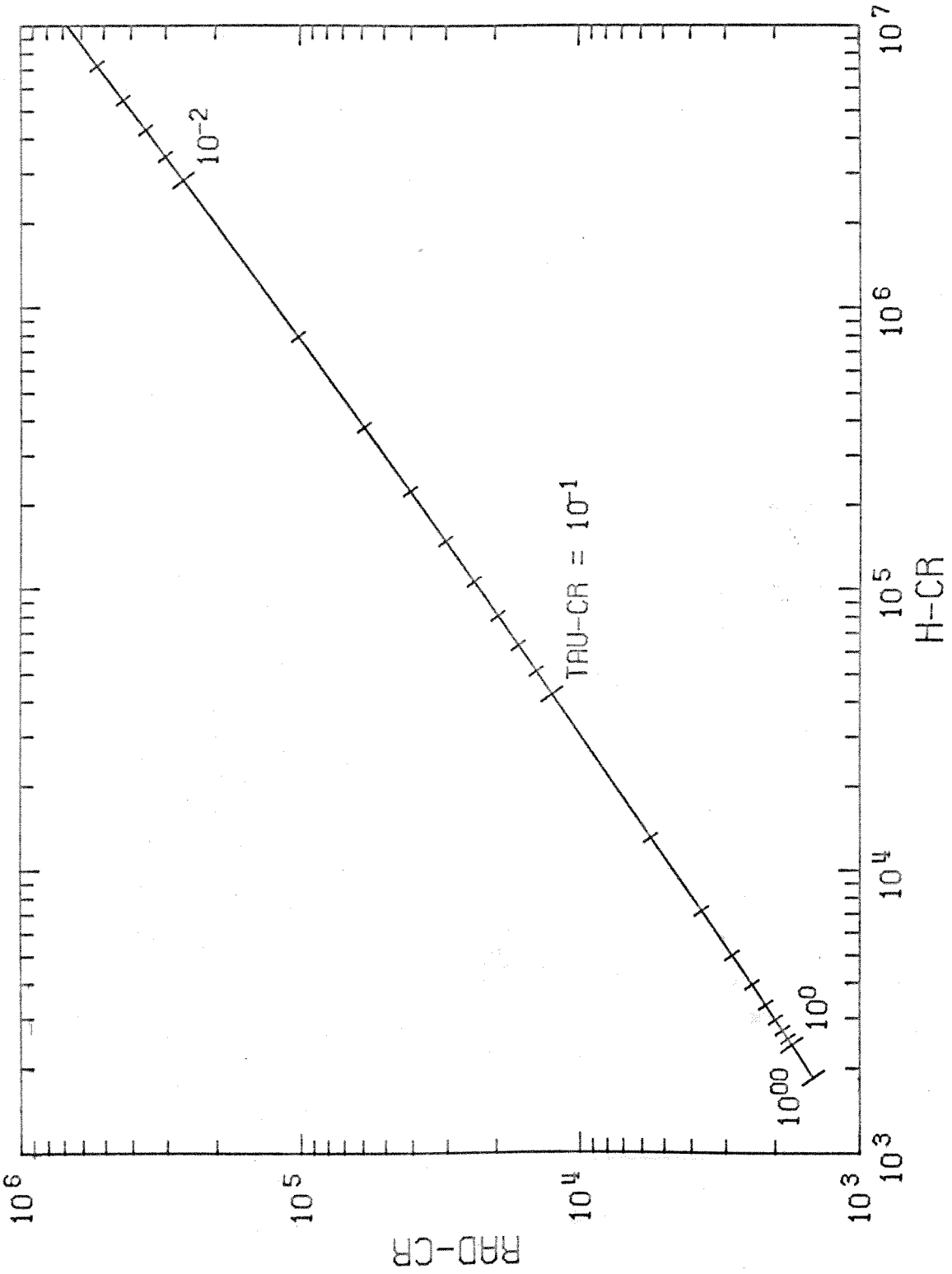

Figure 20. Critical Time as a Function of Critical Rayleigh Number and Critical Lower Surface Heat Flux.

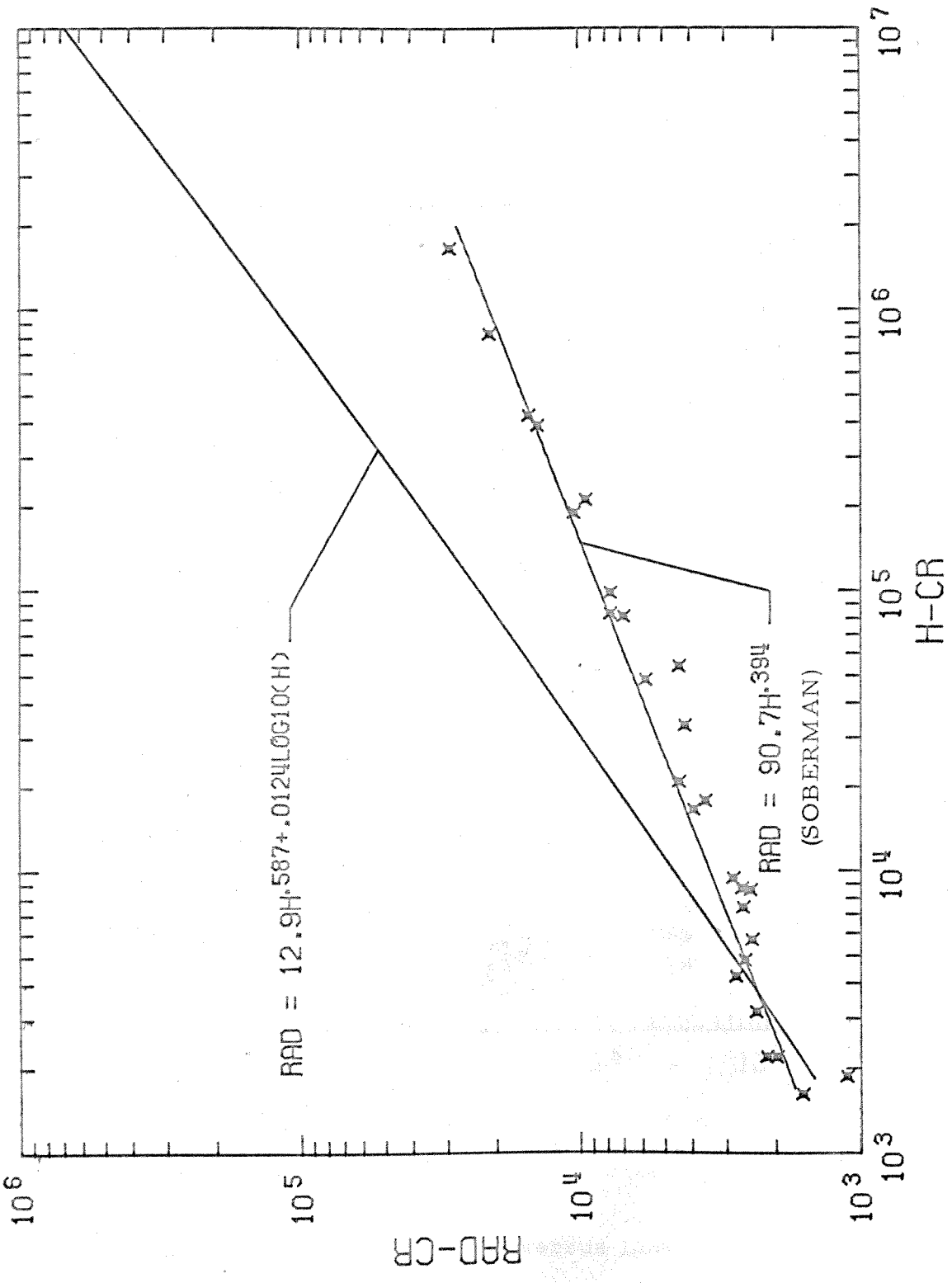

Figure 21. Comparison of Present Results with Results of Soberman (1959).

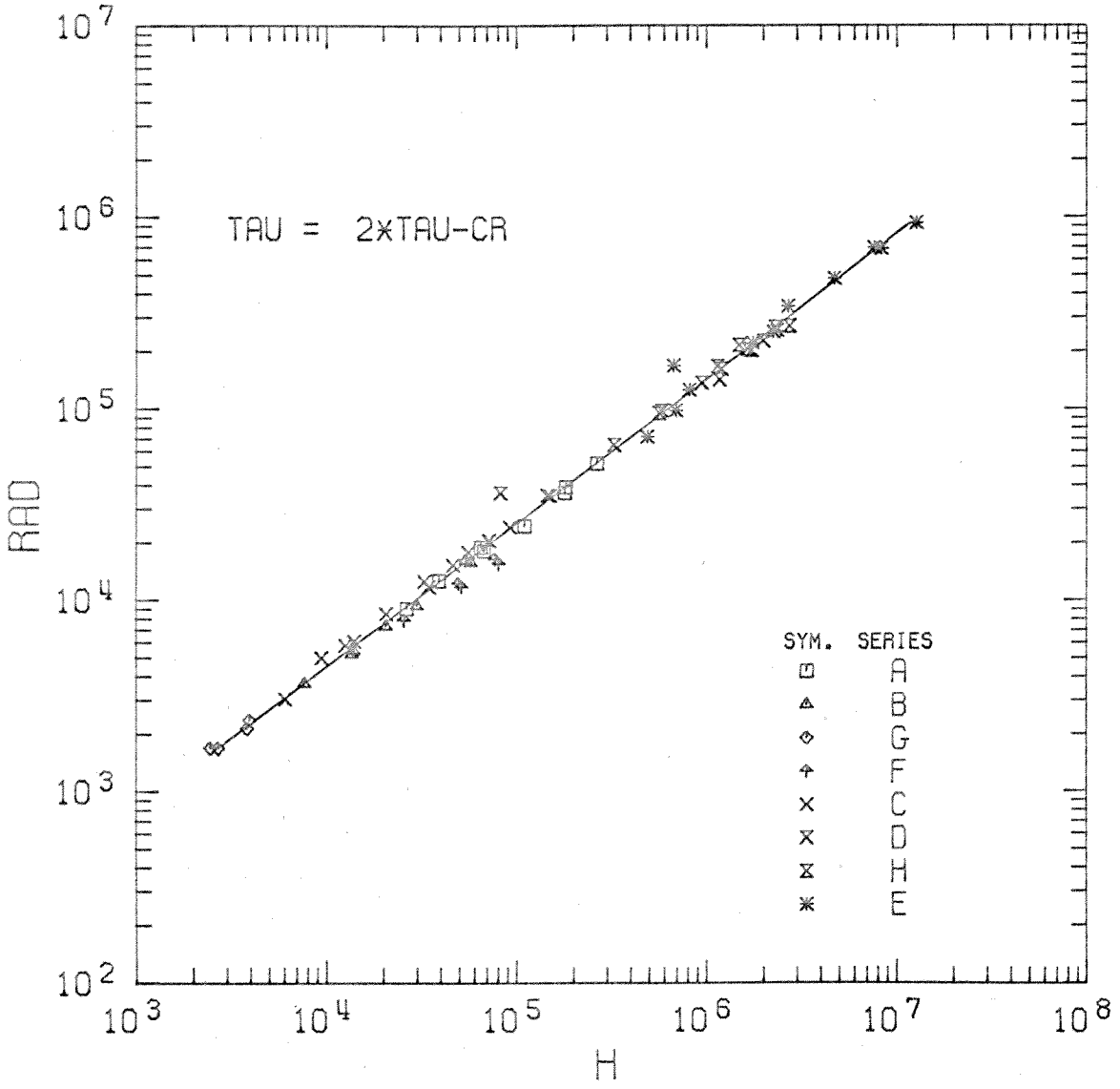

Figure 22. Rayleigh Number versus Lower Surface Heat Flux at $\tau = 2\tau_{cr}$.

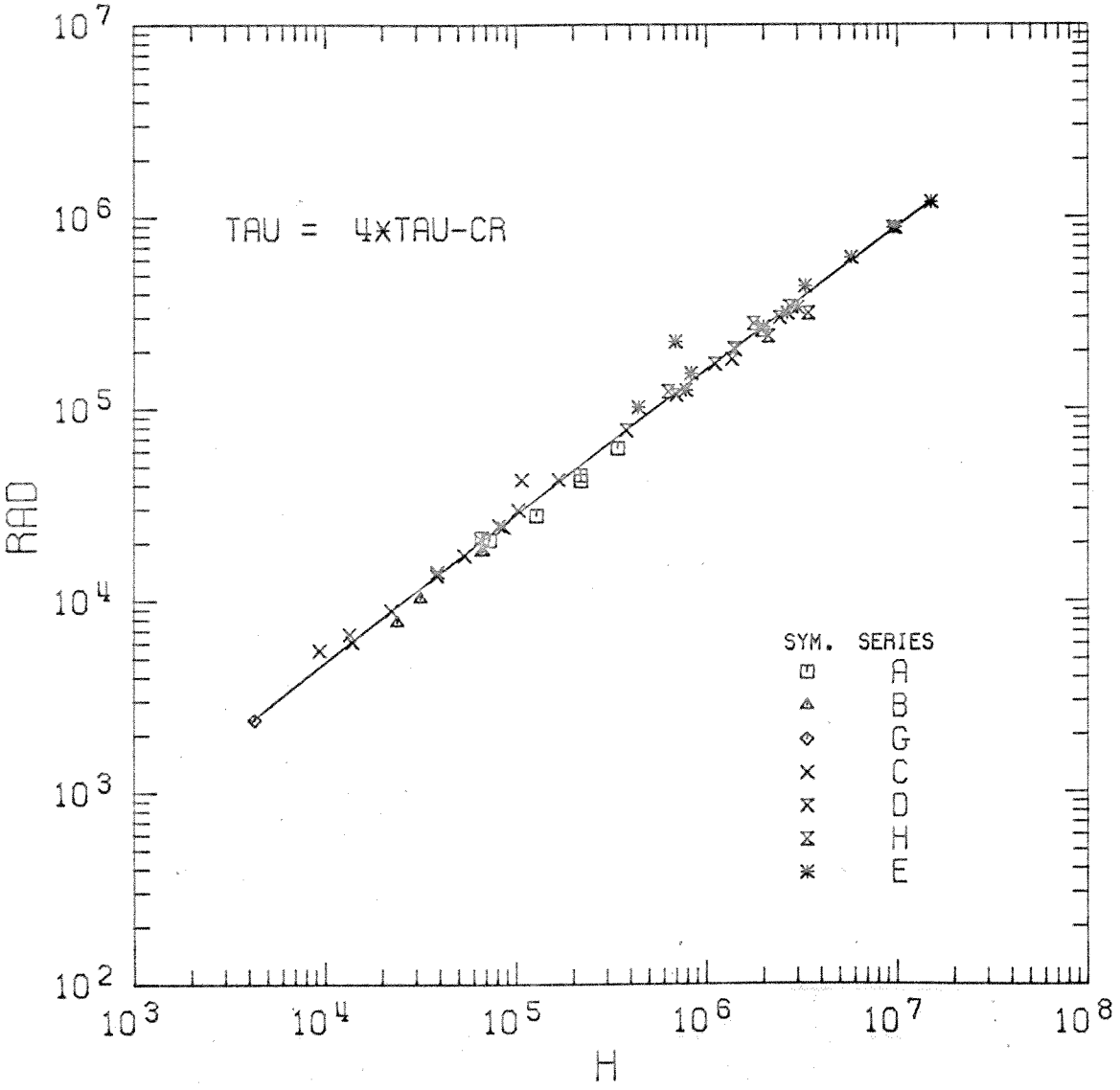

Figure 23. Rayleigh Number versus Lower Surface Heat Flux at $\tau = 4\tau_{cr}$.

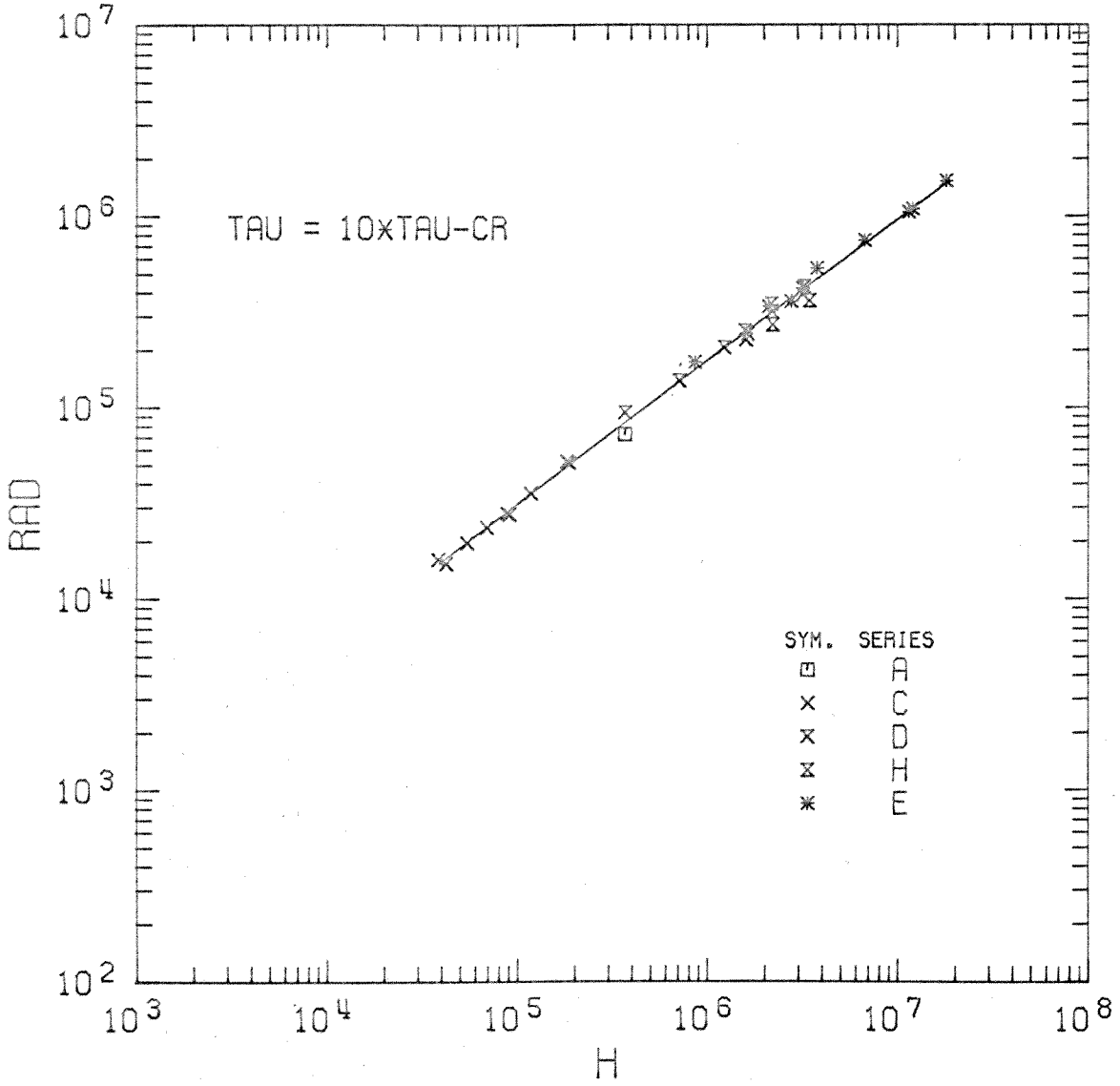

Figure 24. Rayleigh Number versus Lower Surface Heat Flux at $\tau = 10\,\tau_{cr}$.

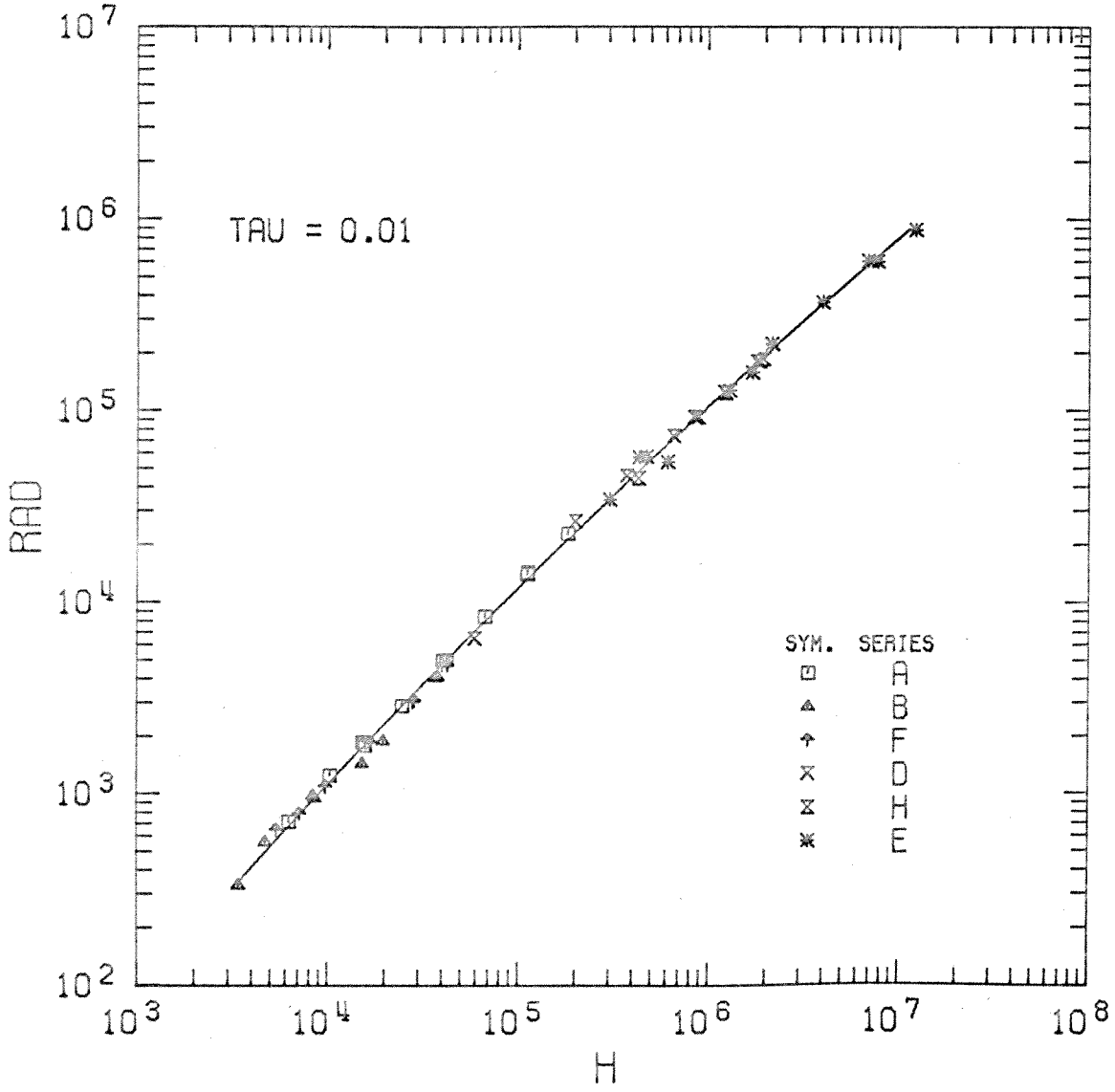

Figure 25. Rayleigh Number versus Lower Surface Heat Flux at $\tau = 0.01$.

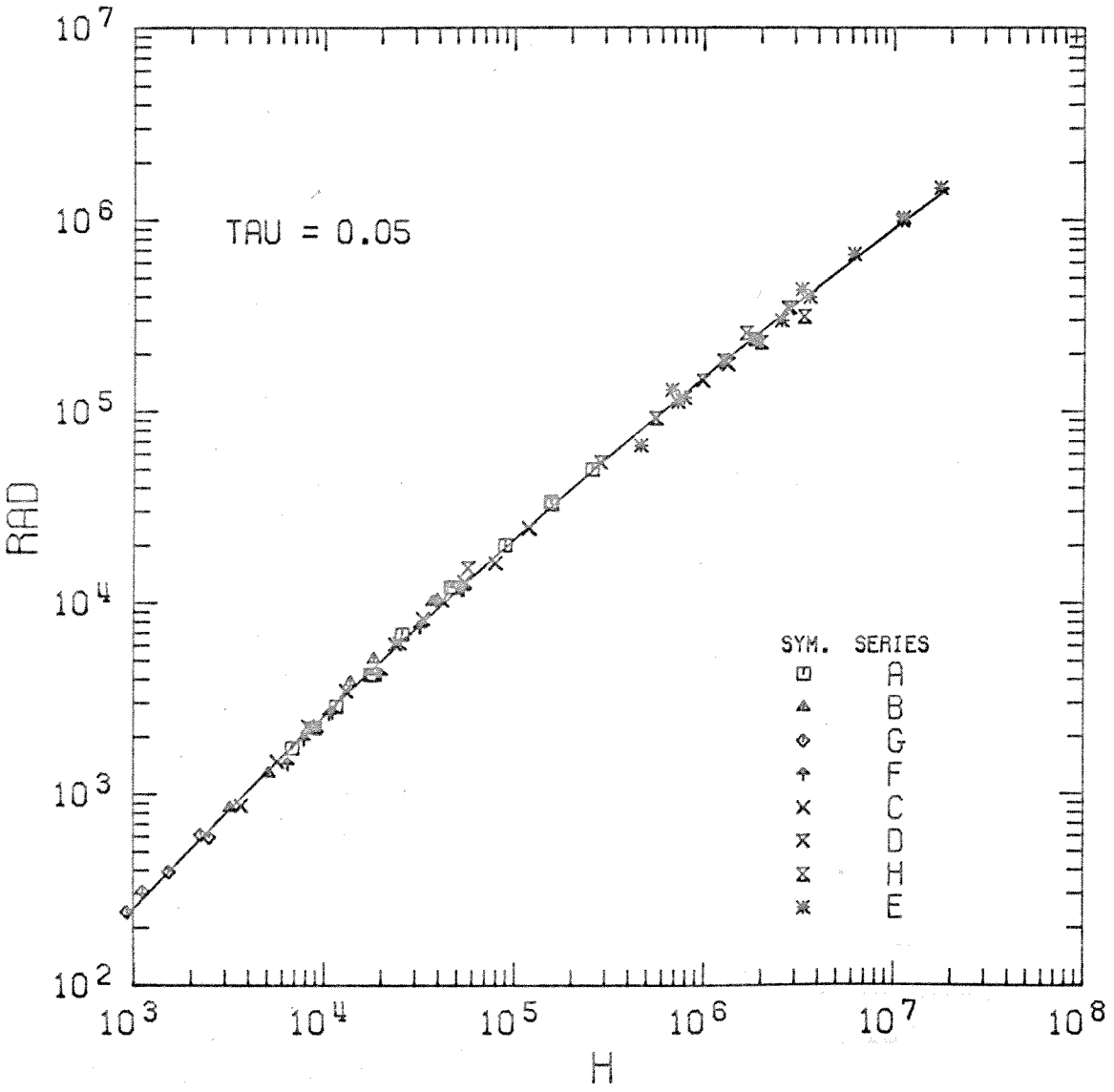

Figure 26. Rayleigh Number versus Lower Surface Heat Flux at $\tau = 0.05$.

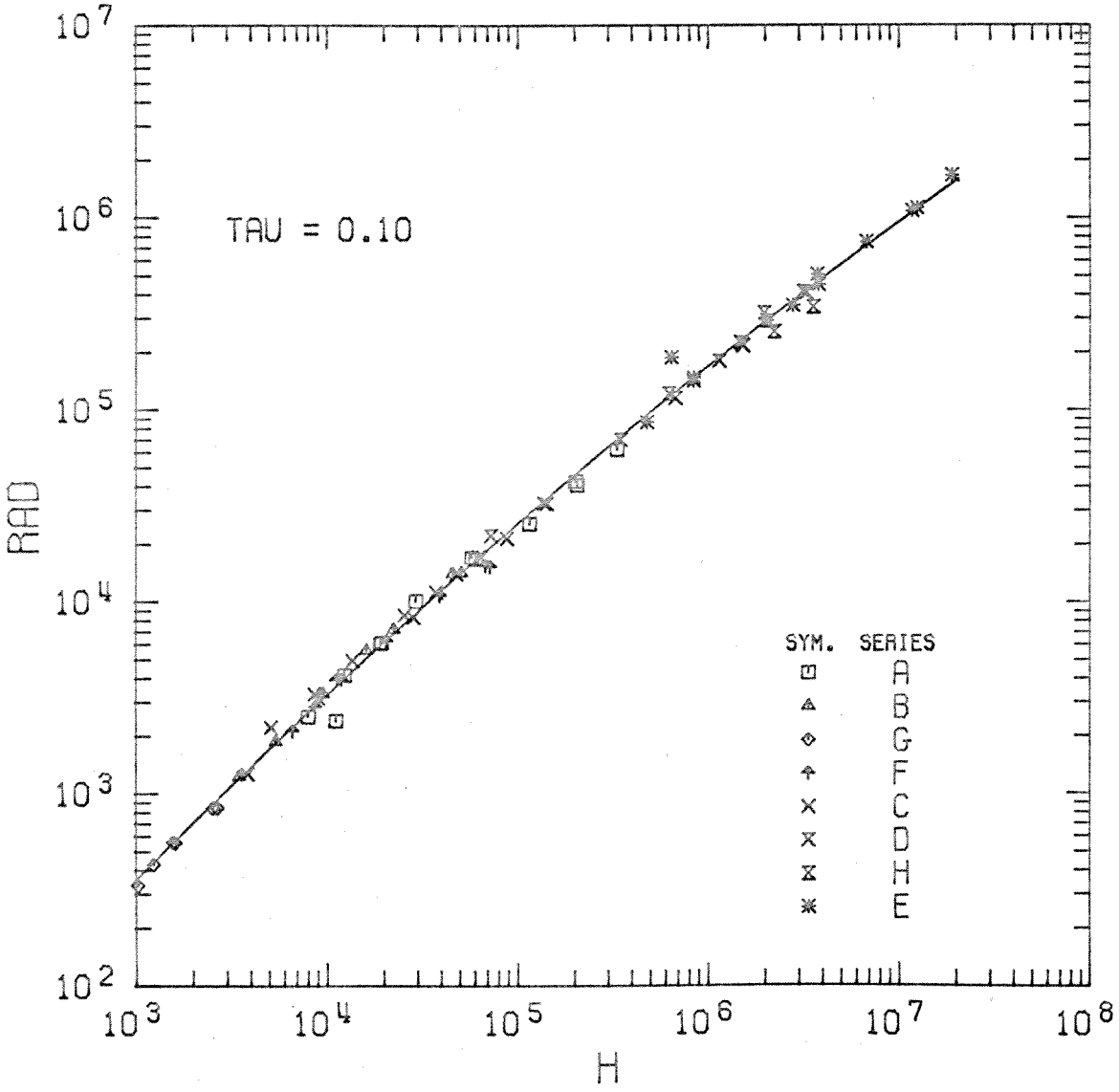

Figure 27. Rayleigh Number versus Lower Surface Heat Flux at $\tau = 0.10$.

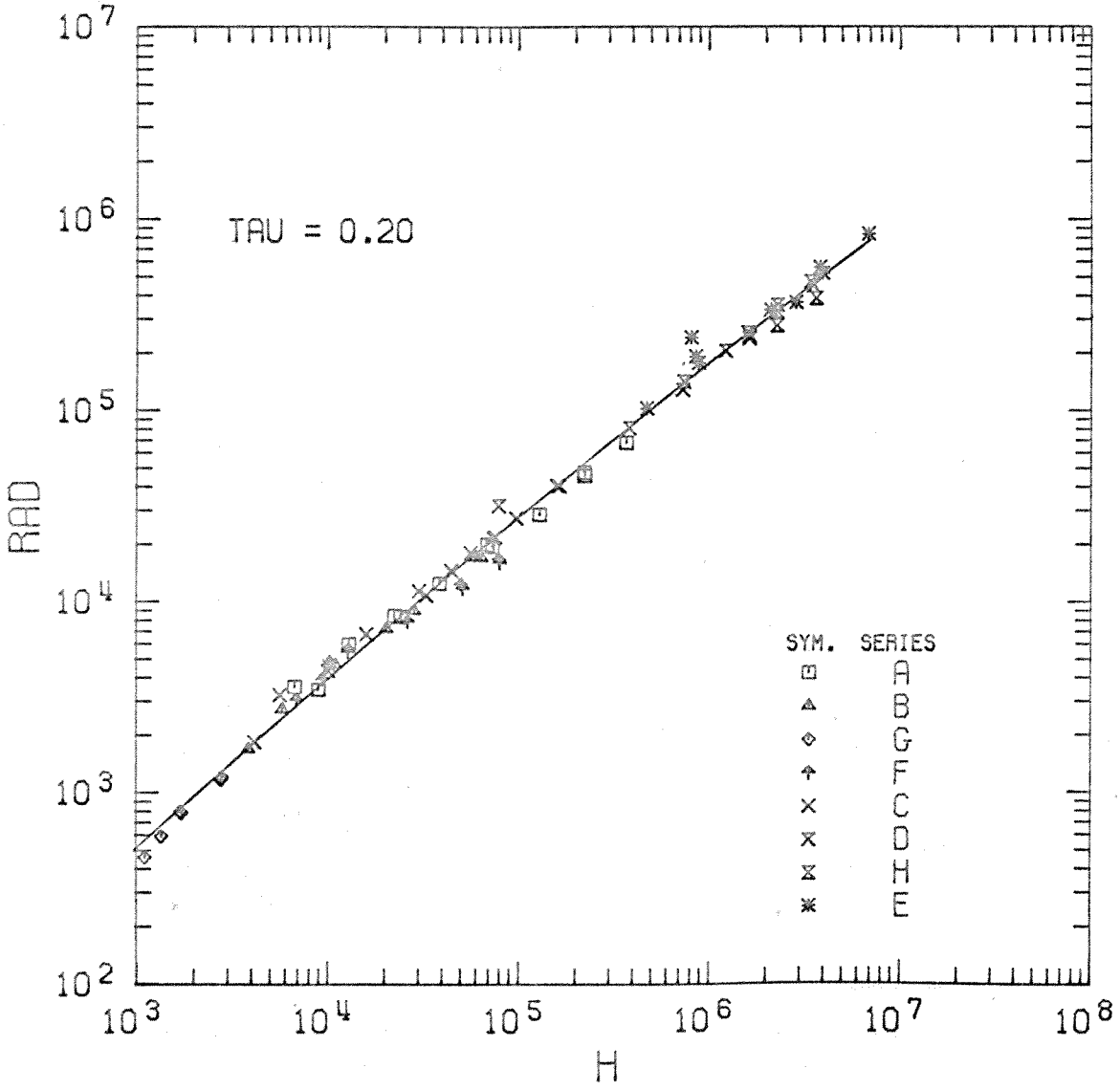

Figure 28. Rayleigh Number versus Lower Surface Heat Flux at $\tau = 0.20$.

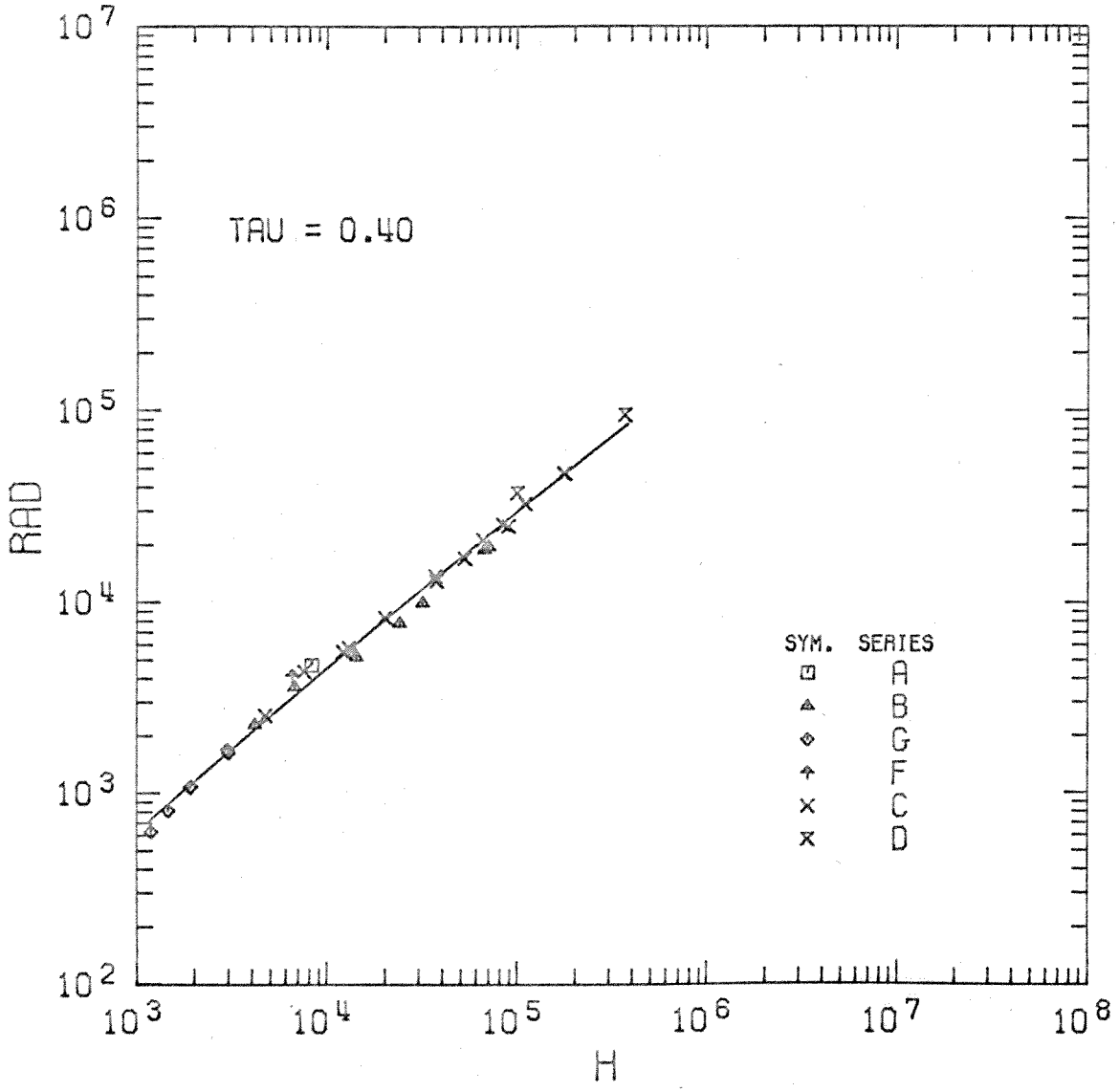

Figure 29. Rayleigh Number versus Lower Surface Heat Flux at $\tau = 0.40$.

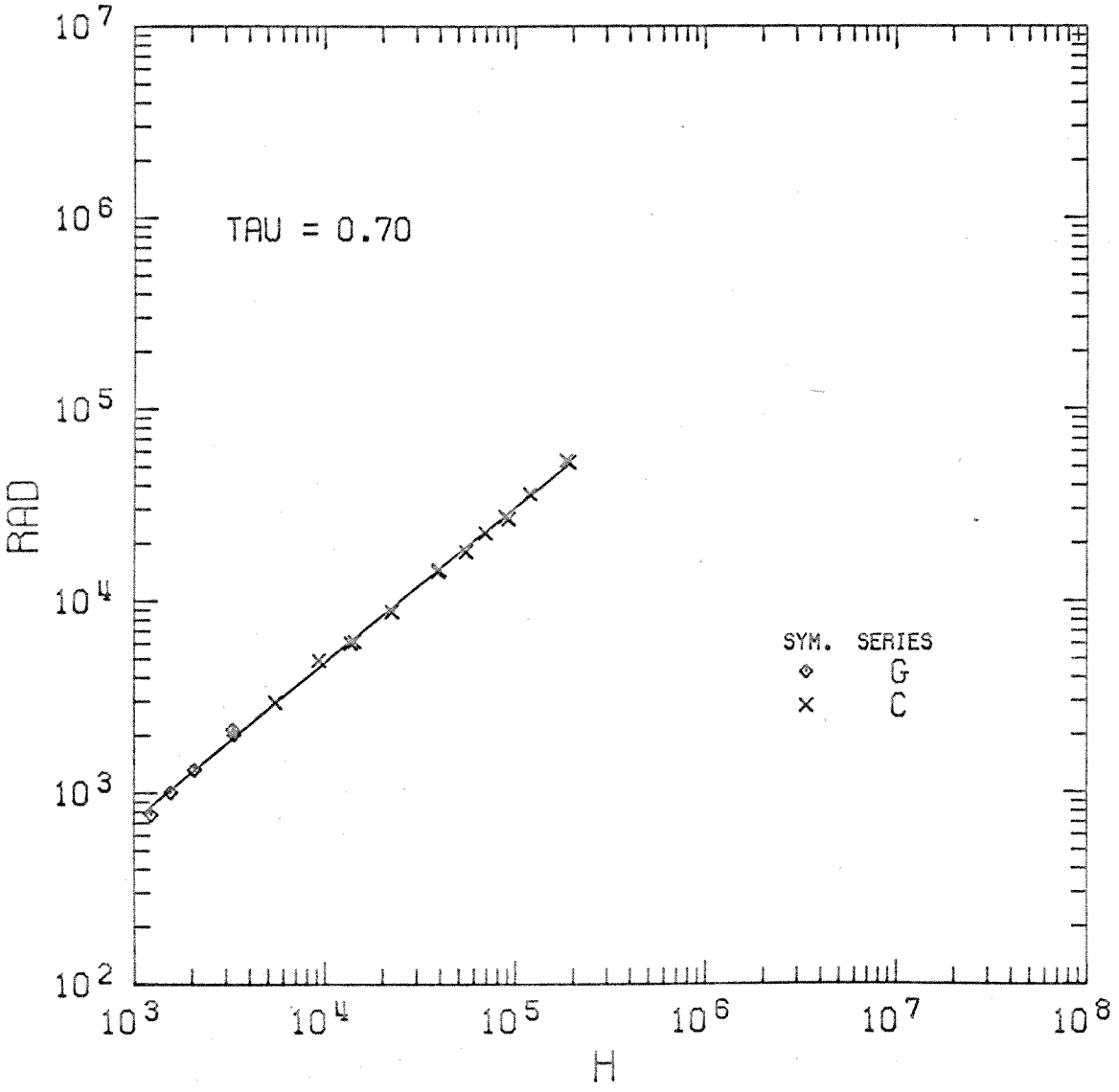

Figure 30. Rayleigh Number versus Lower Surface Heat Flux at $\tau = 0.70$.

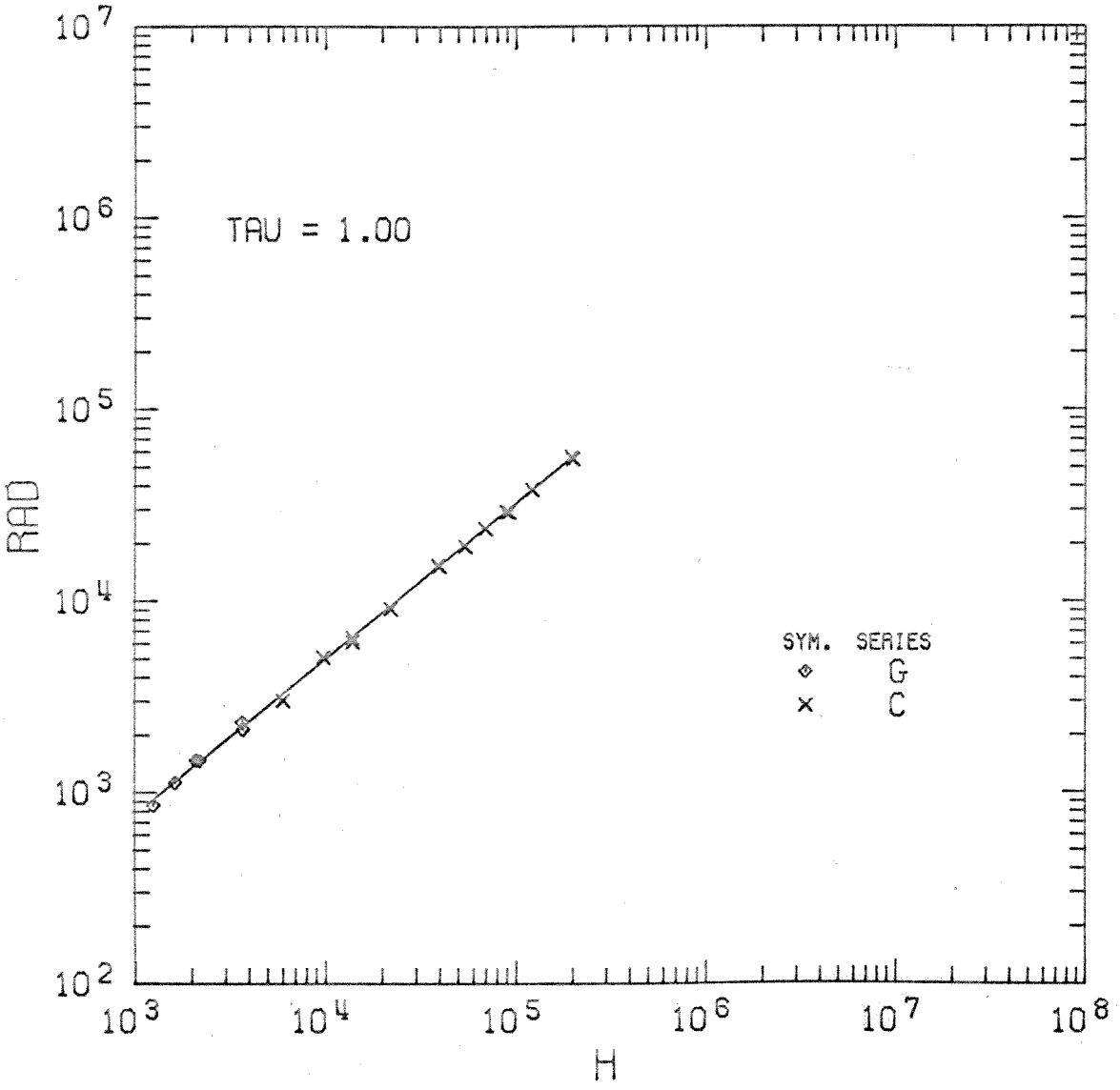

Figure 31. Rayleigh Number versus Lower Surface Heat Flux at $\tau = 1.00$.

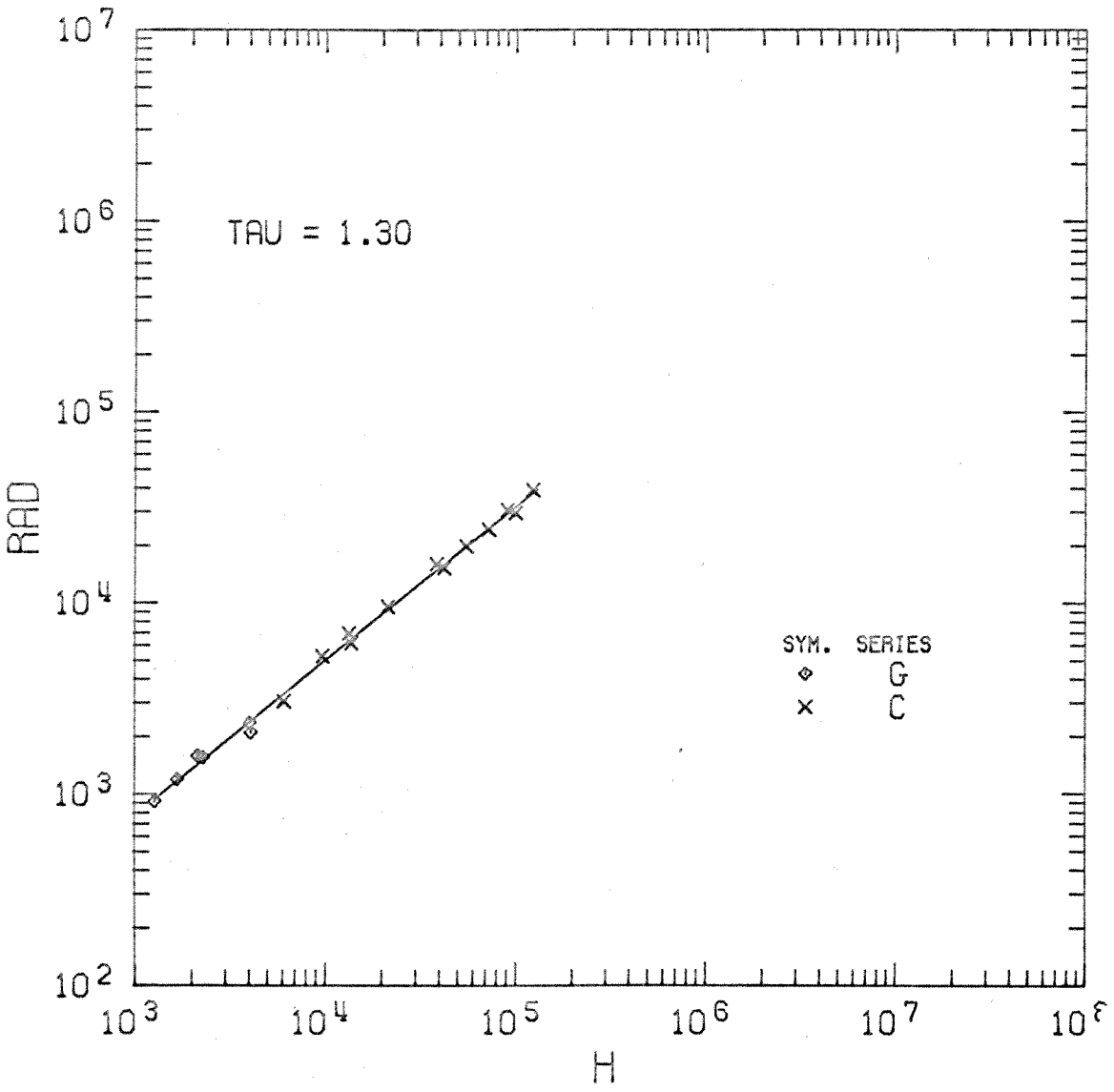

Figure 32. Rayleigh Number versus Lower Surface Heat Flux at $\tau = 1.30$.

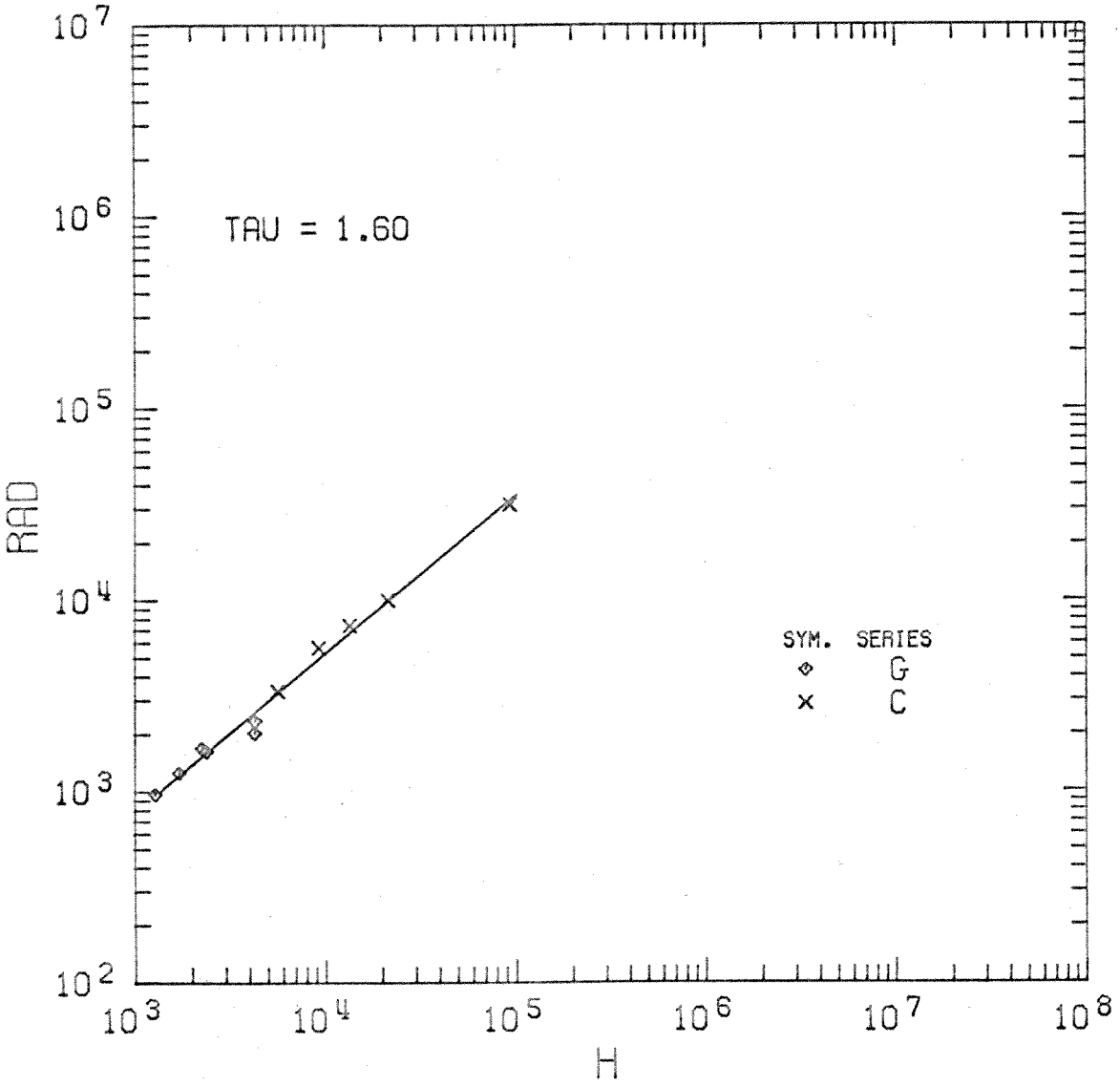

Figure 33. Rayleigh Number versus Lower Surface Heat Flux at $\tau = 1.60$.

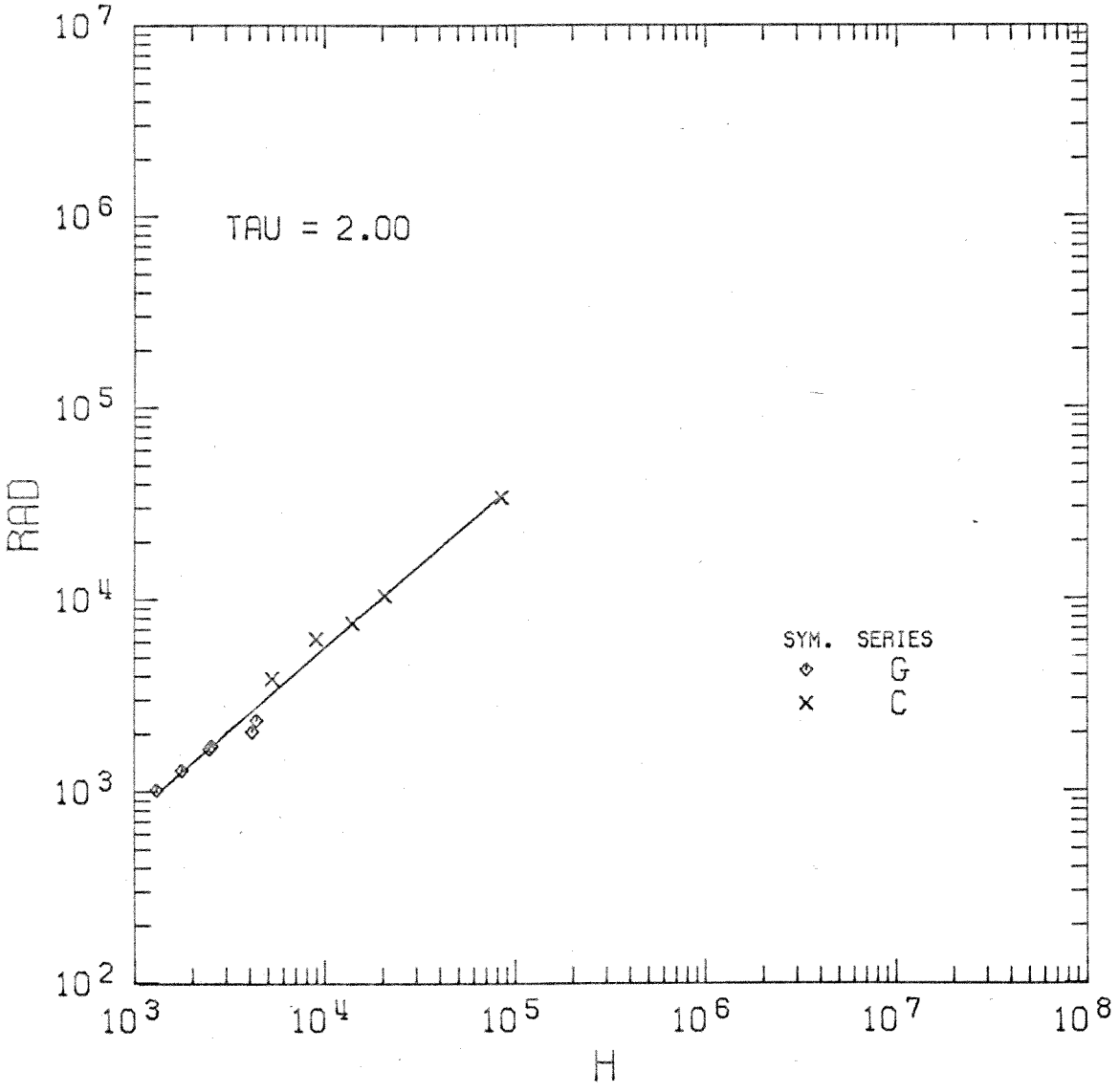

Figure 34. Rayleigh Number versus Lower Surface Heat Flux at $\tau = 2.00$.

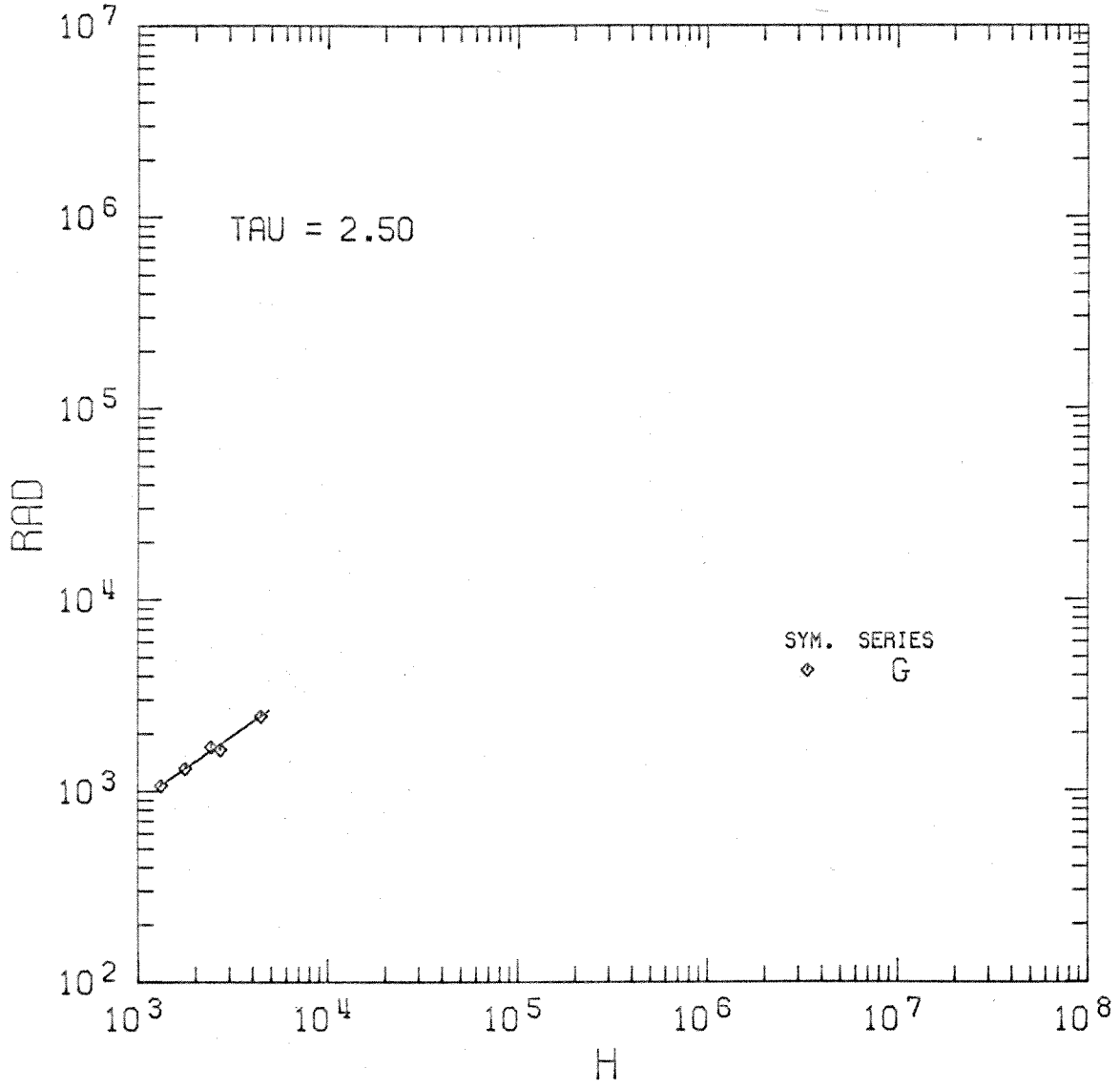

Figure 35. Rayleigh Number versus Lower Surface Heat Flux at $\tau = 2.50$.

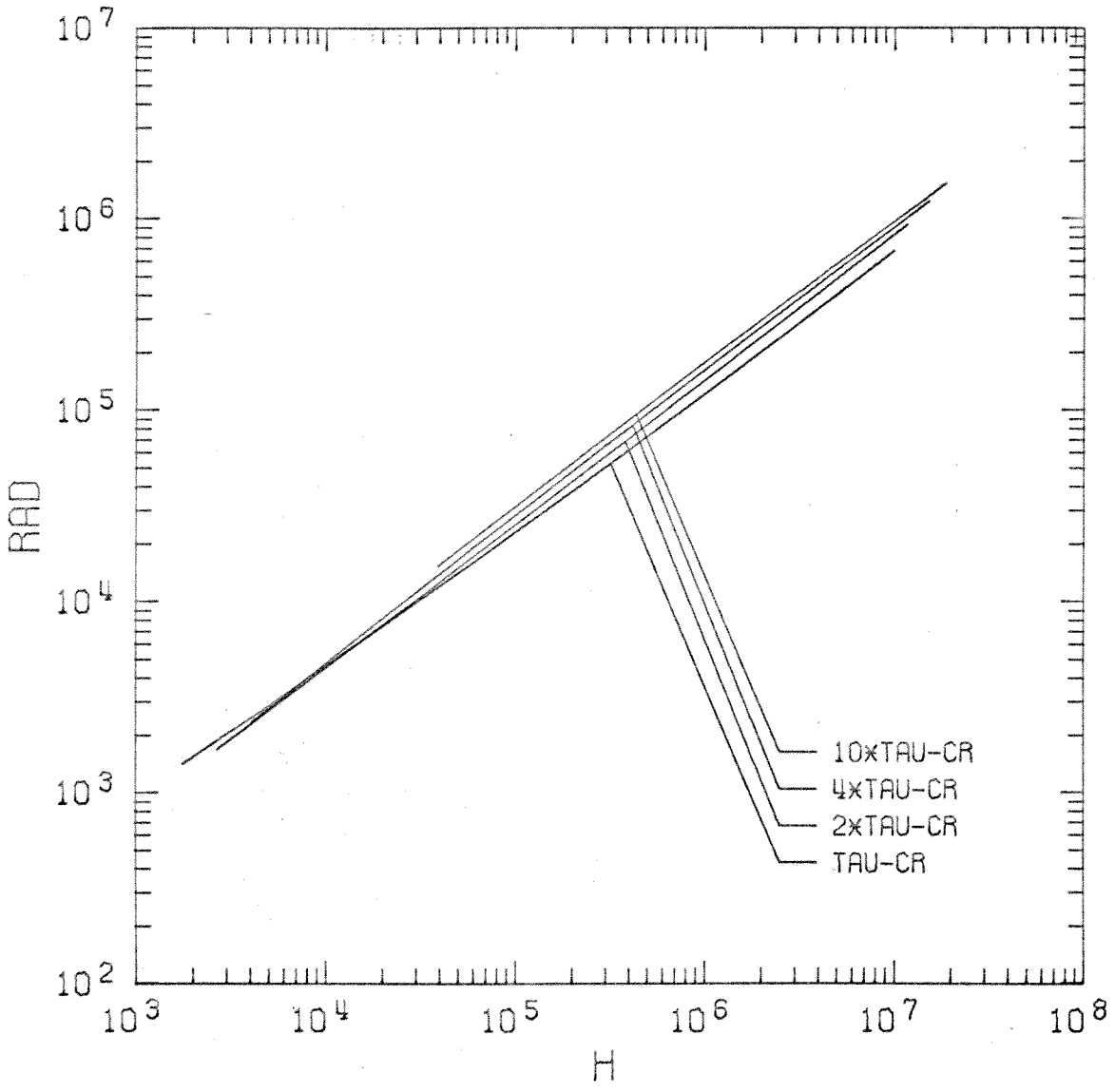

Figure 36. Rayleigh Number versus Lower Surface Heat Flux for $\tau = \tau_{cr}$, $2\,\tau_{cr}$, $4\,\tau_{cr}$, $10\,\tau_{cr}$.

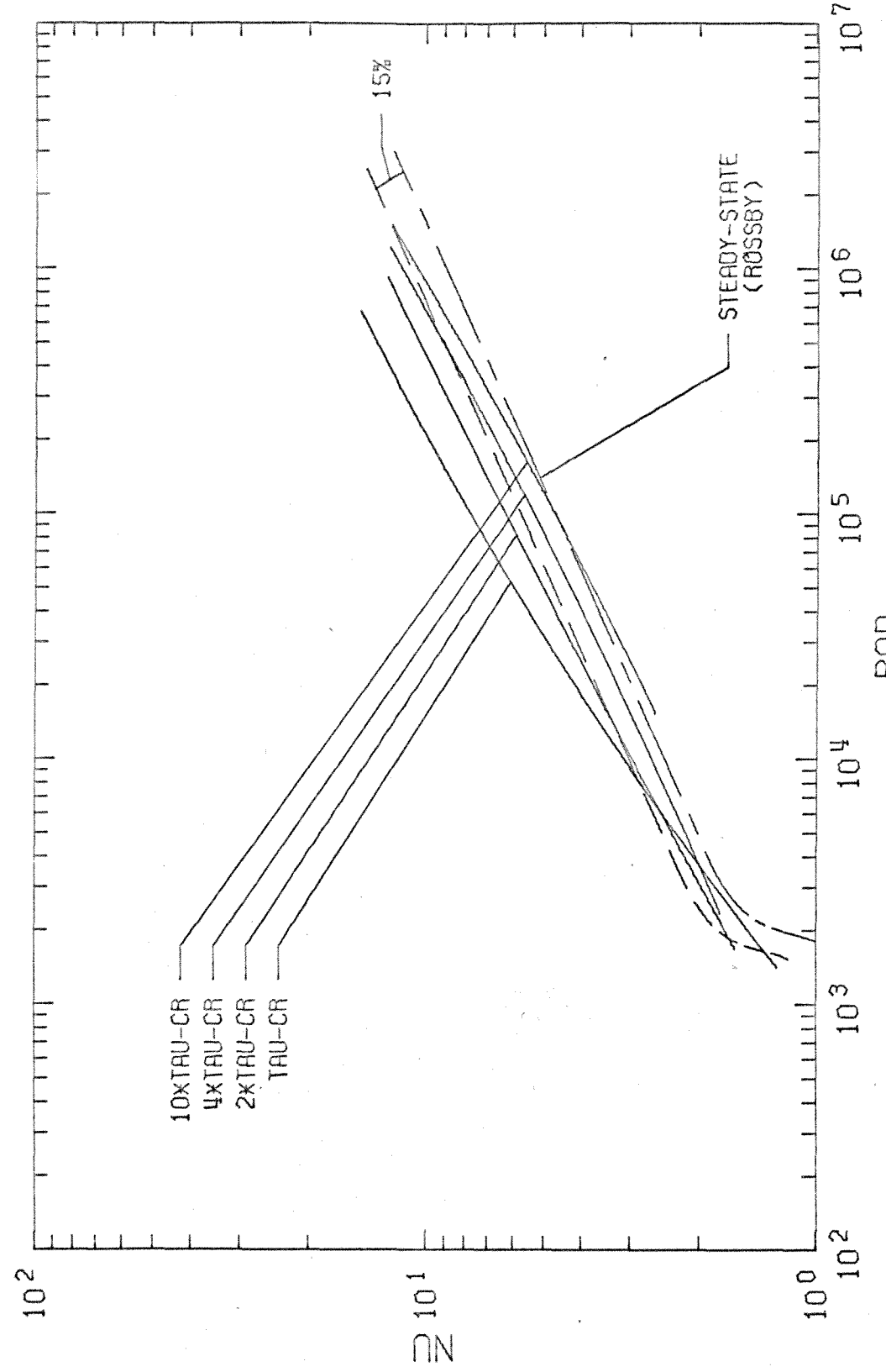

Figure 37. Nusselt Number versus Rayleigh Number for $\tau = \tau_{cr}$, $2\,\tau_{cr}$, $4\,\tau_{cr}$, $10\,\tau_{cr}$ and Results of Rossby (1966, 1969).

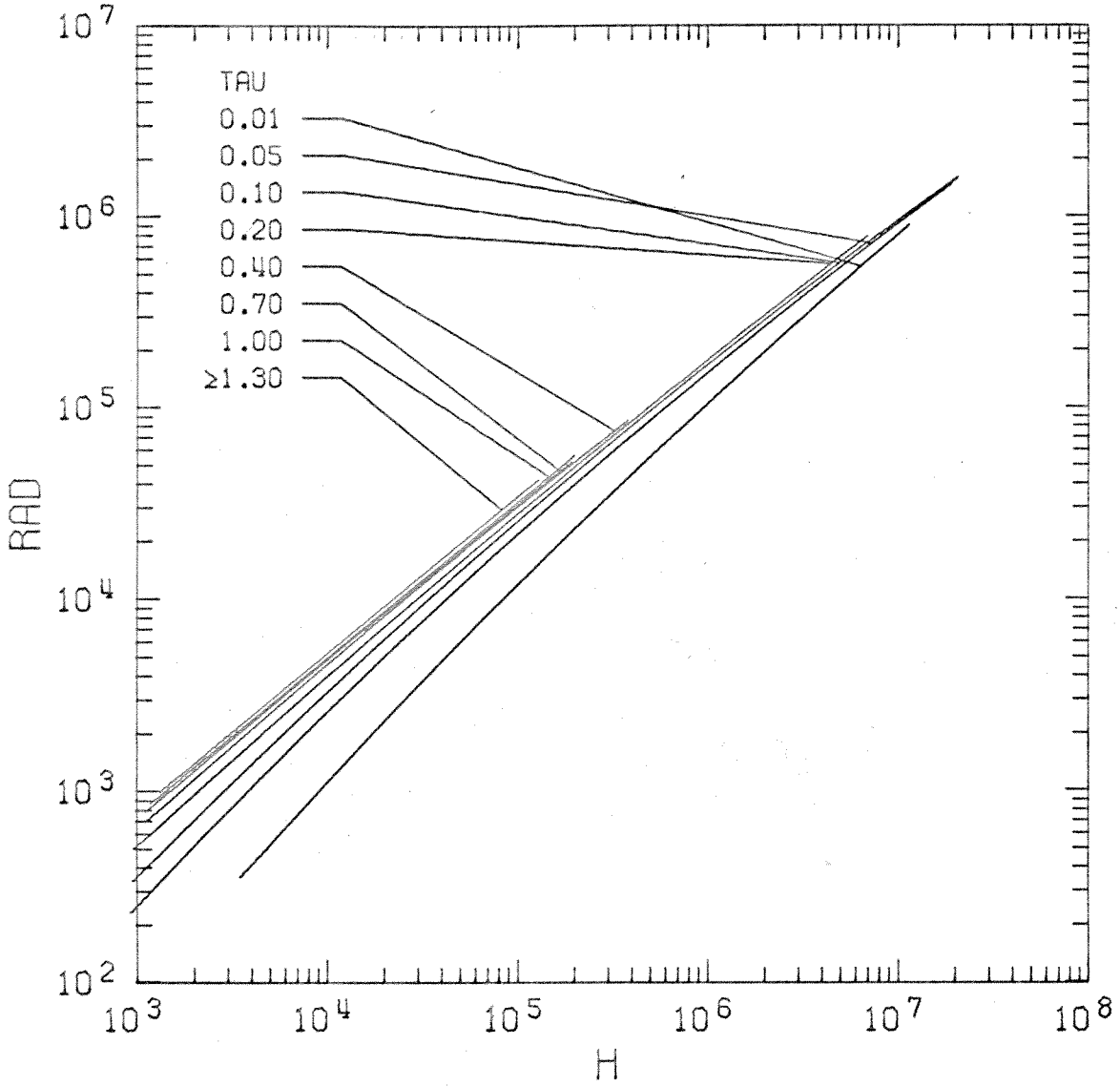

Figure 38. Rayleigh Number versus Lower Surface Heat Flux for τ = 0.01, 0.05, 0.10, 0.20, 0.40, 0.70, 1.00, $\geq$ 1.30.

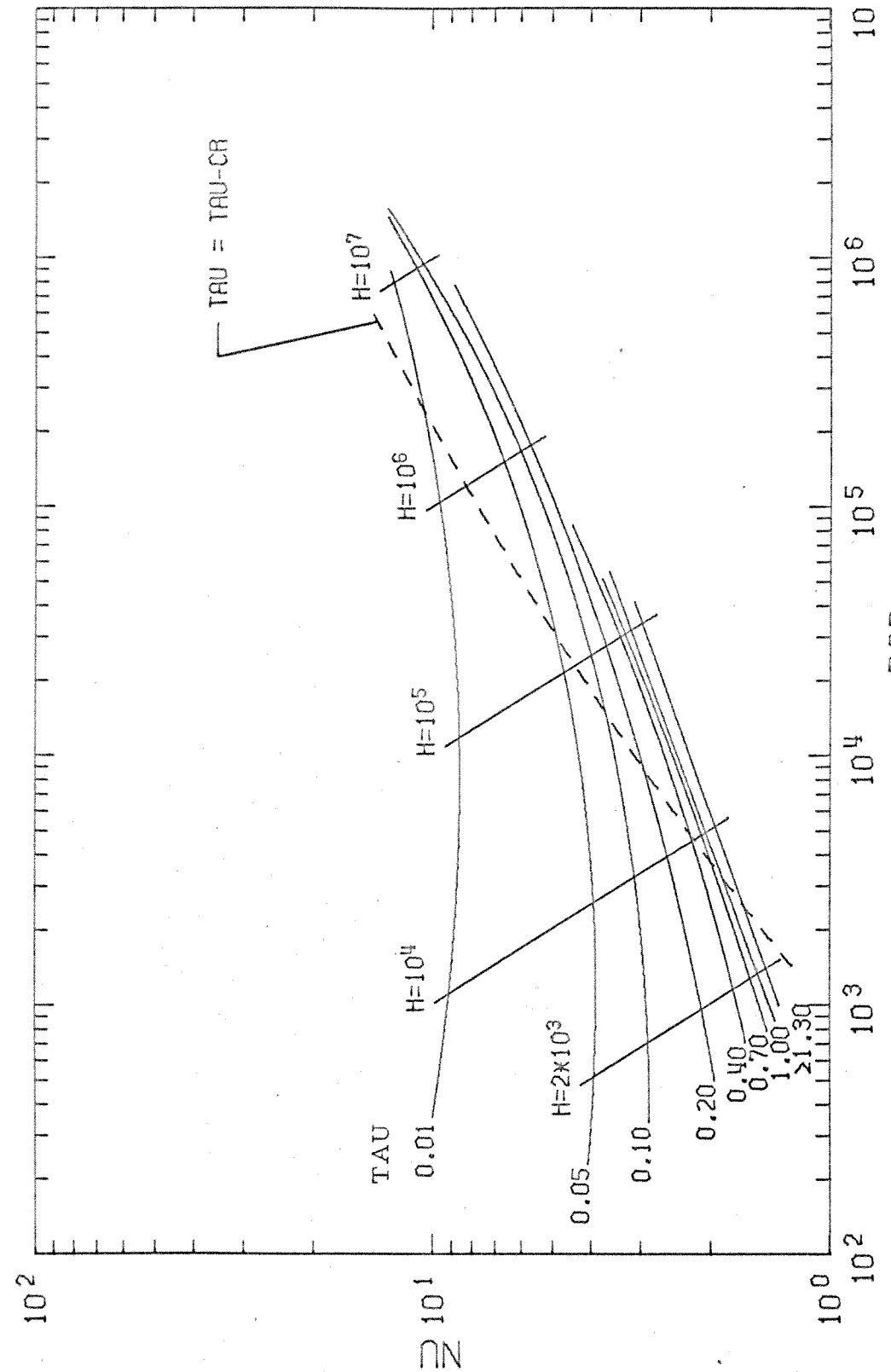

Figure 39. Nusselt Number versus Rayleigh Number for τ = 0.01, 0.05, 0.10, 0.20, 0.40, 0.70, 1.00, ≥1.30 with Result for $\tau = \tau_{cr}$ and Lines of Constant Lower Surface Heat Flux.

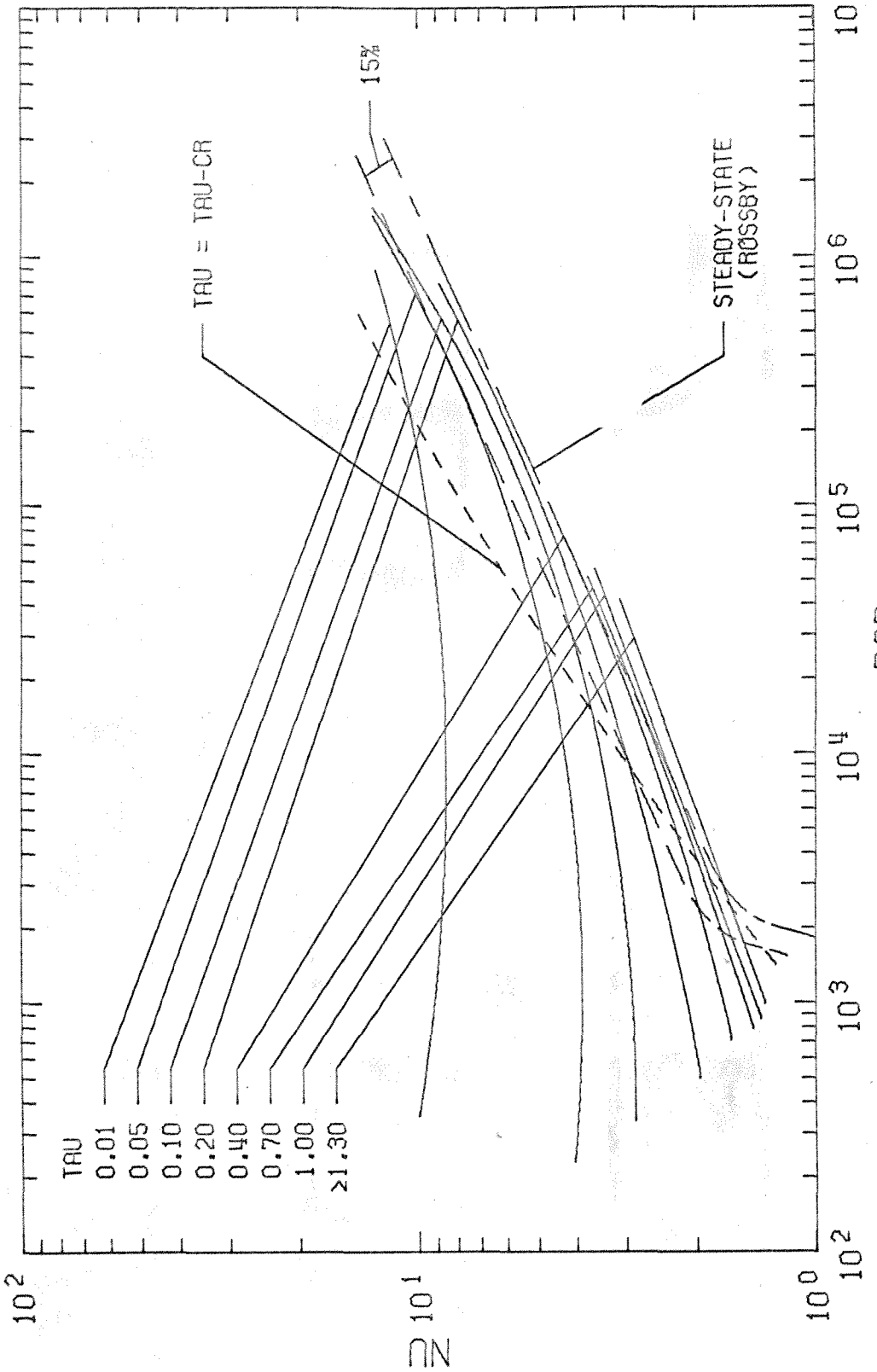

Figure 40. Nusselt Number versus Rayleigh Number for $\tau = 0.01$, 0.05, 0.10, 0.20, 0.40, 0.70, 1.00, ≥1.30 with Result for $\tau = \tau_{cr}$ and Results of Rossby (1966, 1969).

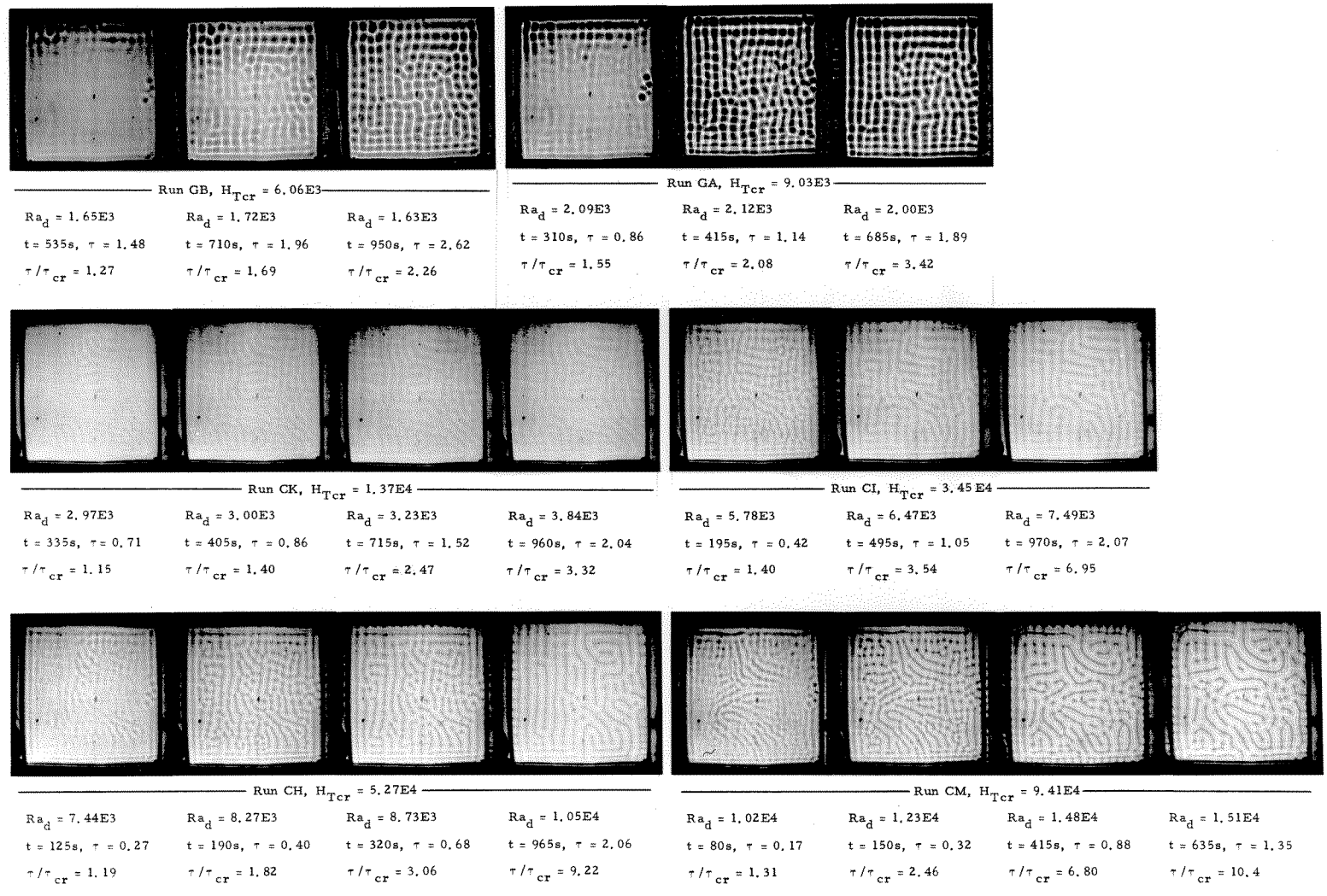

Figure 41. Patterns of Motion for 0.00635 m Depth (Runs GB, GA, CK, CI, CH, CM). See Figure 9 for scaling.

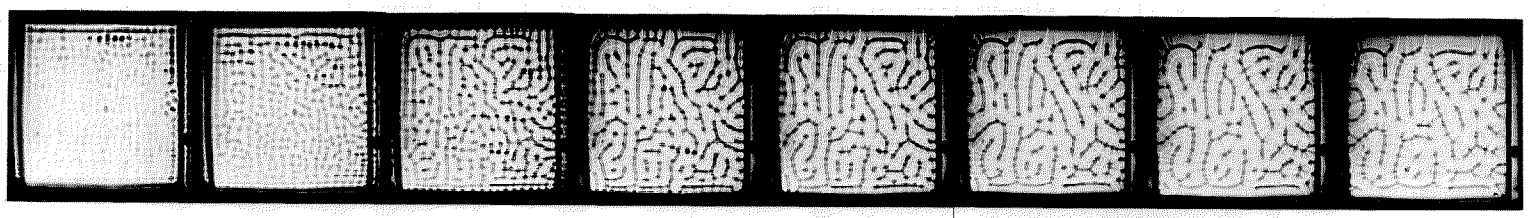

Run CC, H_{Tcr} = 2.02E5

Ra_d = 1.65E4	Ra_d = 2.27E4	Ra_d = 2.59E4	Ra_d = 2.78E4	Ra_d = 2.90E4	Ra_d = 3.10E4	Ra_d = 3.16E4	Ra_d = 3.54E4
t = 45s, τ = 0.10	t = 115s, τ = 0.24	t = 220s, τ = 0.47	t = 380s, τ = 0.81	t = 480s, τ = 1.02	t = 660s, τ = 1.40	t = 810s, τ = 1.72	t = 980s, τ = 2.08
τ/τ_{cr} = 1.13	τ/τ_{cr} = 2.88	τ/τ_{cr} = 5.52	τ/τ_{cr} = 9.51	τ/τ_{cr} = 12.0	τ/τ_{cr} = 16.5	τ/τ_{cr} = 20.9	τ/τ_{cr} = 24.6

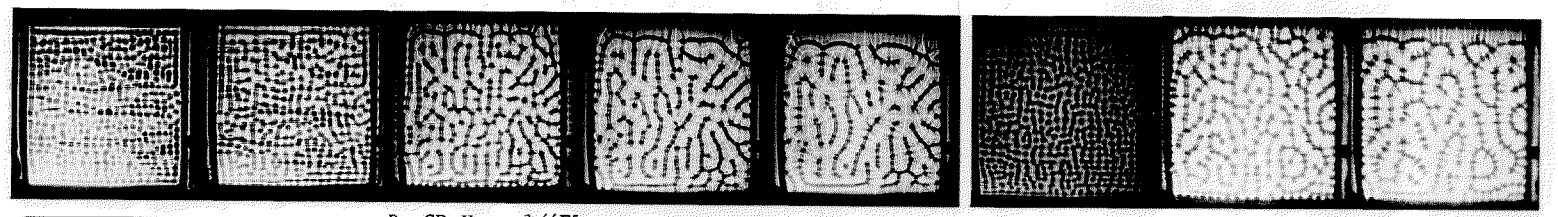

Run CD, H_{Tcr} = 2.66E5

Ra_d = 2.06E4	Ra_d = 2.77E4	Ra_d = 3.40E4	Ra_d = 3.69E4	Ra_d = 3.89E4
t = 45s, τ = 0.10	t = 100s, τ = 0.21	t = 245s, τ = 0.52	t = 400s, τ = 0.85	t = 610s, τ = 1.30
τ/τ_{cr} = 1.41	τ/τ_{cr} = 3.13	τ/τ_{cr} = 7.68	τ/τ_{cr} = 12.5	τ/τ_{cr} = 19.1

Run CA, H_{Tcr} = 4.02E5

Ra_d = 3.29E4	Ra_d = 4.99E4	Ra_d = 5.56E4
t = 50s, τ = 0.11	t = 250s, τ = 0.53	t = 450s, τ = 0.96
τ/τ_{cr} = 1.67	τ/τ_{cr} = 8.32	τ/τ_{cr} = 15.0

Figure 42. Patterns of Motion for 0.00635 m Depth (Runs CC, CD, CA). See Figure 9 for scaling.

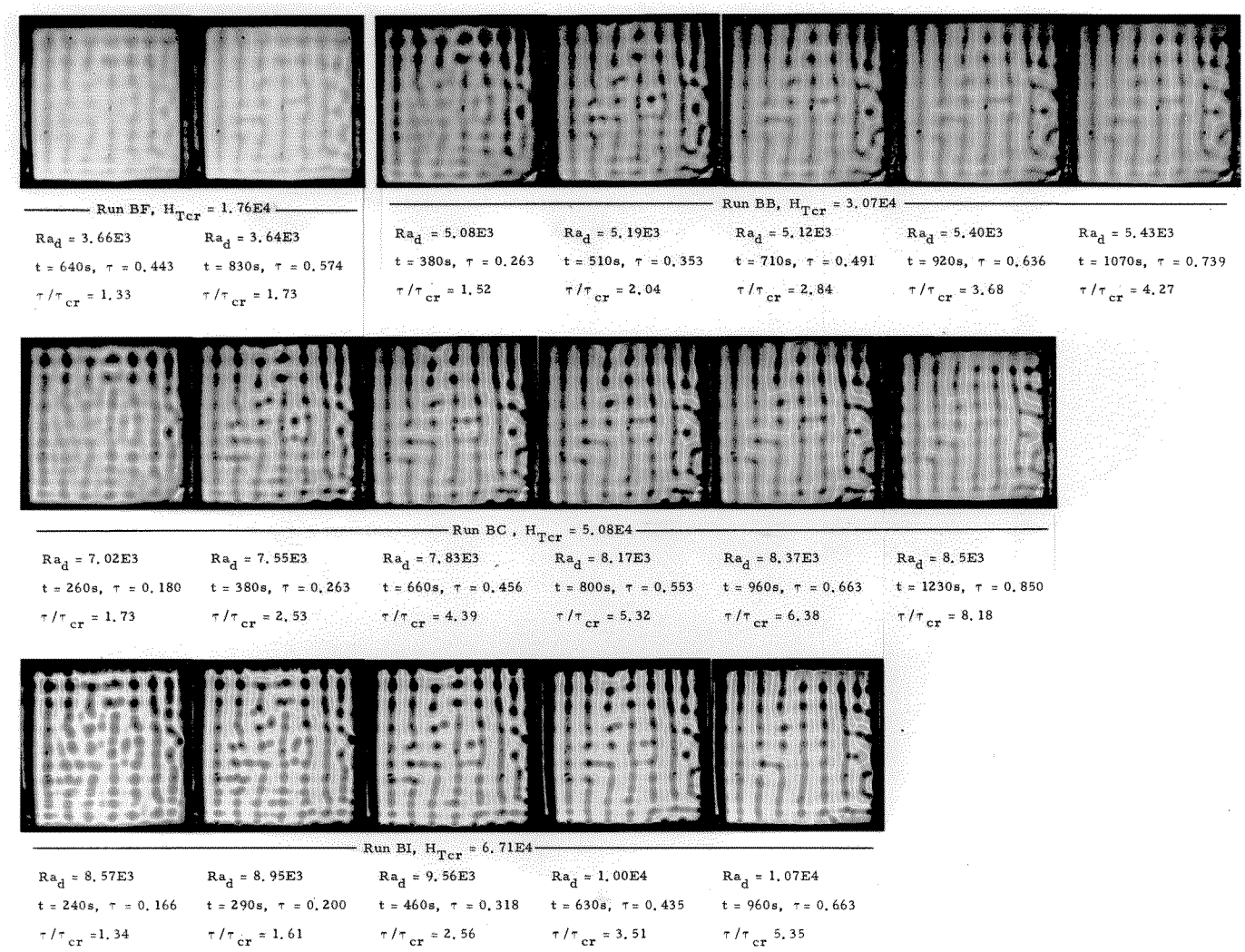

Figure 43. Patterns of Motion for 0.01270 m Depth (Runs BF, BB, BC, BI). See Figure 9 for scaling.

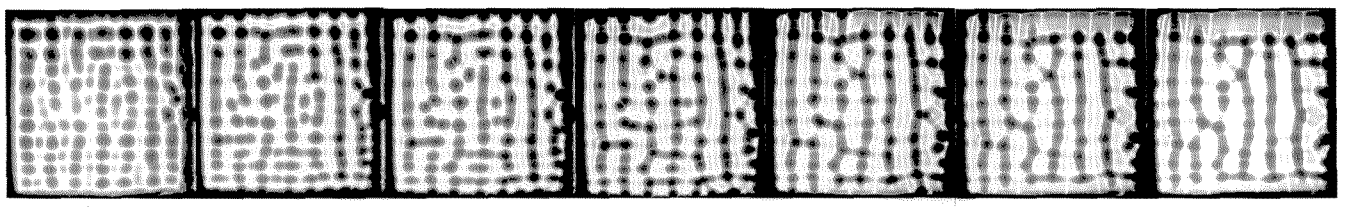

Run BA, H_{Tcr} = 1.36E5

Ra_d = 1.42E4	Ra_d = 1.71E4	Ra_d = 1.79E4	Ra_d = 1.88E4	Ra_d = 1.99E4	Ra_d = 2.06E4	Ra_d = 2.14E4
t = 150s, τ = 0.104	t = 300s, τ = 0.207	t = 420s, τ = 0.290	t = 580s, τ = 0.400	t = 770s, τ = 0.531	t = 900s, τ = 0.620	t = 1000s, τ = 0.689
τ/τ_{cr} = 1.37	τ/τ_{cr} = 2.72	τ/τ_{cr} = 3.82	τ/τ_{cr} = 5.27	τ/τ_{cr} = 7.00	τ/τ_{cr} = 8.16	τ/τ_{cr} = 9.06

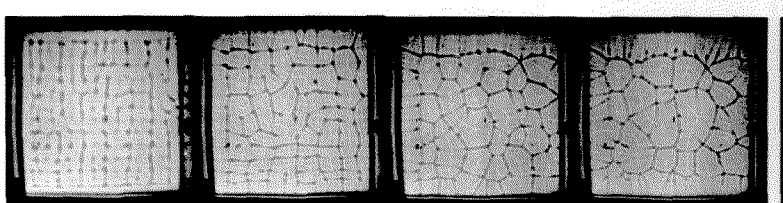

Run DD, H_{Tcr} = 8.60E5

Ra_d = 5.30E4	Ra_d = 7.71E4	Ra_d = 8.96E4	Ra_d = 1.01E5
t = 90s, τ = 0.048	t = 295s, τ = 0.157	t = 620s, τ = 0.330	t = 960s, τ = 0.551
τ/τ_{cr} = 1.20	τ/τ_{cr} = 3.92	τ/τ_{cr} = 8.25	τ/τ_{cr} = 13.8

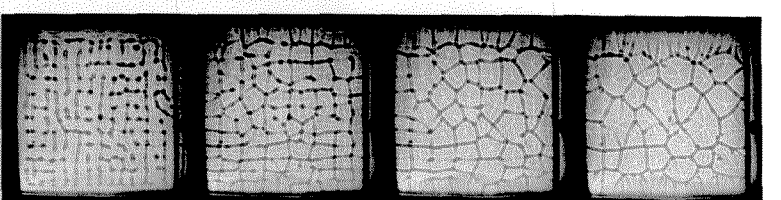

Run DC, H_{Tcr} = 1.54E6

Ra_d = 8.62E4	Ra_d = 1.18E5	Ra_d = 1.30E5	Ra_d = 1.50E5
t = 80s, τ = 0.043	t = 220s, τ = 0.117	t = 420s, τ = 0.224	t = 745s, τ = 0.397
τ/τ_{cr} = 1.48	τ/τ_{cr} = 4.04	τ/τ_{cr} = 7.73	τ/τ_{cr} = 13.7

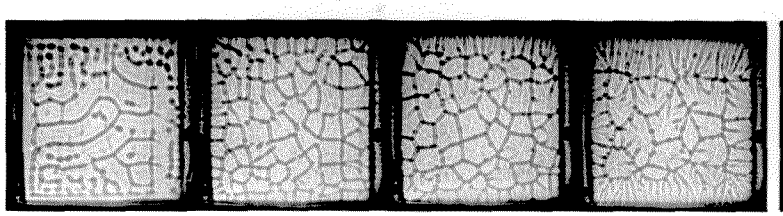

Run DB, H_{Tcr} = 3.23E6

Ra_d = 1.39E5	Ra_d = 2.10E5	Ra_d = 2.44E5	Ra_d = 2.63E5
t = 50s, τ = 0.027	t = 175s, τ = 0.094	t = 435s, τ = 0.232	t = 770s, τ = 0.410
τ/τ_{cr} = 1.93	τ/τ_{cr} = 6.72	τ/τ_{cr} = 16.6	τ/τ_{cr} = 29.3

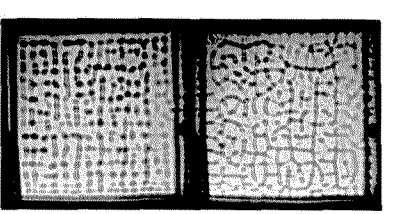

Run DI, H_{Tcr} = 3.25E6

Ra_d = 1.45E5	Ra_d = 1.99E5
t = 50s, τ = 0.027	t = 120s, τ = 0.064
τ/τ_{cr} = 1.50	τ/τ_{cr} = 3.56

Figure 44. Patterns of Motion for 0.01270 m Depth (Runs BA, DD, DC, DB, DI). See Figure 9 for scaling.

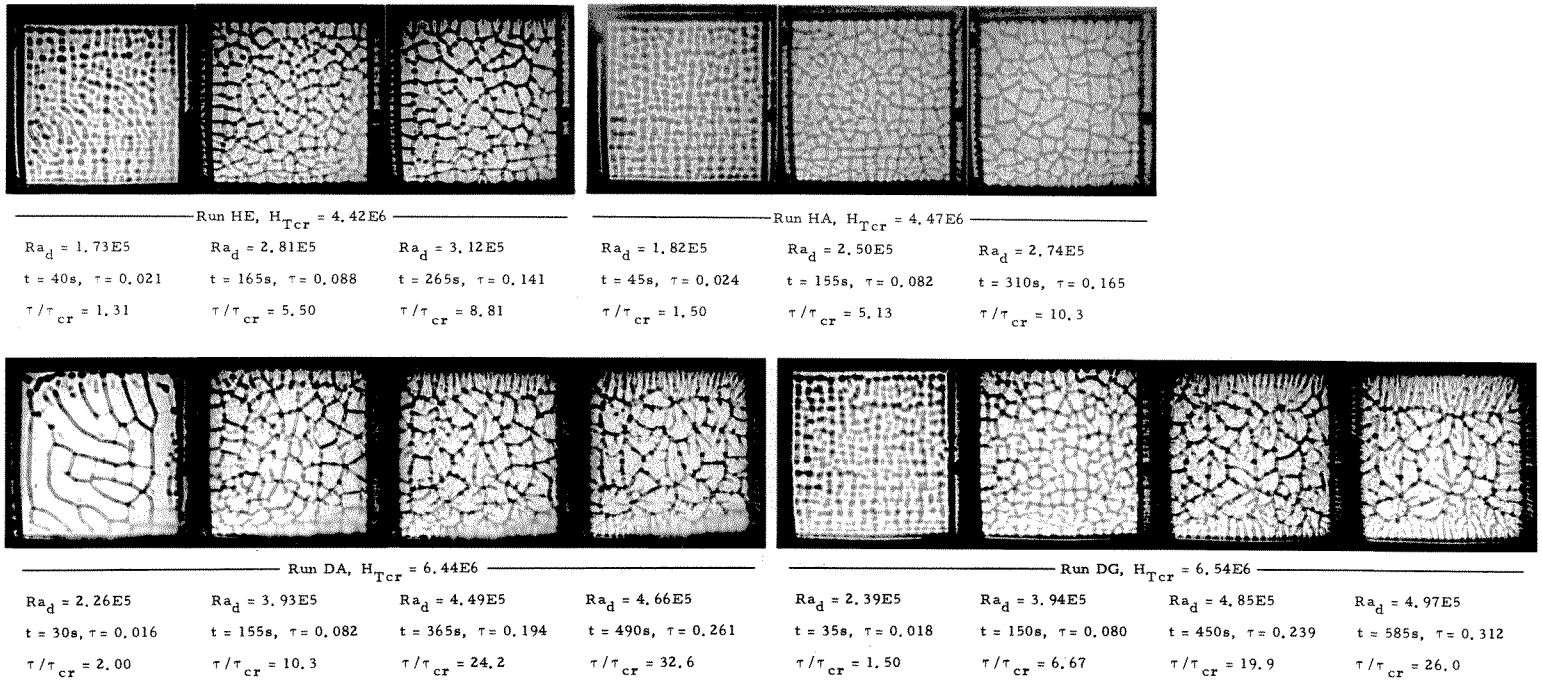

Figure 45. Patterns of Motion for 0.01270 m Depth (Runs HE, HA, DA, DG). See Figure 9 for scaling.

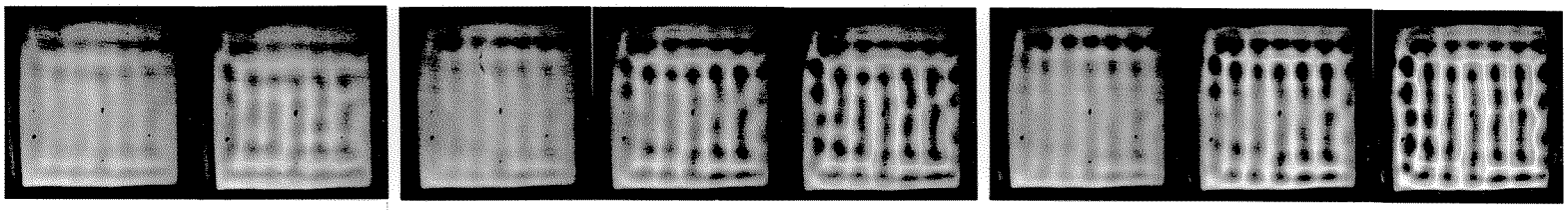

Run FF, H_{Tcr} = 1.93E4

Ra_d = 4.20E3	Ra_d = 4.28E3
t = 1440s, τ = 0.434	t = 1730s, τ = 0.521
τ/τ_{cr} = 1.06	τ/τ_{cr} = 1.28

Run FE, H_{Tcr} = 2.50E4

Ra_d = 4.69E3	Ra_d = 4.81E3	Ra_d = 4.9E3
t = 1035s, τ = 0.312	t = 1210s, τ = 0.364	t = 1345s, τ = 0.405
τ/τ_{cr} = 1.04	τ/τ_{cr} = 1.21	τ/τ_{cr} = 1.35

Run FD, H_{Tcr} = 3.42E4

Ra_d = 5.74E3	Ra_d = 5.91E3	Ra_d = 5.8E3
t = 760s, τ = 0.229	t = 870s, τ = 0.262	t = 1010s, τ = 0.304
τ/τ_{cr} = 1.05	τ/τ_{cr} = 1.21	τ/τ_{cr} = 1.40

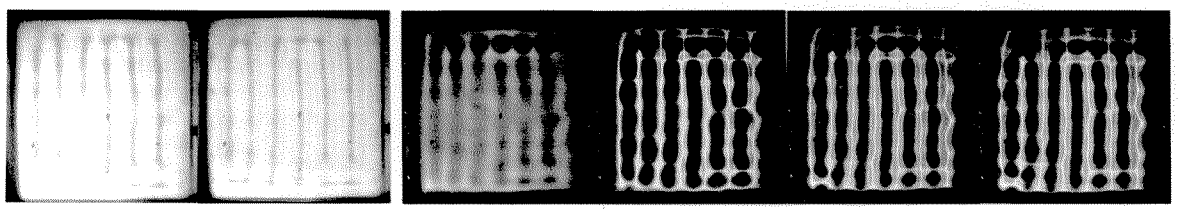

Run AJ, H_{Tcr} = 5.53E4

Ra_d = 8.11E3	Ra_d = 9.16E3
t = 600s, τ = 0.185	t = 1030s, τ = 0.316
τ/τ_{cr} = 1.34	τ/τ_{cr} = 2.29

Run FC, H_{Tcr} = 5.79E4

Ra_d = 7.43E3	Ra_d = 7.78E3	Ra_d = 7.77E3	Ra_d = 7.76E3
t = 495s, τ = 0.150	t = 600s, τ = 0.181	t = 750s, τ = 0.226	t = 935s, τ = 0.282
τ/τ_{cr} = 1.06	τ/τ_{cr} = 1.28	τ/τ_{cr} = 1.59	τ/τ_{cr} = 1.99

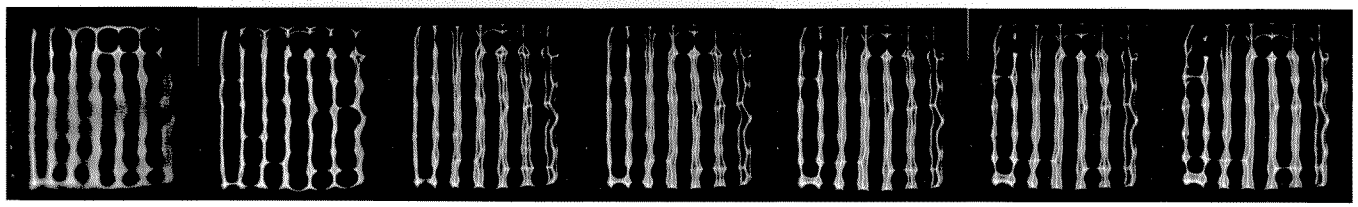

Run FB, H_{Tcr} = 9.88E4

Ra_d = 1.11E4	Ra_d = 1.14E4	Ra_d = 1.16E4	Ra_d = 1.17E4	Ra_d = 1.16E4	Ra_d = 1.19E4	Ra_d = 1.18E4
t = 375s, τ = 0.112	t = 420s, τ = 0.126	t = 495s, τ = 0.148	t = 575s, τ = 0.174	t = 745s, τ = 0.224	t = 885s, τ = 0.266	t = 1005s, τ = 0.302
τ/τ_{cr} = 1.07	τ/τ_{cr} = 1.20	τ/τ_{cr} = 1.41	τ/τ_{cr} = 1.66	τ/τ_{cr} = 2.14	τ/τ_{cr} = 2.58	τ/τ_{cr} = 2.88

Figure 46. Patterns of Motion for 0.01905 m Depth (Runs FF, FE, FD, AJ, FC, FB). See Figure 9 for scaling.

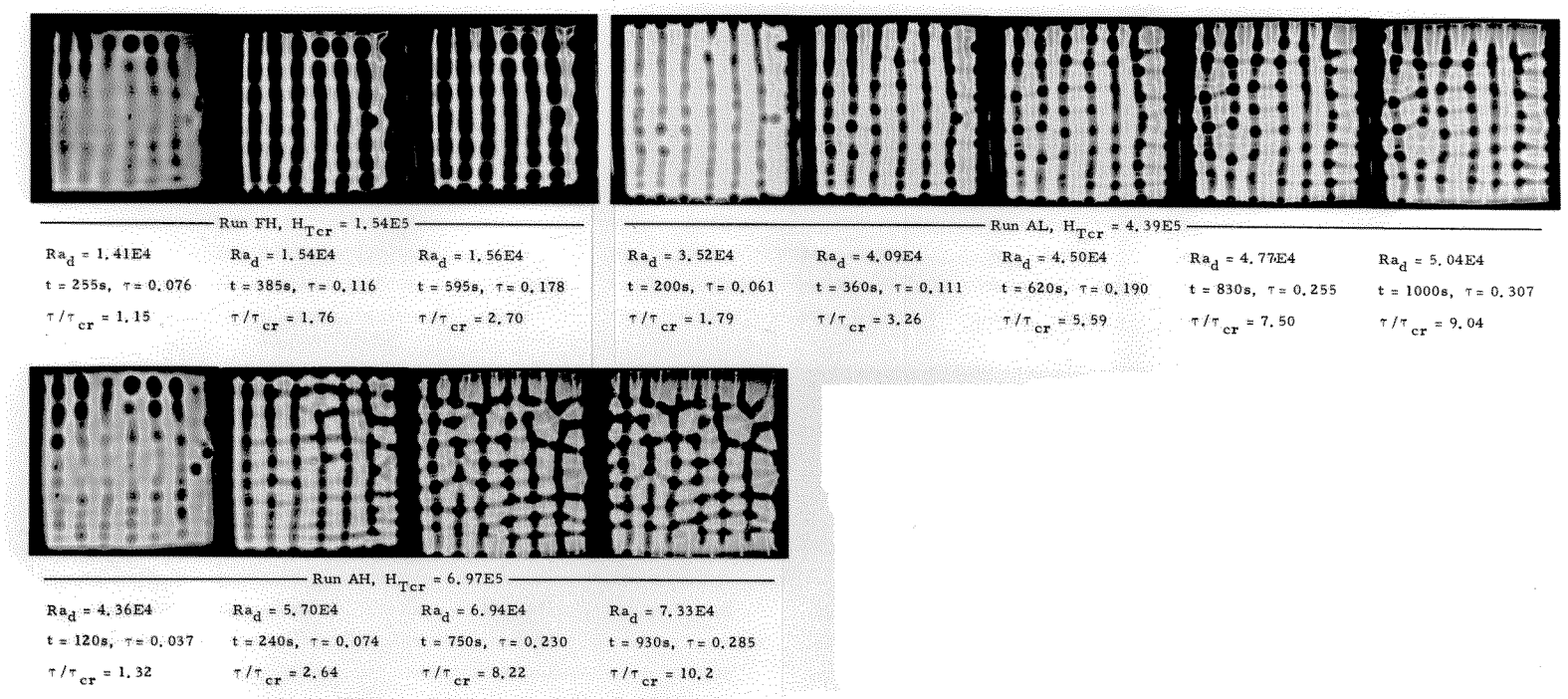

Figure 47. Patterns of Motion for 0.01905 m Depth (Runs FH, AL, AH). See Figure 9 for scaling.

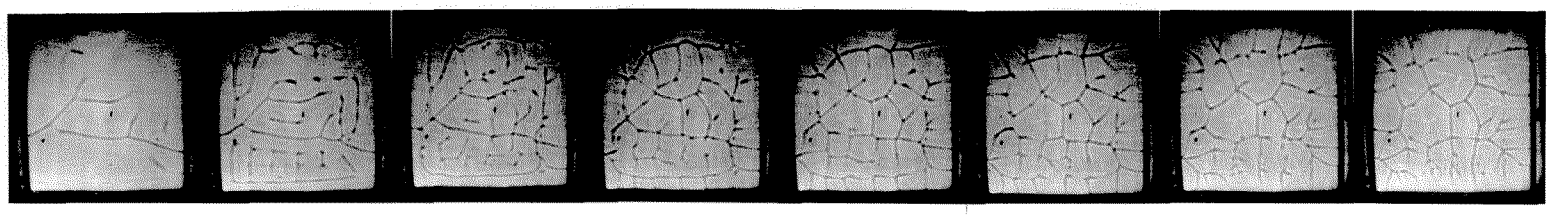

Run EI, H_{Tcr} = 1.89E6

Ra_d = 8.53E4	Ra_d = 9.65E4	Ra_d = 1.18E5	Ra_d = 1.34E5	Ra_d = 1.49E5	Ra_d = 1.67E5	Ra_d = 1.77E5	Ra_d = 1.77E5
t = 110s, τ = 0.026	t = 145s, τ = 0.034	t = 245s, τ = 0.058	t = 365s, τ = 0.086	t = 495s, τ = 0.117	t = 665s, τ = 0.158	t = 845s, τ = 0.200	t = 1010s, τ = 0.238
τ/τ_{cr} = 1.44	τ/τ_{cr} = 1.89	τ/τ_{cr} = 3.22	τ/τ_{cr} = 4.78	τ/τ_{cr} = 6.50	τ/τ_{cr} = 8.78	τ/τ_{cr} = 11.1	τ/τ_{cr} = 13.2

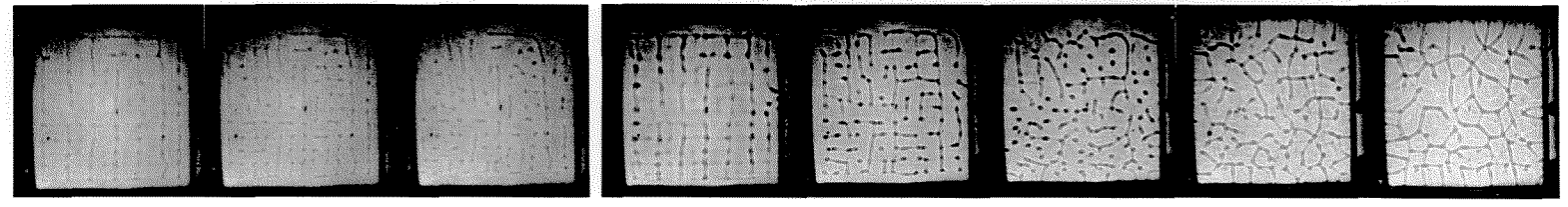

Run EG, H_{Tcr} = 1.90E6

Ra_d = 1.28E5	Ra_d = 1.46E5	Ra_d = 1.61E5
t = 205s, τ = 0.048	t = 260s, τ = 0.062	t = 315s, τ = 0.074
τ/τ_{cr} = 1.20	τ/τ_{cr} = 1.55	τ/τ_{cr} = 1.85

Run EF, H_{Tcr} = 4.30E6

Ra_d = 1.79E5	Ra_d = 2.06E5	Ra_d = 2.38E5	Ra_d = 2.76E5	Ra_d = 3.24E5
t = 95s, τ = 0.022	t = 135s, τ = 0.032	t = 205s, τ = 0.048	t = 355s, τ = 0.084	t = 610s, τ = 0.144
τ/τ_{cr} = 1.16	τ/τ_{cr} = 1.68	τ/τ_{cr} = 2.52	τ/τ_{cr} = 4.42	τ/τ_{cr} = 7.58

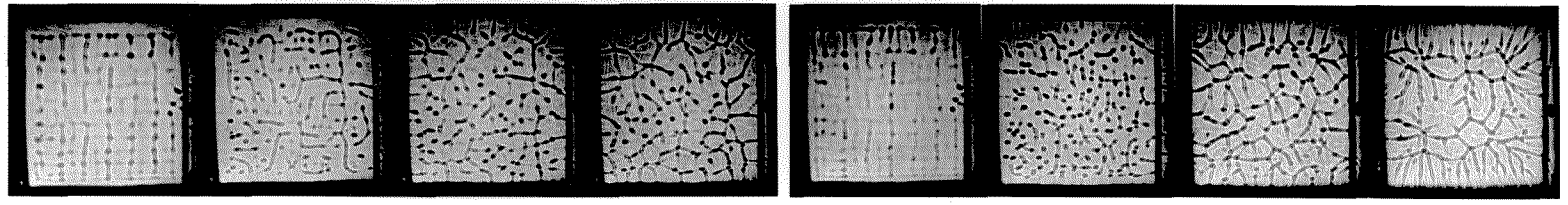

Run EE, H_{Tcr} = 5.63E6

Ra_d = 2.10E5	Ra_d = 2.55E5	Ra_d = 3.04E5	Ra_d = 3.38E5
t = 85s, τ = 0.020	t = 135s, τ = 0.032	t = 220s, τ = 0.084	t = 335s, τ = 0.079
τ/τ_{cr} = 1.33	τ/τ_{cr} = 2.14	τ/τ_{cr} = 3.47	τ/τ_{cr} = 5.27

Run ED, H_{Tcr} = 7.54E6

Ra_d = 2.79E5	Ra_d = 3.83E5	Ra_d = 5.27E5	Ra_d = 5.72E5
t = 70s, τ = 0.017	t = 145s, τ = 0.034	t = 510s, τ = 0.121	t = 895s, τ = 0.212
τ/τ_{cr} = 1.55	τ/τ_{cr} = 3.09	τ/τ_{cr} = 11.0	τ/τ_{cr} = 19.3

Figure 48. Patterns of Motion for 0.01905 m Depth (Runs EI, EG, EF, EE, ED). See Figure 9 for scaling.

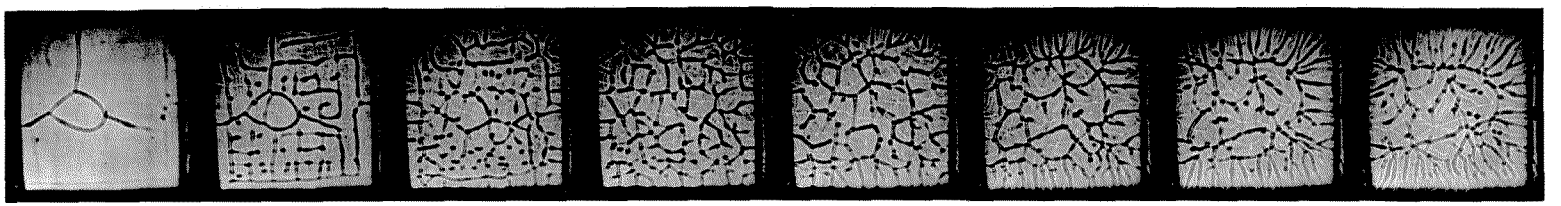

Run EJ, H_{Tcr} = 7.58E6

Ra_d = 2.45E5	Ra_d = 2.98E5	Ra_d = 3.62E5	Ra_d = 4.15E5	Ra_d = 4.60E5	Ra_d = 5.08E5	Ra_d = 5.25E5	Ra_d = 5.38E5
t = 55s, τ = 0.013	t = 85s, τ = 0.020	t = 145s, τ = 0.034	t = 265s, τ = 0.063	t = 470s, τ = 0.111	t = 660s, τ = 0.156	t = 825s, τ = 0.195	t = 1000s, τ = 0.236
τ/τ_{cr} = 1.86	τ/τ_{cr} = 2.86	τ/τ_{cr} = 4.86	τ/τ_{cr} = 9.00	τ/τ_{cr} = 15.9	τ/τ_{cr} = 22.3	τ/τ_{cr} = 27.8	τ/τ_{cr} = 33.8

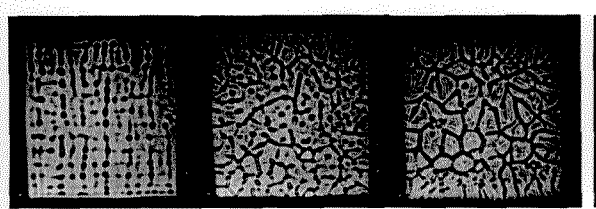

Run EC, H_{Tcr} = 1.29E7

Ra_d = 3.89E5	Ra_d = 5.91E5	Ra_d = 7.73E5
t = 50s, τ = 0.012	t = 140s, τ = 0.033	t = 505s, τ = 0.120
τ/τ_{cr} = 1.33	τ/τ_{cr} = 3.67	τ/τ_{cr} = 13.3

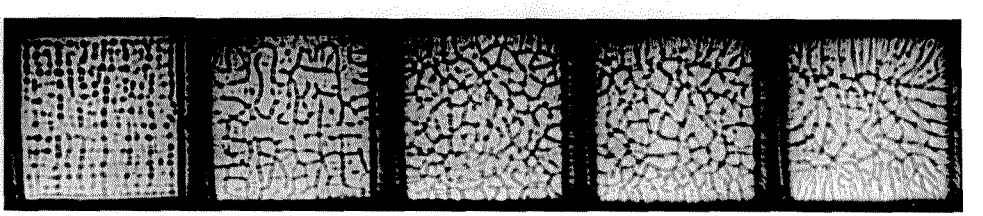

Run EK, H_{Tcr} = 2.16E7

Ra_d = 5.84E5	Ra_d = 7.14E5	Ra_d = 1.03E6	Ra_d = 1.09E6	Ra_d = 1.15E6	
t = 40s, τ = 0.009	t = 65s, τ = 0.016	t = 250s, τ = 0.059	t = 405s, τ = 0.096	t = 690s, τ = 0.163	
τ/τ_{cr} = 1.29	τ/τ_{cr} = 2.28	τ/τ_{cr} = 8.43	τ/τ_{cr} = 13.7	τ/τ_{cr} = 23.3	

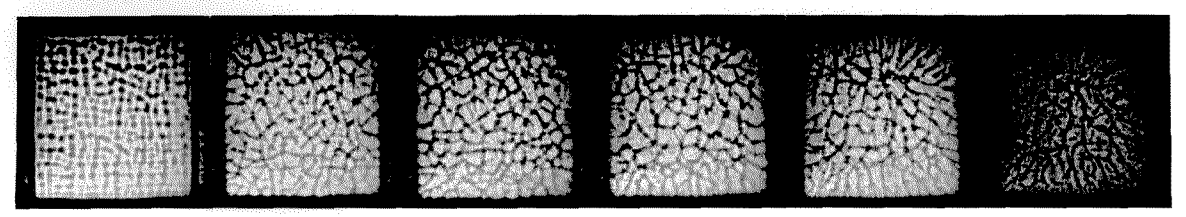

Run EA, H_{Tcr} = 3.31E7

Ra_d = 8.01E5	Ra_d = 1.31E6	Ra_d = 1.53E6	Ra_d = 1.66E6	Ra_d = 1.76E6	Ra_d = 1.82E6
t = 35s, τ = 0.008	t = 130s, τ = 0.031	t = 250s, τ = 0.059	t = 400s, τ = 0.095	t = 595s, τ = 0.140	t = 735s, τ = 0.174
τ/τ_{cr} = 1.33	τ/τ_{cr} = 5.17	τ/τ_{cr} = 9.84	τ/τ_{cr} = 15.8	τ/τ_{cr} = 23.3	τ/τ_{cr} = 29.0

Figure 49. Patterns of Motion for 0.01905 m Depth (Runs EJ, EC, EK, EA). See Figure 9 for scaling.

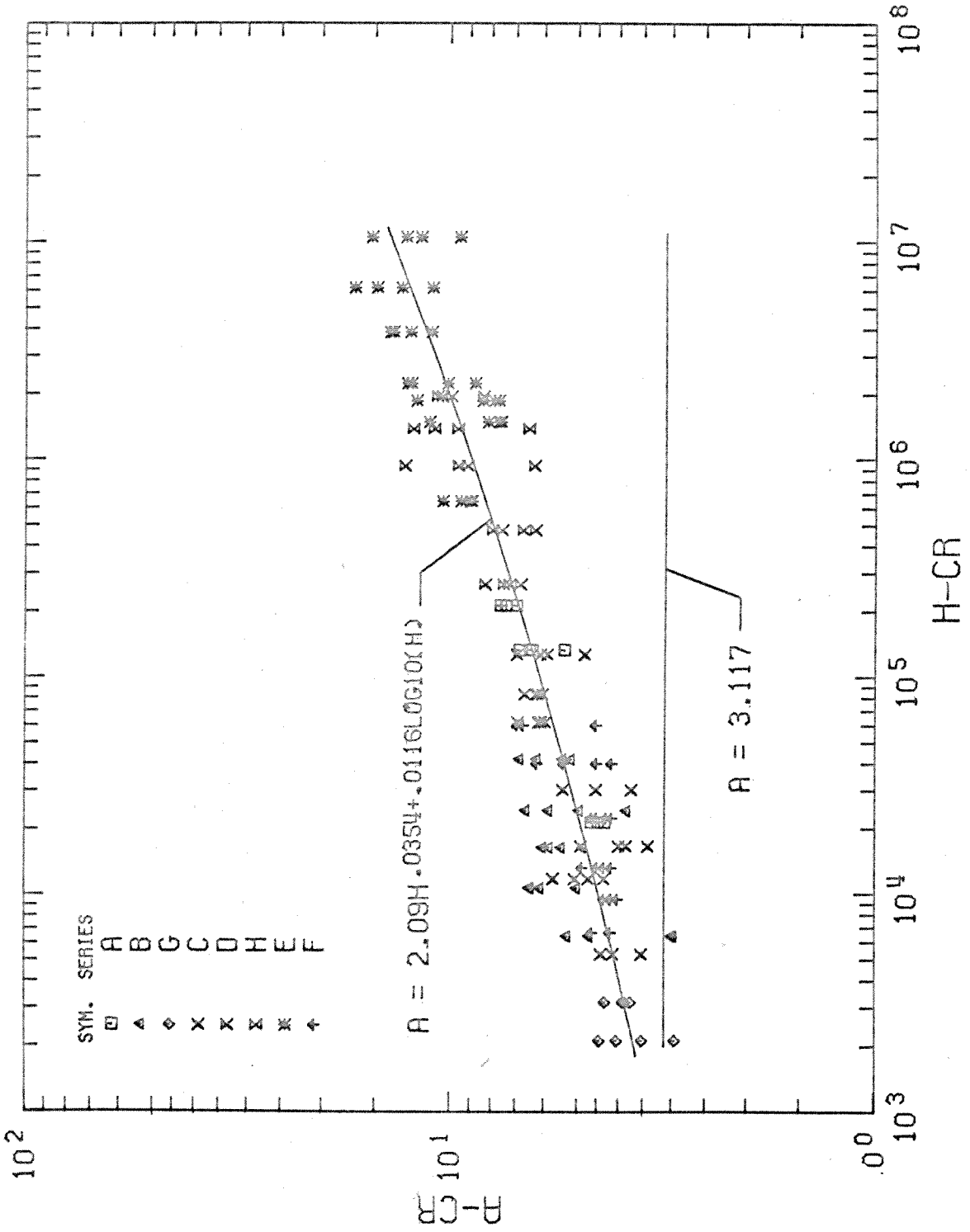

Figure 50. Critical Wave Number versus Critical Lower Surface Heat Flux .

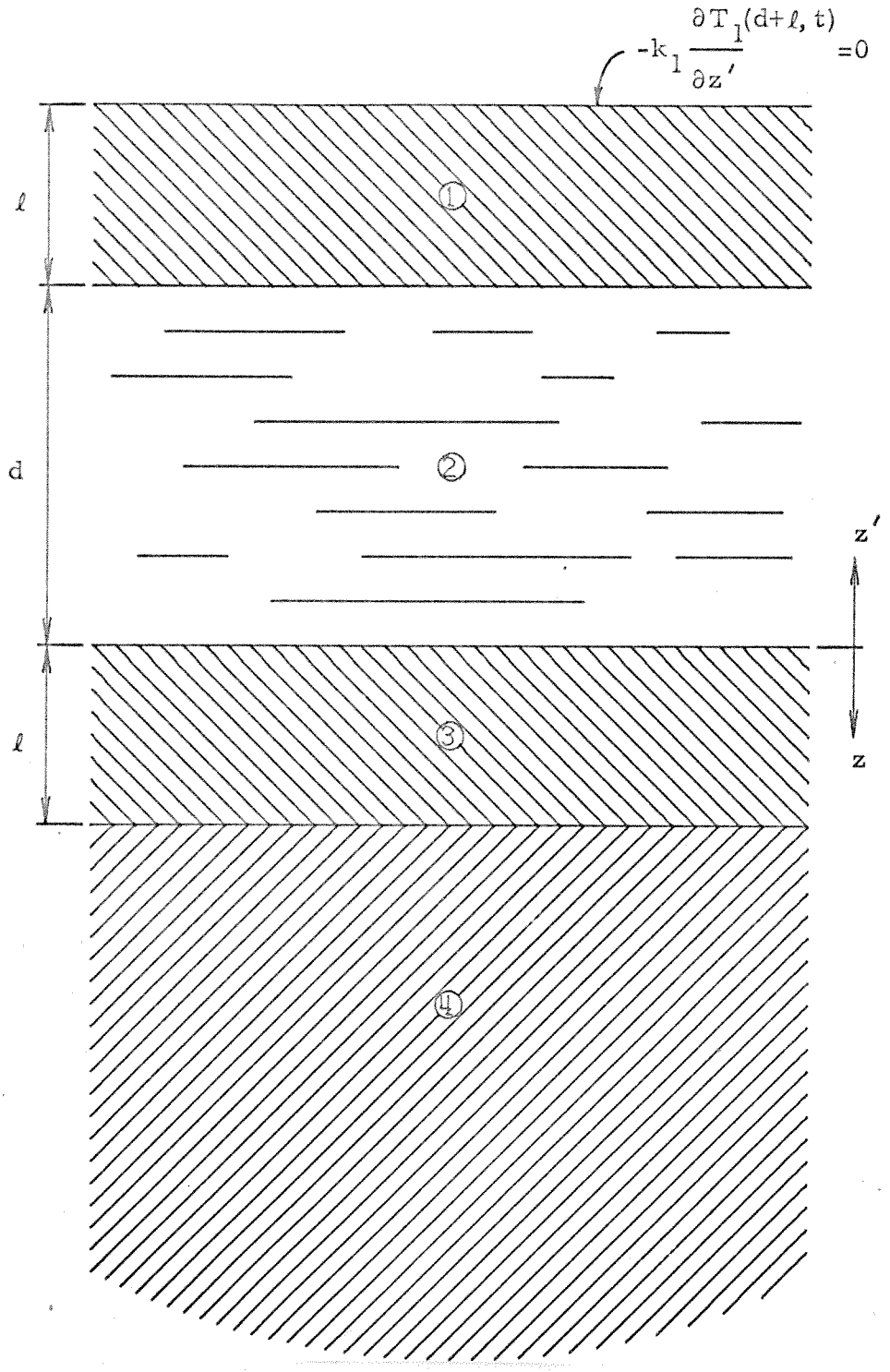

Figure 51. Composite Heat Transfer Medium.

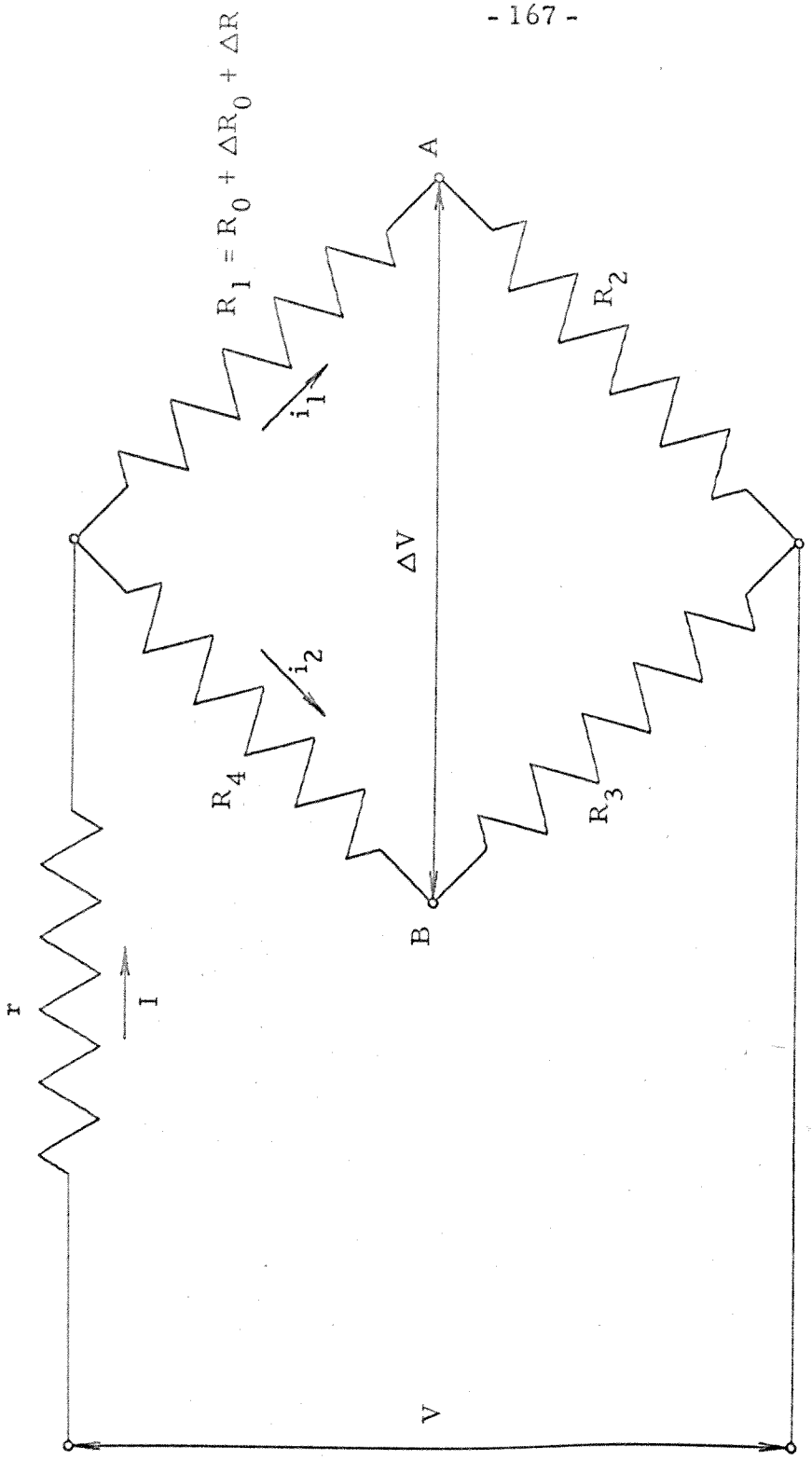

Figure 52. Wheatstone Bridge Circuit.

APPENDIX B

DETAILS OF THE STABILITY BOUNDARY ANALYSIS

APPENDIX B

DETAILS OF THE STABILITY BOUNDARY ANALYSIS

A. Introduction.

For any given conduction profile the stability of the fluid layer is determined from the solution of the eigenvalue problem given by Equation (40) of Chapter III. That is,

$$\det\left|\frac{2a^2 E_{rn}}{(a^2 + r^2\pi^2)^3} - \frac{1}{R}\,\delta_{rn}\right| = 0 \qquad \text{at} \qquad t = t_{cr}. \tag{B1}$$

The effect of the conduction profile is contained in the term $E_{rn}(t_{cr})$, which is given by

$$E_{rn}(t_{cr}) = \int_0^1 \left(-\frac{\partial \overline{T}}{\partial z}(z, t_{cr})\right) \sin r\pi z\, W_n(z)\, dz \tag{B2}$$

For the rigid-rigid boundary conditions the vertical velocity components, $W_n(z)$, can be written as

$$W_n(z) = \sin n\pi z - \frac{(A_n - F_n z)}{2} e^{az} + \frac{(A_n - E_n z)}{2} e^{-az} \tag{B3}$$

where

$$A_n = (c_n - d_n)\ , \quad B_n = (c_n + d_n)\ , \quad E_n = A_n + B_n e^{a}\ , \quad F_n = A_n + B_n e^{-a}$$

$$c_n = \frac{n\pi[1-(-1)^n]}{2(\sinh a + a)} \quad , \quad d_n = \frac{n\pi[1+(-1)^n]}{2(\sinh a - a)}$$

In the following sections the E_{rn} will be calculated for the steady-state profile, the approximate two-step profile and the approximate exponential profile.

B. Steady-State Profile.

The steady-state temperature profile and the corresponding temperature gradient are given by

$$\overline{T}(z) = (1-z) \quad , \quad -\frac{d\overline{T}}{dz}(z) = 1 \tag{B4}$$

Using the temperature gradient, the E_{rn} can be written as

$$\begin{aligned} 2E_{rn} = &\int_0^1 \cos (r-n)\pi z \, dz - \int_0^1 \cos (r+n)\pi z \, dz \\ &- \int_0^1 (A_n - F_n z) e^{az} \sin r\pi z \, dz \\ &+ \int_0^1 (A_n - E_n z) e^{-az} \sin r\pi z \, dz \end{aligned} \tag{B5}$$

$$2E_{rn} \equiv I_1 - I_2 - I_3 + I_4$$

The terms I_1, I_2, I_3 and I_4 are

$$\begin{aligned} I_1 &= \delta_{rn} \\ I_2 &= 0 \\ I_3 &= \frac{1}{a^2 + r^2\pi^2} \left\{ \left(A_n r\pi + F_n \frac{2ar\pi}{a^2 + r^2\pi^2} \right) [1-(-1)^r e^a] + F_n r\pi (-1)^r e^a \right\} \\ I_4 &= \frac{1}{a^2 + r^2\pi^2} \left\{ \left(A_n r\pi - E_n \frac{2ar\pi}{a^2 + r^2\pi^2} \right) [1-(-1)^r e^{-a}] + E_n r\pi (-1)^r e^{-a} \right\} \end{aligned} \tag{B6}$$

Using the definitions of A_n, E_n and F_n, the E_{rn} can be simplified to

$$E_{rn} = \frac{\delta_{rn}}{2} - \frac{4ar\pi}{(a^2 + r^2\pi^2)^2} \left\{ c_n (\cosh a + 1) \frac{[1-(-1)^r]}{2} + d_n (\cosh a - 1) \frac{[1+(-1)^r]}{2} \right\} \tag{B7}$$

C. Two-Step Profile.

The Two-step approximate temperature profile and the corresponding temperature gradient are given by

$$\overline{T}_a(z;\, t_{cr}) = \begin{cases} 1 - \dfrac{z}{\delta} & 0 \le z \le \delta \\ 0 & \delta \le z \le 1 \end{cases}, \qquad -\frac{d\overline{T}_a}{dz} = \begin{cases} \dfrac{1}{\delta} & 0 \le z \le \delta \\ 0 & \delta \le z \le 1 \end{cases} \tag{B8}$$

Using the temperature gradient, the E_{rn} can be written as

$$2\delta E_{rn} = \int_0^\delta \cos(r-n)\pi z\, dz - \int_0^\delta \cos(r+n)\pi z\, dz$$

$$- \int_0^\delta (A_n - F_n z) e^{az} \sin r\pi z\, dz$$

$$+ \int_0^\delta (A_n - E_n z) e^{-az} \sin r\pi z\, dz$$

$$2\delta E_{rn} \equiv I_1 - I_2 - I_3 + I_4$$

The terms I_1, I_2, I_3 and I_4 are

$$I_1 = \delta\, \delta_{rn} + \frac{1}{(r-n)\pi} \sin(r-n)\pi\delta(1-\delta_{rn})$$

$$I_2 = \frac{1}{(r+n)\pi} \sin(r+n)\pi\delta$$

$$I_3 = \frac{1}{a^2 + r^2\pi^2} \left\{ \left(A_n r\pi + F_n \frac{2ar\pi}{a^2 + r^2\pi^2} \right) [1 - \cos r\pi\delta e^{a\delta}] \right. \tag{B10a}$$

$$+ F_n r\pi\delta \cos r\pi\delta e^{a\delta}$$

$$\left. + \left[(A_n - F_n\delta)a + F_n \left(\frac{a^2 - r^2\pi^2}{a^2 + r^2\pi^2} \right) \right] \sin r\pi\delta\, e^{a\delta} \right\}$$

$$I_4 = \frac{1}{a^2+r^2\pi^2}\left\{\left(A_n r\pi - E_n \frac{2ar\pi}{a^2+r^2\pi^2}\right)\left[1-\cos r\pi\delta\, e^{-a\delta}\right]\right.$$

$$+ E_n r\pi\delta \cos r\pi\delta\, e^{-a\delta} \qquad \text{(B10b)}$$

$$\left. + \left[-(A_n - E_n\delta)a + F_n\left(\frac{a^2-r^2-\pi^2}{a^2+r^2\pi^2}\right)\right]\sin r\pi\delta\, e^{-a\delta}\right\}$$

D. Exponential Profile.

The exponential approximate temperature profile and the corresponding temperature gradient are given by

$$\overline{T}_a(z; t_{cr}) = (1-z)e^{-\alpha z} \quad , \quad -\frac{d\overline{T}_a}{dz} = [(1+\alpha)-\alpha z]e^{-\alpha z} \tag{B11}$$

Using the temperature gradient, the E_{rn} can be written as

$$\begin{aligned} 2E_{rn} = &\int_0^1 [(1+\alpha)-\alpha z]^{-\alpha z} \cos(r-n)\pi z\, dz \\ &- \int_0^1 [(1+\alpha)-\alpha z]e^{-\alpha z} \cos(r+n)\pi z\, dz \\ &- \int_0^1 \left\{A_n(1+\alpha) - [A_n\alpha + F_n(1+\alpha)]z + F_n\alpha z^2\right\} e^{-(\alpha-a)z} \sin r\pi z\, dz \\ &+ \int_0^1 \left\{A_n(1+\alpha) - [A_n\alpha + E_n(1+\alpha)]z + E_n\alpha z^2\right\} e^{-(\alpha+a)z} \sin r\pi z\, dz \end{aligned} \tag{B12}$$

$$2E_{rn} \equiv I_1 - I_2 - I_3 + I_4$$

The terms I_1, I_2, I_3 and I_4 are

$$I_1 = \frac{1}{\alpha^2+(r-n)^2\pi^2}\left\{\left[(1+\alpha)\alpha-\alpha\left(\frac{\alpha^2-(r-n)^2\pi^2}{\alpha^2+(r-n)^2\pi^2}\right)\right][1-(-1)^{r+n}e^{-\alpha}] + \alpha^2(-1)^{r+n}e^{-\alpha}\right\} \tag{B13a}$$

$$I_2 = \frac{1}{\alpha^2+(r+n)^2\pi^2}\left\{\left[(1+\alpha)\alpha-\alpha\left(\frac{\alpha^2-(r+n)^2\pi^2}{\alpha^2+(r+n)^2\pi^2}\right)\right][1-(-1)^{r+n}e^{-\alpha}] + \alpha^2(-1)^{r+n}e^{-\alpha}\right\}$$

$$I_3 = \frac{1}{(\alpha-a)^2+r^2\pi^2}\left\{\left[A_n(1+\alpha)-[A_n\alpha+F_n(1+\alpha]\,\frac{2(\alpha-a)r\pi}{(\alpha-a)^2+r^2\pi^2}\right.\right.$$
$$\left.+2F_n\alpha\,\frac{r\pi[3(\alpha-a)^2-r^2\pi^2]}{[(\alpha-a)^2+r^2\pi^2]^2}\right][1-(-1)^r e^{-(\alpha-a)}]$$
$$\left.-\left[-(A_n\alpha+F_n)r\pi+2F_n\alpha\,\frac{2(\alpha-a)r\pi}{(\alpha-a)^2+r^2\pi^2}\right](-1)^r e^{-(\alpha-a)}\right\}$$

$$I_4 = \frac{1}{(\alpha+a)^2+r^2\pi^2}\left\{\left[A_n(1+\alpha)-[A_n\alpha+E_n(1+\alpha)]\,\frac{2(\alpha+a)r\pi}{(\alpha+a)^2+r^2\pi^2}\right.\right. \qquad \text{(B13b)}$$
$$\left.+2E_n\alpha\,\frac{r\pi[3(\alpha+a)^2-r^2\pi^2]}{[(\alpha+a)^2+r^2\pi^2]^2}\right][1-(-1)^r e^{-(\alpha+a)}]$$
$$\left.-\left[-(A_n\alpha+E_n)r\pi+2E_n\alpha\,\frac{2(\alpha+a)r\pi}{(\alpha+a)^2+r^2\pi^2}\right](-1)^r e^{-(\alpha+a)}\right\}$$

E. Asymptotic Expansions for Infinite Heating Rate.

For the special cases of $\delta \to 0$ and $\alpha \to \infty$, which corresponds to an infinite rate of heating or an infinitely deep fluid layer, the resulting expressions, obtained from making asymptotic expansions of the E_{rn}, simplify to the same terms within a constant. In the limit of infinite heating the E_{rn} can be written as

$$E_{rn} \approx a(r\pi)(n\pi)\left[\frac{[1-(-1)^n]}{2}\left(\frac{\cosh a+1}{\sinh a+a}\right)+\frac{[1+(-1)^n]}{2}\left(\frac{\cosh a-1}{\sinh a-a}\right)\right]\begin{Bmatrix}\frac{\delta^3}{4}\\ \frac{6}{\alpha^3}\end{Bmatrix} \quad \text{(B14)}$$

The terms of the determinant (B1) are

$$\frac{2a^3(r\pi)(n\pi)}{(a^2+r^2\pi^2)^3}e_n - \frac{1}{R}\delta_{rn} \quad \text{(B15)}$$

where

$$e_n = \left[\frac{[1-(-1)^n]}{2}\left(\frac{\cosh a+1}{\sinh a+a}\right)+\frac{[1+(-1)^n]}{2}\left(\frac{\cosh a-1}{\sinh a-a}\right)\right]\begin{Bmatrix}\frac{\delta^3}{4}\\ \frac{6}{\alpha^3}\end{Bmatrix}$$

If row r is multiplied by $(a^2+r^2\pi^2)^3/r\pi$ and column n is multiplied by $1/n\pi$, the terms become

$$2a^3e_n - \frac{1}{R}\frac{(a^2+r^2\pi^2)^3}{(r\pi)(n\pi)}\delta_{rn} \equiv 2a^3e_n - \frac{1}{R}\frac{(a^2+n^2\pi^2)^3}{n^2\pi^2}\delta_{rn} \quad \text{(B16)}$$

Multiplying column n by $(a^2+n^2\pi^2)^3/n^2\pi^2$, the terms can be written as

$$\frac{2a^3n^2\pi^2}{(a^2+n^2\pi^2)^3}e_n - \frac{1}{R}\delta_{rn} \quad \text{(B17)}$$

The left-hand side of the terms are now functions of n only. By

successive approximations, it is possible to show that for this special case the solution of the determinant is given by

$$\frac{1}{R} = \sum_{n=1}^{\infty} \frac{2a^2 n^2 \pi^2}{(a^2+n^2\pi^2)^3} e_n \qquad \text{(B18)}$$

APPENDIX C

ANALYTICAL CONDUCTION PROFILE

APPENDIX C

ANALYTICAL CONDUCTION PROFILE

In the determination of the response of the fluid layer to hea from below, use was made of the analytical conduction solution. T solution was used because the type of heating, a plane of constant h generation, leads in its initial stages to the temperature at the plan increasing as the square root of time. This behavior is difficult to handle with the normal finite difference scheme used in numerical heat transfer calculations. If the conduction solution is known, the onset of motion can be quickly determined by examining the deviation of the experimental heat transfer data from the theoretical conduction results. The conduction solution also represents a check of the data during times when the fluid layer is known to be conducting.

The idealized conduction problem consisting of a semi-infinite composite solid is shown in Figure 51. The fluid layer is bounded on either side by equal thickness layers of identical material (Pyrex glass). The upper plane is assumed to be a surface of zero heat flux; in the experiments the bounding fluid was air. Below the lower layer of glass is a semi-infinite layer of another material (phenolic plastic).

The basic technique is to make a Laplace transform of the governing equations, solve them in the transform plane and then take the inverse transform to obtain the desired solution. The diffictult part of the solution is that the equations lead to a series expansion, the terms

of which must be determined one by one. The number of terms to be calculated was determined by the material properties, the maximum time for a run, 2000 s, and the maximum error of the results, set at ±0.00001.

The starting place of the analysis is the heat conduction equation which for the various layers can be written as

$$\frac{\partial T_1}{\partial t} = \kappa_1 \frac{\partial^2 T_1}{\partial z'^2} \quad , \quad \frac{\partial T_2}{\partial t} = \kappa_2 \frac{\partial^2 T_2}{\partial z'^2} \quad , \quad \frac{\partial T_3}{\partial t} = \kappa_3 \frac{\partial^2 T_3}{\partial z^2} \quad , \quad \frac{\partial T_4}{\partial t} = \kappa_4 \frac{\partial^2 T_4}{\partial z^2} \tag{C1}$$

The initial conditions for the problem are

$$T_1(z', 0) = T_2(z', 0) = T_3(z, 0) = T_4(z, 0) = 0 \tag{C2}$$

The boundary conditions can be stated as

$$T_1(d, t) = T_2(d, t) \quad , \quad T_2(0, t) = T_3(0, t) \quad , \quad T_3(\ell, t) = T_4(\ell, t)$$

$$-k_1 \frac{\partial T_1}{\partial z'}(d, t) = -k_2 \frac{\partial T_2}{\partial z'}(d, t) \quad , \quad -k_3 \frac{\partial T_3}{\partial z}(\ell, t) = -k_4 \frac{\partial T_4}{\partial z}(\ell, t) \tag{C3}$$

$$T_4(\infty, t) = 0 \quad , \quad -k_1 \frac{\partial T_1}{\partial z'}(d+\ell, t) = 0$$

$$-k_2 \frac{\partial T_2}{\partial z'}(0, t) - k_3 \frac{\partial T_3}{\partial z}(0, t) = Q_T$$

Take the Laplace transfor of Equations (C1), (C2) and (C3). Let a bar over the temperature denote the transform quantity. That is,

$$\overline{T_i}(z) = \int_0^\infty T_i(z, t) e^{-pt} dt \tag{C4}$$

The governing equations become

$$\frac{d^2\overline{T}_1}{dz'^2} - q_1^2\overline{T}_1 = 0 \quad , \quad \frac{d^2\overline{T}_2}{dz'^2} - q_2^2\overline{T}_2 = 0 \quad , \quad \frac{d^2\overline{T}_3}{dz^2} - q_3^2\overline{T}_3 = 0 \quad , \quad \frac{d^2\overline{T}_4}{dz^2} - q_4^2\overline{T}_4 = 0 \quad \text{(C5)}$$

where

$$q_i \equiv \sqrt{\frac{p}{\kappa_i}}$$

The boundary conditions are transformed to

$$\overline{T}_1(d) = \overline{T}_2(d) \quad , \quad \overline{T}_2(0) = \overline{T}_3(0) \quad , \quad \overline{T}_3(\ell) = \overline{T}_4(\ell)$$

$$-k_1 \frac{d\overline{T}_1}{dz'}(d) = -k_2 \frac{d\overline{T}_2}{dz'}(d) \quad , \quad -k_3 \frac{d\overline{T}_3}{dz}(\ell) = -k_4 \frac{d\overline{T}_4}{dz}(\ell)$$

$$\overline{T}_4(\infty) = 0 \quad , \quad -k_1 \frac{d\overline{T}_1}{dz'}(d+\ell) = 0 \qquad \text{(C6)}$$

$$-k_2 \frac{d\overline{T}_2}{dz'}(0) - k_3 \frac{d\overline{T}_3}{dz}(0) = \frac{Q_T}{p}$$

The solutions to the governing equations (C5) can be written in the form

$$\overline{T}_1(z') = Ae^{q_1(z'-d-\ell)} + Be^{-q_1(z'-d-\ell)}$$

$$\overline{T}_2(z') = Ce^{q_2 z'} + De^{-q_2 z'} \qquad \text{(C7)}$$

$$\overline{T}_3(z) = Ee^{q_3 z} + Fe^{-q_3 z}$$

$$\overline{T}_4(z) = Ge^{-q_4(z-\ell)} + He^{q_4(z-\ell)}$$

Substituting the solutions (C7) into the boundary conditions (C6), the coefficients must satisfy the relationships

$$Ae^{-q_1\ell} + Be^{q_1\ell} = Ce^{q_2 d} + De^{-q_2 d}$$

$$C + D = E + F$$

$$Ee^{q_3\ell} + Fe^{-q_3\ell} = G + H$$

$$-k_1q_1Ae^{-q_1\ell} + k_1q_1Be^{q_1\ell} = -k_2q_2Ce^{q_2 d} + k_2q_2De^{-q_2 d}$$

$$-k_3q_3Ee^{q_3\ell} + k_3q_3Fe^{-q_3\ell} = k_4q_4G - k_4q_4H \qquad \text{(C8)}$$

$$H = 0 \quad , \quad -k_1q_1A + k_1q_1B = 0$$

$$-k_2q_2C + k_2q_2D - k_3q_3E + k_3q_3F = \frac{Q_T}{p}$$

For compactness of notation introduce the following quantities, making use of the fact that layers 1 and 3 are identical materials

$$\sigma_2 = k_2/k_1\sqrt{\kappa_1/\kappa_2} \quad , \quad \sigma_3 = k_3/k_1\sqrt{\kappa_1/\kappa_3} \equiv 1 \quad , \quad \sigma_4 = k_4/k_1\sqrt{\kappa_1/\kappa_4}$$

$$\xi = (1+\sigma_4)(1+\sigma_2)^2 \quad , \quad \zeta_1 = 2\left(1-\sigma_2^2\right)/\xi \quad , \quad \zeta_2 = (1+\sigma_4)(1-\sigma_2)^2/\xi$$

$$\zeta_3 = (1-\sigma_4)(1+\sigma_2)^2/\xi \quad , \quad \zeta_4 = (1-\sigma_4)(1-\sigma_2)^2/\xi \qquad \text{(C9)}$$

$$\varphi = \zeta_1 e^{-2q_1\ell} + \zeta_2 e^{-2q_2 d} - \zeta_1 e^{-2q_1\ell - 2q_2 d} + \zeta_3 e^{-4q_1\ell - 2q_2 d} - \zeta_4 e^{-4q_1\ell}$$

Using these quantities, the coefficients can be written as

$$A = B = \frac{Q_T}{k_1q_1p}\,\frac{2\sigma_2 e^{-q_1\ell - q_2 d}}{\xi}\,\frac{(1+\sigma_4) + (1-\sigma_4)e^{-2q_1\ell}}{(1-\varphi)} \qquad \text{(C10a)}$$

$$C = -\frac{Q_T}{k_1q_1p}\,\frac{e^{-2q_2 d}\left[(1+\sigma_4)(1-\sigma_2) - 2(\sigma_4+\sigma_2)e^{-2q_1\ell} - (1-\sigma_4)(1+\sigma_2)e^{-4q_1\ell}\right]}{\xi(1-\varphi)}$$

$$D = \frac{Q_T}{k_1 q_1 p} \frac{\left[(1+\sigma_4)(1+\sigma_2)-2(\sigma_4-\sigma_2)e^{-2q_1\ell}-(1-\sigma_4)(1-\sigma_2)e^{-4q_1\ell}\right]}{\xi(1-\varphi)}$$

$$E = \frac{Q_T}{k_1 q_1 p} \frac{(1-\sigma_4)e^{-2q_1\ell}}{\xi(1-\varphi)} \left[(1+\sigma_2)-(1-\sigma_2)e^{-2q_1\ell}-(1-\sigma_2)e^{-2q_2 d} + (1+\sigma_2)e^{-2q_1\ell-2q_2 d}\right]$$

$$F = \frac{Q_T}{k_1 q_1 p} \frac{(1+\sigma_4)}{\xi(1-\varphi)} \left[(1+\sigma_2)-(1-\sigma_2)e^{-2q_1\ell}-(1-\sigma_2)e^{-2q_2 d} + (1+\sigma_2)e^{-2q_1\ell-2q_2 d}\right] \qquad \text{(C10b)}$$

$$G = \frac{Q_T}{k_1 q_1 p} \frac{2e^{-2q_1\ell}}{\xi(1-\varphi)} \left[(1+\sigma_2)-(1-\sigma_2)e^{-2q_1\ell}-(1-\sigma_2)e^{-2q_2 d} + (1+\sigma_2)e^{-2q_1\ell-2q_2 d}\right]$$

With the coefficients (C10) the general solution (C7) can now in principle be inverted to give the actual temperatures through the composite medium as a function of time and spatial position. A direct inverse transformation cannot be performed, however, because of the presence of the term $(1-\varphi)$ in the denominator of the coefficients. This difficulty is circumvented by making a series expansion of the term. This procedure will yield solutions that are useful for short times. The range of validity of the expansion will be increased by including more terms of the expansion in the analysis. The term is expressed as

$$\frac{1}{(1-\varphi)} = \sum_{n=0}^{\infty} \varphi^n \tag{C11}$$

When the expansion is performed, the resulting terms can be grouped in matching powers of the exponent arguments. Symbolically, this grouping can be written as

$$\sum_{n=0}^{\infty} \varphi^n = \sum_{i=1}^{\infty} \sum_{j=1}^{\infty} \beta_{ij} e^{-2(i-1)q_1 \ell - 2(j-1)q_2 d} \tag{C12}$$

In the present experiments a detailed spatial behavior of the temperature and the heat flux in the composite medium was not required. Instead, only the temperature and heat flux at selected planes are needed. The quantities for which transformations had to be obtained were

$$T_2(d,t) \quad , \quad T_2(0,t) \quad , \quad T_3(\ell,t) \quad , \quad -k_2 \frac{\partial T_2}{\partial z'}(0,t) \quad , \quad -k_3 \frac{\partial T_3}{\partial z}(0,t)$$

$$-k_4 \frac{\partial T_4}{\partial z}(\ell,t) \quad , \quad \frac{1}{d}\int_0^d T_2(z',t)\,dz' \tag{C13}$$

The integral expression was used in the calculation of the thermal thickness. In the transformed plane the required quantities are

$$\overline{T}_2(d) = Ce^{q_2 d} + De^{-q_2 d} \quad , \quad \overline{T}_2(0) = C + D \quad , \quad \overline{T}_3(\ell) = G$$

$$-k_2 \frac{d\overline{T}_2}{dz'}(0) = -k_2 q_2 (C-D) \quad , \quad -k_3 \frac{d\overline{T}_3}{dz}(0) = -k_3 q_3 (E-F) \tag{C14}$$

$$-k_4 \frac{d\overline{T}_4}{dz}(\ell) = k_4 q_4 G \quad , \quad \frac{1}{d}\int_0^d \overline{T}_2(z')dz' = \frac{1}{q_2 d}\left(D - C + Ce^{q_2 d} - De^{-q_2 d}\right)$$

Using Equations (C14), the inverse transformation can be performed term by term in the series expansion. For the heat flux quantities a typical term with its transform would be

$$\frac{e^{-\mu_{ij} q_1 \ell}}{p} \rightarrow \operatorname{erfc}\left(\frac{\mu_{ij}\ell}{2\sqrt{\kappa_1 t}}\right) \tag{C15}$$

For the temperatures a typical term with its transform would be

$$\frac{e^{-\mu_{ij} q_1 \ell}}{p q_1} \rightarrow 2\sqrt{\kappa_1 t}\, \operatorname{ierfc}\left(\frac{\mu_{ij}\ell}{2\sqrt{\kappa_1 t}}\right) \tag{C16}$$

For the integral a typical term would be

$$\frac{e^{-\mu_{ij} q_1 \ell}}{p q_1^2} \rightarrow 4\kappa_1 t\, i^2\operatorname{erfc}\left(\frac{\mu_{ij}\ell}{2\sqrt{\kappa_1 t}}\right) \tag{C17}$$

In the above expressions erfc(x) is the complementary error function. The other functions ierfc(x) and i^2erfc(x) are the first and second integrals of the complementary error function. They can be written as

$$\begin{aligned} \operatorname{ierfc}(x) &= \frac{1}{\sqrt{\pi}} e^{-x^2} - x \operatorname{erfc}(x) \\ i^2\operatorname{erfc}(x) &= \frac{1}{4}\left[(1+2x^2)\operatorname{erfc}(x) - \frac{2}{\sqrt{\pi}} x e^{-x^2}\right] \end{aligned} \tag{C18}$$

In the present experiments the various quantities (C13) were calculated at ten second intervals over the span of two thousand se seconds. This procedure was carried out for the three different oils and three different depths. The results were punched on computer cards, which then formed a data set that was part of the two data reduction computer programs.

APPENDIX D

WHEATSTONE BRIDGE CALCULATIONS

APPENDIX D

WHEATSTONE BRIDGE CALCULATIONS

The temperatures of the two bounding glass surfaces were determined by measuring the change in resistance of the two coatings through the use of Wheatstone bridges. These resistance changes were then converted to temperature changes by a calibration factor that had been predetermined in a series of constant temperature bath experiments. For the lower surface the value of the calibration factor was $0.00436\Omega/K$, while the upper surface value was $0.00575\Omega/K$.

The resistance change of the coating is determined from the voltage imbalance of the bridge and the total voltage drop across the bridge when the other three leg resistances of the bridge are known. Using the Wheatstone bridge shown in Figure 52 for notation, the analysis begins with Kirkhoff's laws

$$(R_1+R_2)i_1=(R_3+R_4)i_2, \quad i_1+i_2=I \tag{D1}$$

Solving for i_1 and i_2,

$$i_1=\left(\frac{R_3+R_4}{\Sigma R}\right)I, \quad i_2=\left(\frac{R_1+R_2}{\Sigma R}\right)I \tag{D2}$$

where

$$\Sigma R \equiv R_1+R_2+R_3+R_4$$

The total voltage drop can be written as

$$V=I\left[r+\frac{1}{1/(R_1+R_2)+1/(R_3+R_4)}\right]=I\left[\frac{(R_1+R_2)(R_3+R_4)+r\Sigma R}{\Sigma R}\right] \qquad (D3)$$

The voltage imbalance of the bridge is

$$V_B-V_A\equiv\Delta V=R_3 i_2-R_2 i_1,\quad \Delta V=\left(\frac{R_1R_3-R_2R_4}{\Sigma R}\right)I$$

$$\Delta V=\left[\frac{R_1R_3-R_2R_4}{(R_1+R_2)(R_3+R_4)+r\Sigma R}\right]V \qquad (D4)$$

Introduce the following notation:

$$\delta=\frac{\Delta V}{V},\quad R_1=R_0+\Delta R_0+\Delta R,\quad R_0=\frac{R_2R_4}{R_3},\quad \Sigma R_0=R_0+R_2+R_3+R_4 \qquad (D5)$$

where ΔR_0 is the initial resistance "imbalance" at temperature T_0 and ΔR is the additional change in resistance due to heating to temperature T. Using the notation in Equations (D5), the voltage imbalance Equation (D4) can be rewritten as

$$\delta=\frac{(\Delta R_0+\Delta R)R_3}{(R_0+\Delta R_0+\Delta R+R_2)(R_3+R_4)+r(\Sigma R_0+\Delta R_0+\Delta R)}$$

$$\delta_0=\frac{\Delta R_0 R_3}{(R_0+\Delta R_0+R_2)(R_3+R_4)+r(\Sigma R_0+\Delta R_0)} \qquad (D6)$$

Solving for the change in resistance,

$$\Delta R_0+\Delta R=\frac{\delta[(R_0+R_2)(R_3+R_4)+r\Sigma R_0]}{R_3-\delta(R_3+R_4+r)}$$

$$\Delta R_0=\frac{\delta_0[(R_0+R_2)(R_3+R_4)+r\Sigma R_0]}{R_3-\delta_0(R_3+R_4+r)} \tag{D7}$$

$$\Delta R=\frac{(\delta-\delta_0)R_3[(R_0+R_2)(R_3+R_4)+r\Sigma R_0]}{[R_3-\delta(R_3+R_4+r)][R_3-\delta_0(R_3+R_4+r)]}$$

The change in resistance is converted to a change in temperature through a calibration constant, α_R:

$$\Delta T=\frac{\Delta R}{\alpha_R} \tag{D8}$$

An additional quantity that is needed in the calculations is the total heat generation rate at the lower surface, Q_T. The heat generation rate is per unit area, which means that the effective heating area of the glass surface, A, must be determined. From voltage drop measurements across the plate the effective area was found to be 0.04848 m^2 (8.35" x 9.00"). Using the effective heating area, the total heat generation rate is determined from Joule's law:

$$Q_T A=i_1^2 R_1=\left(\frac{R_3+R_4}{(R_1+R_2)(R_3+R_4)+r\Sigma R}\right)^2 R_1 V^2 \tag{D9}$$

Eliminating R_1, the heat generation rate can be rewritten as

$$Q_T = C_Q \left\{ \begin{matrix} R_0 R_3^2 + \delta R_3 [(R_2 - R_0)(R_3 + R_4 + r) - r(R_3 + R_4)] \\ - \delta^2 (R_3 + R_4 + r)[R_2(R_3 + R_4 + r) + r(R_3 + R_4)] \end{matrix} \right\} \frac{V^2}{A} \qquad \text{(D10)}$$

where

$$C_Q = \left[\frac{1}{R_3} \frac{R_3 + R_4}{(R_0 + R_2)(R_3 + R_4) + r\Sigma R_0} \right]^2$$

If r=0, the expression can be reduced to

$$Q_T = \left[\frac{R_3 R_4}{R_2 (R_3 + R_4)^2} + \delta \frac{1}{R_2} \left(\frac{R_3 - R_4}{R_3 + R_4} \right) - \delta^2 \frac{1}{R_2} \right] \frac{V^2}{A} \qquad \text{(D11)}$$

In the present experiments the resistances of the legs of the two Wheatstone bridges were

Lower surface bridge	Upper surface bridge
$R_2 = 15.434\Omega$	$R_2 = 15.521\Omega$
$R_3 = 15.536\Omega$	$R_3 = 15.579\Omega$
$R_4 = 12.868\Omega$	$R_4 = 15.468\Omega$
$r = 0.000\Omega$	$r = 0.018\Omega$
$R_0 = 12.784\Omega$	$R_0 = 15.410\Omega$

Balancing resistors, ranging in value from 1500Ω to 4000Ω, were used in parallel with R_3 to correct any slight changes in resistance during the course of the experiments.

APPENDIX E

PROPERTY VALUES

APPENDIX E

PROPERTY VALUES

In calculating the response of the fluid layer to transient heating, use is made of the physical properties of the fluid and the bounding materials. For the bounding solids the thermal conductivity, density and specific heat at constant pressure are required. For the fluid the kinematic viscosity and the thermal coefficient of expansion are needed in addition to the properties mentioned for the solids.

For silicone oils it is highly advisable to measure at least the viscosity because the value quoted by the manufacturer is only nominal, varying from batch to batch. Other physical properties seem to be less affected by slight variations in actual viscosity. For the present experiments both the density (hence, the thermal coefficient of expansion) and the viscosity were measured as a function of temperature by Mr. W. R. Hodson of Cal-Colonial Chemsolve. The densities of the three grades of oil were measured with a pycnometer, using distilled water as a standard. The viscosity of the 5 cs oil was measured with a Uboldtype viscometer with amyl alcohol as the reference. The

viscosities of the 100 cs and 500 cs oils were measured with a Brookfield viscometer, where iso propyl alcohol was the standard. The thermal coefficient of expansion was determined from the density data.

The remaining fluid properties, the thermal conductivity and the specific heat, were obtained from various sources. The thermal conductivity was obtained from Bates (1949), who from his experiments recommended the following correlation:

$$k = 0.1661\left(\frac{4.66+\nu_{25}-.000003\nu_{25}^{2}}{8.00+\nu_{25}}\right)(1-.000601t) \qquad \text{(E1)}$$

where ν_{25} is the nominal viscosity at 25 C in centistokes and t is the temperature in C. The specific heat at constant pressure was chosen after a thorough search of the available literature.

Of the properties used, the one subject to the largest error is probably the specific heat. The large possible error arises because of the differences in the reported values from various sources. The temperature dependence of the specific heat is subject to even more uncertainty. These discrepancies point up the need for detailed measurements of the silicone oil properties, such as was carried out by Bates, to determine the temperature dependence of the properties and any possible batch variation.

For use in the computer calculations correlations were fit to the various properties, which are summarized in Table E1. The density, thermal conductivity and specific heat were fit to linear relationships. The thermal coefficient of expansion was extracted from the linear dependence of the density. The kinematic viscosity was fit to the empirical Walther equation used for heavy oils. The equation is of the form:

$$\log_{10}\left(\log_{10}(\nu+0.8)\right)=A+B\log_{10}T \qquad (E2)$$

where the kinematic viscosity is measured in centistokes (10^{-6} m^2 s^{-1}) and T is the absolute temperature in K.

For the bounding surfaces of Pyrex glass a search was made of the literature to find the values of the properties. The density and specific heat data were taken from the recommended curves found in Touloukian (1967). These books are compilations of properties from various sources. The thermal conductivity data proved to be widely scattered. The final choice was to use the results of Plummer, Campbell and Comstock (1962), who made measurements of the thermal diffusivity in a transient experiment. The various data were fit to polynomial equations in temperature for use in the computer calculations. The resulting equations are shown in Table E1.

In the analytical calculations of the conduction problem (Appendix C) the properties of phenolic plastic were needed in addition to those of Pyrex glass and silicone oil. The values used, shown in Table E1, were obtained from Muller (1966).

In choosing the values of the properties to be used for silicone oil an extensive search was made of the literature. A listing of the properties, used and suggested, has been made in Table E2. The properties are given at 25C, unless otherwise noted. The properties listed are the kinematic viscosity, $\nu(m^2 s^{-1})$, the density, $\rho(kg\, m^{-3})$, the coefficient of thermal expansion, $\beta(K^{-1})$, the thermal conductivity, $k(W\, m^{-1} K^{-1})$, the specific heat, $c_p(J\, kg^{-1} K^{-1})$, the thermal diffusivity, $\varkappa(m^2 s^{-1})$, the Prandtl number, Pr, and the viscosity temperature coefficient, VTC [$\equiv 1-\nu(50C)/\nu(25C)$]. The viscosity temperature coefficient is defined differently than the manufacturer's coefficient, which uses the temperatures 98.9 C and 37.8 C. The different temperatures were chosen to cover the usual experimental range of mean temperatures reported in the literature. Properties which were not actually reported by the source, but could be calculated from the given information, are enclosed in brackets. If extrapolations or interpolations were required to evaluate the property at 25 C, least square techniques were used. All viscosity corrections were done using the Walther equation, unless another equation was recommended by the source. A listing of the sources of the data and notes about any different temperatures are given at the end of the Table E2.

TABLE E1

PROPERTY CORRELATIONS USED IN EXPERIMENTS

Silicone Oils:

$$\log_{10}(\log_{10}(\nu + 0.8)) = a + b \log_{10} T$$

$$\rho = \rho_0 - \Delta\rho t, \quad \beta = \beta_0/(1 - \beta_0 t), \quad k = k_0 - \Delta k t$$

$$c_p = c_{p0} + \Delta c_p t, \quad \varkappa = k/\rho c_p, \quad Pr = \nu/\varkappa$$

Grade	a	b	ρ_0	$\Delta\rho$	$\beta_0 \times 10^3$
5.0	5.61086	-2.338	936.2	0.902	0.9637
100	2.99679	-1.089	985.3	0.858	0.8708
500	2.54713	-0.854	992.3	0.928	0.9352

Grade	k_0	Δk	c_{p0}	Δc_p
5.0	0.1234	0.742	1528.	0.837
100	0.1609	0.967	1453.	0.837
500	0.1648	0.991	1511.	0.837

Properties at 25 C:

Grade	$\nu \times 10^6$	ρ	$\beta \times 10^3$	k	c_p	$\varkappa \times 10^7$	Pr
5.0	3.86	913.7	0.987	0.1215	1549.	0.858	45.0
100	100.	963.9	0.890	0.1585	1473.	1.116	896.
500	523.	969.1	0.958	0.1623	1532.	1.093	4770

Pyrex glass:

$$\rho = 2221.(1 - 9.11\times10^{-6} t - 7.7\times10^{-9} t^2) = 2221. \text{ at } 25 \text{ C}$$

$$c_p = 681.4 + 1.76t - 0.00084t^2 = 724.9 \text{ at } 25 \text{ C}$$

$$\varkappa\times10^7 = 5.590 - 3.86\times10^{-3} t + 9.5\times10^{-6} t^2 = 5.50 \text{ at } 25 \text{ C}$$

$$k = \varkappa \rho c_p = 0.886 \text{ at } 25 \text{ C}$$

Phenolic plastic:

$$\rho = 1330, \quad k = 0.29, \quad c_p = 1460, \quad \varkappa = 1.50\times10^{-7}$$

TABLE E2

1. VISCOSITY

Grade	$\nu \times 10^6$	Source	Grade	$\nu \times 10^6$	Source
0.65	0.65	1, 2, 3	500	500	1, 2, 3, 4
	0.675[a]	9		532.	19
1.0	1.0	1, 2, 3		523.	20
1.5	1.5	1, 2, 3	1000	1000	1, 2, 3, 4
	1.60[a]	9		977.	18
2.0	2.0	1, 2, 3		937.	19
	[2.09]	17	10000	10000	4
3.0	3.0	1, 2, 3		[10245]	7
	[2.91]	15			
5.0	5.0	1, 2, 3			
	3.86	20			
7.0	7.0	4			
10.	10.	1, 2, 3, 4			
	11.3	19			
20.	20.	1, 2, 3, 4			
	19.04	14			
50.	50.	1, 2, 3, 4			
	50.[d]	8			
	[48.4]	16			
100	100	1, 2, 3, 4			
	157.	19			
	100.	20			
200	200	1, 2, 3, 4			
	206.	19			
350	350	1, 2, 3, 4			
	[423.]	15			

TABLE E2

2. DENSITY

Grade	ρ	Source
0.65	761	1, 2
	761[b]	3
1.0	818	1, 2
	818[b]	3
1.5	853	1, 2
	853[b]	3
2.0	873	1, 2
	873[b]	3
3.0	900	1, 2
	900[b]	3
	[908.]	15
5.0	920	1, 2
	920[b]	3
	913.7	20
7.0	930	4
10.	940	1, 2, 4
	940[b]	3
	932.	19
20.	955	1, 2
	955[b]	3
	950	4
	955.0	14
50.	960	1, 2, 4
	960[b]	3
	963.[a]	8
	960.	19
100	970	1, 2, 4
	968[b]	3
	968	10
	968[a]	11
	965.	19
	963.9	20
200	971	1, 2, 4
	971[b]	3
	965.	19
350	972	1, 2, 4
	972[b]	3
	[976.]	15
500	972	1, 2
	972[b]	3
	973	4
	965.	19
	969.1	20
1000	973	1, 2, 4
	972[b]	3
	969.7	18
	965.	19
10000	973	4

TABLE E2

3. THERMAL COEFFICIENT OF EXPANSION

Grade	$\beta \times 10^3$	Source
0.65	1.34[a]	2, 3
	1.598	5
1.0	1.34[a]	2, 3
1.5	1.34[a]	2, 3
2.0	1.17[a]	2, 3
	1.247	5
3.0	1.06[a]	2, 3
	[1.08]	15
5.0	1.05[a]	2, 3
	0.987	20
7.0	1.11[a]	4
10.	1.08[a]	2, 3, 4
	1.035	5
	0.964	19
20.	1.07[a]	2, 3, 4
	1.025	5
50.	1.04[a]	2, 3, 4
	0.96[a]	8
	0.903	19
100	0.96[a]	2, 3
	0.97[a]	4
	0.969	5
	0.903	19
	0.890	20
200	0.96[a]	2, 3
	0.97[a]	4
200	0.900	19
350	0.96[a]	2, 3
	0.97[a]	4
	0.966	5
	[0.925]	15
500	0.96[a]	2, 3
	0.97[a]	4
	0.900	19
	0.958	20
1000	0.96[a]	2, 3
	0.97[a]	4
	0.963	5
	0.936	18
	0.893	19
10000	0.97[a]	4

TABLE E2

4. THERMAL CONDUCTIVITY

Grade	k	Source	Grade	k	Source
0.65	0.100[c]	1,2	20.	[0.144]	5
	0.100[b]	3		0.141	14
	[0.100]	5	50.	0.151[c]	1,2
1.0	0.100[c]	1,2		0.151[b]	3
	0.100[b]	3		0.145[a]	4
	[0.103]	5		[0.154]	5
1.5	0.105[c]	1,2		0.155[a]	8
	0.105[b]	3	100	0.155[c]	1,2
	[0.106]	5		0.155[b]	3
2.0	0.109[c]	1,2		0.149[a]	4
	0.109[b]	3		[0.159]	5
	[0.109]	5		0.155[a]	10,11
3.0	0.113[c]	1,2	200	0.155[c]	1,2
	0.113[b]	3		0.155[b]	3
	[0.114]	5		0.151[a]	4
	[0.147]	15		[0.161]	5
5.0	0.117[c]	1,2		0.155[a]	12
	0.117[b]	3	350	0.159[c]	1,2
	[0.122]	5		0.159[b]	3
7.0	0.128[a]	4		0.152[a]	4
	[0.127]	5		[0.162]	5
10.	0.134[c]	1,2		[0.201]	15
	0.134[b]	3	500	0.159[c]	1,2
	0.128[a]	4		0.159[b]	3
	[0.133]	5		0.152[a]	4
20.	0.142[c]	1,2		[0.162]	5
	0.142[b]	3	1000	0.159[c]	1,2
	0.137[a]	4		0.159[b]	3

TABLE E2

4. THERMAL CONDUCTIVITY

(CONTINUED)

Grade	k	Source
1000	0.152[a]	4
	[0.163]	5
10000	0.152[a]	4
	[0.159]	5

TABLE E2

5. SPECIFIC HEAT

Grade	c_p	Source	Grade	c_p	Source
0.65	[2050]	3	350	1550	6
1.0	1821	14		[1502]	15
2.0	[1620]	3	500	1550	6
	1352[a]	5		1532	20
	1683	14	1000	1461[a]	5
3.0	1616	14		1550	6
	[1622]	15		1599	18
5.0	1549	14			
	1549	20			
10.	[1780]	3			
	1507[a]	5			
	1409	14			
20.	[1520]	3			
	1448	14			
50.	1550	6			
	1470	8			
100	1473[a]	5			
	1550	6			
	1420[f]	10			
	1470[a]	11			
	1402	14			
	1473	20			
200	1550	6			
	1386[e]	12			
350	[1390]	2			
	[1470]	3			
	1423[a]	5			

TABLE E2

6. THERMAL DIFFUSIVITY

Grade	$\kappa \times 10^7$	Source
0.65	[0.722][a]	9
1.0	0.674	14
1.5	[0.737][a]	9
2.0	0.741	14
	[0.914]	17
3.0	0.780	14
	[0.985]	15
5.0	0.88[a]	13
	0.824	14
	0.858	20
10.	0.98[a]	13
	0.955	14
	0.935[a]	19
20.	1.020	14
50.	[1.095][a]	8
	[0.962]	16
	0.983[a]	19
100	[1.13][a]	10
	[1.09][a]	11
	1.16[a]	13
	1.14	14
	0.930[a]	19
	1.116	20
200	1.1[a]	12
	0.983[a]	19
350	[1.368]	15
500	0.958[a]	19
	1.093	20
1000	1.18[a]	13
	[1.049]	18
	0.944[a]	19

TABLE E2

7. PRANDTL NUMBER

Grade	Pr	Source	Grade	Pr	Source
0.65	9.35[a]	9	500	[5550][a]	19
1.0	14.8	14		4770	20
1.5	21.72[a]	9	1000	8500[a]	13
2.0	27	14		[9310]	18
	[22.9]	17		[9930][a]	19
3.0	38.5	14			
	[29.5]	15			
5.0	57[a]	13			
	61	14			
	45.0	20			
10.	102[a]	13			
	105	14			
	[121][a]	19			
20.	187	14			
50.	[457][a]	8			
	[503]	16			
	[591][a]	19			
100	[885][a]	10			
	[917][a]	11			
	860[a]	13			
	877	14			
	[1688][a]	19			
	896	20			
200	[1820][a]	12			
	[2100][a]	19			
350	[3090]	15			

TABLE E2

8. VISCOSITY TEMPERATURE COEFFICIENT

Grade	VTC	Source
0.65	[0.178]	1,2,3
1.0	[0.213]	1,2,3
1.5	[0.278]	1,2,3
2.0	[0.290]	1,2,3
	[0.315]	17
3.0	[0.312]	1,2,3
	[0.315]	15
5.0	[0.343]	1,2,3
	0.280	20
7.0	[0.332]	4
10.	[0.357]	1,2,3,4
	[0.217]	19
20.	[0.370]	1,2,3,4
	[0.395]	14
50.	[0.363]	1,2,3,4
	[0.352]	16
	[0.217]	19
100	[0.368]	1,2,3,4
	[0.217]	19
	0.324	20
200	[0.382]	1,2,3,4
	[0.217]	19
350	[0.379]	1,2,3,4
	[0.370]	15
500	[0.377]	1,2,3,4
	[0.217]	19
500	0.341	20
1000	[0.375]	1,2,3,4
	[0.364]	18
	[0.217]	19
10000	[0.360]	4
	[0.296]	7

TABLE E2

9. SOURCES AND NOTATIONS

Superscript notation:

Superscript	Temperature
a	none specified
b	23 C
c	50 C
d	24 C
e	20 C
f	40 C

Sources:

Number	Source
1	Dow Corning (1952)
2	Dow Corning (1957)
3	Dow Corning (1967)
4	Union Carbide (1970)
5	Bates (1949)
6	Noll (1968)
7	Goldstein and Graham (1969)
8	Hoard, Robertson and Acrivos (1970)
9	Ingersoll (1966)
10	Koschmieder (1966)
11	Koschmieder (1967, 1969)
12	Krishnamurti (1967, 1968b)
13	Krishnamurti (1968c, 1970b)
14	Rossby (1966, 1969)
15	Silveston (1958)
16	Somerscales and Dropkin (1966)
17	Somerscales and Gazda (1968, 1969)
18	Somerscales and Dougherty (1969, 1970)
19	Sun and Edwards (1970)
20	Present experiments

APPENDIX F

CALCULATIONS AND ERROR ANALYSIS

APPENDIX F

CALCULATIONS AND ERROR ANALYSIS

A. Measurement Precision

1. Temperature measurement

The temperatures of the two bounding surfaces were measured with Wheatstone bridges. The legs of the bridges, excluding the glass plates, were constructed of Manganin wire. The resistances of the wires were measured with a minimum accuracy of ± 0.06%.

For the upper surface the total voltage drop across the bridge was maintained at 1.000 V within ± 0.05%. For the lower surface the initial total voltage drop ranged between 0.798 V and 0.856 V. The maximum error in this measurement was ± 0.01 V, which corresponds to a minimum accuracy of ± 1.3%. During a run the total voltage drop across the lower surface bridge had a value between 10.4 V and 55.8 V. For voltages less than 30 V the accuracy of the measurement was ± 0.3 V. For voltages greater than 30 V the accuracy of the measurement was ± 1. V. On a percentage basis the error ranged between ± 1.0% and ± 2.9%.

The voltage imbalance for the upper surface bridge was measured on either a 0.001 V or 0.0032 V full-scale meter reading. The maximum voltage readings were less than 0.0013 V. The minimum accuracy of the meter readings was ± 1.% of the full-scale reading. For the lower surface bridge the initial imbalance was always less than 0.001 V and could be measured to within ± 0.00003 V.

The voltage imbalance of the lower surface bridge was measured on one of four full scale settings, 0.003 V, 0.010 V, 0.030 V or 0.100 V, depending on the total voltage drop across the bridge. The accuracy of the readings were ± 3.% of the full scale reading.

As seen in equation (D7) of Appendix D, the calculation of the change in resistance involves the resistances of the bridge legs, the voltage imbalance and the total voltage drop. Using the best possible cases, the change in resistance for the upper surface could be measured to within ± 1.3%; the lower surface change in resistance could be measured to within ± 4.2%. This error obviously increased for a decreasing change in resistance.

In computing the change in temperature of the surfaces one additional quantity has to be considered, which is the change in resistance with temperature, α_R. This quantity was measured experimentally, using a constant temperature bath; and its value was determined within ± 1.0%. The absolute accuracy of the temperature difference was set at ± 0.05K. Thus, including all these errors, the minimum accuracy of the lower surface temperature difference was ± 0.05K or ± 5.2%, whichever was the largest. For the upper surface temperature difference the numbers were ± 0.05 K or ± 2.3%.

The ambient temperature, which was measured by a thermometer located near the apparatus, was accurate to within ±0.1K. The minimum accuracy of the mean temperature, which is the ambient temperature plus the average of the two surface temperature differences, was ± 0.2K.

2. Heat flux measurement

Two heat flux measurements were made during the course of a run, the total rate of heat generation at the oil-glass interface and the heat passing through the glass-phenolic plastic interface.

As seen from equation (D11) of Appendix D, the total heat generation rate is a function of the resistances of the lower surface Wheatstone bridge, the total voltage drop across the bridge, the voltage imbalance of the bridge and the surface heating area. The surface area was determined within ± 0.5%. Using the error bounds cited in part 1, the total error on the heat generation rate at the lower surface can be set at ± 2.8%. Of all the heat transfer measurements made in the experiments, this was the most accurately determined.

The heat passing downward was measured with a heat flux meter, which had a gauge constant of 1.58×10^5 W/m^2/V. The manufacturer listed the accuracy at ± 2%. The output of the meter was read either on a 0.001 V or 0.0032 V scale with an accuracy of ± 1.% of the full scale setting. Thus, for a 0.001 V output the accuracy of the heat flux reading was ± 3.%. Another source of error arose because the heat flux meter measured only steady-state heating. The size of the error depended on the rapidity of the heating relative to the "time constant" of the meter, which was listed by the manufacturer as less than one second. The error was greatest during the first thirty to forty seconds of the run and was usually less than ± 1%.

These two heat flux measurements, along with the surface temperatures, were used to calculate the amount of heat being transferred upwards at the lower surface. The determination of this heat flux also required a knowledge of the thicknesses of the glass plate and the oil layer, and the physical properties of the two media. The depths of the two media were accurate to within ± 0.2%. The errors in the properties will be neglected in the present analysis. Their accuracy will be discussed in Section B of this appendix. Using an error of ± 5% for the measurement of the lower surface temperature, the accuracy of the heat flux at the lower surface can be set at ± 9%.

3. Property evaluation

In the present experiments the viscosity, the density and the thermal coefficient of expansion were measured for the three grades of silicone oil. All other physical properties were obtained from various sources. The results have been summarized in Appendix E. The table below summarizes the accuracy of the property data. When the information was obtained from other sources, use has been made of the accuracy set by the source. When none was given, an "educated guess" was made as to the probable error.

Material	Property						
	ν	ρ	β	k	c_p	$\varkappa$	Pr
Silicone oil	±2%	±0.05%	±1%	± 2.5%	± 5%	± 7%	±9.5%
Pyrex glass	-	±0.50%	-	±18.0%	± 3%	±15%	-
Phenolic plastic	-	±1.00%	-	±20.0%	±15%	±36%	

4. Dimensionless quantites measurement

There are two sources of error in the determination of the various dimensionless quantities used in the presentation of the data: the accuracy of the dimensional measurements and the error in the property evaluation. The table below lists these two sources of error for the various dimensionless quantities.

Dimensionless Quantity	Error	
	Measurement	Property
H_T	± 3.6%	±13.0%
H	± 9.8%	±13.0%
Ra	± 8.6%	±11.5%
Nu	±17.0%	± 2.5%
ε	±17.0%	-
a	±10.0%	-
τ	± 0.9%	± 7.5%
τ_{cr}	±15.0%	± 7.5%

B. Non-Ideality

In making a theoretical analysis the physical model is generally an idealization of the situation that can be realized in the laboratory. For Bénard convection the effects of some of these non-ideal conditions have been examined (see Chapter III). For the present experiments the effect and contribution of some non-ideal conditions is discussed below.

1. Non-Boussinesq effects

The maximum temperature difference encountered in the experiments was approximately 12 K. Because of the temperature variation, there will be changes of the physical properties over the depth of the fluid layer. The effect of property variation is partially accounted for by evaluating the properties at the average temperature of the fluid layer. For a temperature difference of 12 K the difference of the physical properties between the top and bottom surfaces is for the viscosity 17%, density 1.1%, thermal coefficient of expansion 1.2%, thermal conductivity 0.7%, specific heat 0.7%, thermal diffusivity 1.1% and the Prandtl number 16%.

2. Lateral boundaries

The effects of the lateral boundaries have been discussed in Chapters VI and VII.

3. The finite conductivity of the horizontal boundaries

The glass boundaries are approximately five times better as conductors of heat than the silicone oil. As mentioned in Chapter III, a non-infinitely conducting boundary will lead to a reduction of the

critical Rayleigh number. Approximate calculations indicate that for the glass boundaries the critical Rayleigh number would be reduced about 9 percent. The effect of the finite conductivity boundaries on the general behavior of the fluid layer has received little attention.

4. Constant heat flux at the lower surface

In the experiments the true thermal boundary condition at the lower surface is that it is a plane of constant heat generation. In dimensionless form the total rate of heat generation would increase approximately ten percent because of increases in the mean temperature. For the heat flux at the lower surface increases in its dimensionless value could be as much as one hundred percent during the course of a run. Ten percent of the variation would again be due to property changes. About twenty to thirty percent of the change was due to the composite nature of the apparatus. The remaining and largest contribution of the increase was due to the increased effectiveness of the fluid layer to transfer heat once motion occurred. Because the lower boundary was not heat flux controlled, this variation could amount to a seventy to eighty percent increase in the lower surface heat flux.

5. Heat losses

The apparatus was constructed to minimize the loss of heat through the sidewalls by using a layer of styrofoam. It is estimated that the total loss of heat through the sidewalls as a fraction of the total heat generation rate was at most ten percent.